DOE/ER/61488--T1-PT.4

A SEDIMENTOLOGICAL APPROACH TO HYDROLOGIC CHARACTERIZATION: A DETAILED THREE-DIMENSIONAL STUDY OF AN OUTCROP OF THE SIERRA LADRONES FORMATION, ALBUQUERQUE BASIN

by

Ruth C. Lohmann

Submitted in Partial Fulfillment

of the Requirements for the Degree of

Master of Science in Hydrology

New Mexico Institute of Mining and Technology

Socorro, New Mexico

January, 1992

DISCLAIMER

ACKNOWLEDGMENTS

This research was funded by the U.S. Department of Energy (#DE-FG04-89ER60843). I wish to thank Dr. Fred Phillips, my advisor, for his guidance, especially in helping me to see the "big picture." I also thank Dr. John Wilson and Dr. Alan Gutjhar for their valuable technical advice. My special thanks goes to Dr. Dave Love whose extensive geologic wisdom, tireless love of fieldwork, and quirky sense of humor truly inspired me.

I am truly indebted to Matt Davis whose kindness and support helped get me through even the most difficult times. His work formed the springboard for this independent study, and he served as my mentor for much of my research.

I extend thanks also to Susan Colarullo for her input and technical knowledge, as well as to Annette Schaeffer-Perrini whose computer savvy helped me immensely when I needed it most. Finally, I would like to thank Paula Arnet, Daphne Neel, and all my other hydrology friends who supported me throughout my time here at New Mexico Tech.

ABSTRACT

Hydrologists are today realizing that in order to accurately predict the movement of contaminants within a groundwater aquifer, the permeability correlation structure of the aquifer must be characterized. Three-dimensional geologic outcrop studies which quantitatively describe the geologic architecture of deposits of a specific depositional environment are a necessary requirement for characterization of the permeability structure of an aquifer. The objective of this study is to address this need for quantitative, three-dimensional outcrop studies. For this study, a 10,000 m^2 by 25 m high outcrop of Pliocene-Pleistocene Sierra Ladrones Formation located near Belen, New Mexico was mapped in detail, and the geologic architecture was quantified using geostatistical variogram analysis.

The geologic units chosen for mapping are called "architectural elements", following the definitions by Miall (1985) and Miall (1988). Six architectural elements were delineated at the site: 1) a gravel element (CH-1); 2) a sand element (CH-2); 3) overbank clays and silts (element OF); 4) sand paleosols Ps; 4) clay paleosols (Pc); and 6) gravel sand paleosols Pgs.

Analysis of the sedimentary structures within the elements as well as the overall three-dimensional geometry of the elements suggests that the sediments record primarily floodplain deposition by the Rio Puerco and its tributary (Rio San Jose) and the Rio Grande. The primary axis of deposition in the area appears to have been approximately N30W. Moreover, a wetter climate may have set in during the deposition of the sediments mapped higher in the section.

Variogram analysis of the geologic data shows that the deposits are statistically anisotropic. Variograms estimated parallel to the inferred axis of deposition exhibit a nested exponential linear structure, indicating that the average dimensions of the elements exceed the dimensions of the domain when sampled in this direction. Variograms estimated perpendicular

to the paleoflow direction exhibit a nested exponential behavior with a finite range of correlation. The presence of a sill suggests that at least one scale of variability is indeed captured. The small-scale exponential behavior witnessed in both the parallel and perpendicular directions is tentatively attributed to the average width of the sand (CH-2) scours. Finally, the vertical variogram is strongly periodic which agrees with the discrete layered nature of the system.

In general, the information contained in this study should be useful for hydrologists working on the characterization of aquifers from similar depositional environments such as this one. However, for the permeability correlation study to be truly useful, the within-element correlation structure needs to be superimposed on the elements themselves instead of using mean log (k) values, as was done for this study. Such information is derived from outcrop permeability sampling such as the work of Davis (1990) and Goggin et al (1988).

TABLE OF CONTENTS

LIST OF FIGURES

LIST OF TABLES

LIST OF PLATES

CHAPTER 1: INTRODUCTION

In contrast to the first half of the 20th century when water supply was the primary concern, hydrogeologists today are faced with the need to predict the travel path, rate of movement and spread of contaminant plumes in the subsurface, all of which are dependent on the spatial distribution of aquifer properties. In order to predict solute movement in the subsurface, hydrologists generally begin with the Advection Dispersion Equation (ADE). The ADE models solute transport through the subsurface by both advection with the mean groundwater velocity and dispersion in the porous media. Hydrodynamic dispersion refers to the process of solute mixing in the subsurface due to the phenomena of molecular diffusion and aquifer dispersivity.

Dispersivity describes the phenomena whereby solute particles moving through porous medium follow different tortuous paths. In doing so, the velocities of the individual particles differ, causing mixing of the solutes in the subsurface. At the pore scale (micrometers to mms), differential particle pathways are related primarily to pore geometries. However, at the laboratory and the field scale (cms to kms) larger scale geologic heterogeneities such as variations within and between lithologies give rise to dramatically different particle velocities and pathways.

The value of the aquifer dispersivity is required to predict where and how fast a contaminant will move via the advection-dispersion model. However, dispersivity is generally considered to be a fitting parameter for matching observed tracer test breakthrough data. Moreover, there is growing evidence to suggest that dispersivity is a scale-dependent phenomena (Neuman, 1990), whose value appears to increase with increasing scale. In order

to circumvent this dilemna, hydrologists are today realizing that dispersivity is in essence a measure of the aquifer heterogeneity. Instead of trying to quantify a single value of dispersivity for an aquifer, one should instead try to characterize the spatial variability of aquifer parameters. According to Davis (1986), "heterogeneities should be represented carefully in order to characterize the flow field of an aquifer adequately and to realistically simulate dispersion."

The aquifer property which exerts the largest influence on fluid flow in porous medium is permeability. This finding is largely based on tracer tests. The simplest type of test involves tracing flow thru man-made "sand boxes" with varying permeability configurations (Silliman and Simpson, 1977; Schincariol and Schwartz, 1990) The results of these studies show that the larger the contrasts in permeability values, the greater the range of tracer velocities. Moreover, increased heterogeniety in the configuration of units results in increased dispersion of the tracer plume.

Field tracer tests of contaminant and tracer plumes have also shown the control which three-dimensional aquifer heterogeneity exerts on fluid flow in the subsurface. The anomalous migration of tritium across the Hanford Site in Washington state is a notable example of how relatively small contrasts of permeability in the aquifer control the shape and direction of the contaminant plume (Poeter and Gaylord, 1990). The splitting of the contaminant plume at the Borden Site into two independent plumes shortly after it was introduced into the aquifer is another example of how field scale heterogenieties have been shown to profoundly influence subsurface fluid flow (Sudicky et al, 1983).

Numerical studies also demonstrate that permeability contrasts control fluid flow.

Schwartz (1977) studied flow thru idealized 2-D sand-shale sequences by tracing particles through a variety of checkerboard-like grids of low and high conductivity blocks. The results indicated that tracer dispersion increased when a) the pattern became more heterogeneous, and b) the hydraulic conductivity contrast between the blocks was increased. Desbarats (1990) performed a numerical tracer test similar to that of Schwartz (1977) with the exception that sand-shale sequences were represented by multiple realizations of hydraulic conductivity in a binary spatially correlated random function. Desbarats found, as did Schwartz (1977), that the spatial configuration of the sands and shales significantly affected tracer velocities and spreading.

1.1 Characterization of Permeability Distributions

Out of this growing understanding of the importance of the spatial distribuution of permeability within an aquifer arises the question: How does one describe the permeability structure such that the characterization will allow useful prediction of contaminant transport through the aquifer? In order to address this question it is first necessary to discuss what contaminant transport prediction techniques are commonly used by hydrologists, and what types of information these prediction techniques require.

As discussed above, the transport of contaminants through the subsurface is predicted by solving the Advection Dispersion Equation (ADE). Solution of the ADE requires solution of the flow equation, which in turn requires input of the hydraulic conductivity K. A common approach to input of the hydraulic conductivity is to assign an effective K for the entire aquifer, and thereby look at the average flow within the system.

A second and more realistic approach, is to acknowledge that hydraulic conductivity (and hence permeability) varies spatially within the aquifer. If this approach is adopted, the aquifer is subdivided according to zones of varying hydraulic conductivity, and the flow equations for all the zones are solved numerically.

The simplest way to subdivide the aquifer into zones of hydraulic conductivity is to subjectively assign K values to different zones based on hydrogeological knowledge of the aquifer. A more sophisticated approach involves simulating a continuous K field for the aquifer of interest.

Currently, the most widely used simulation method is based upon a stochastic/geostatistical approach. Stochastic theory assumes that the permeability distribution in geologic deposits can be represented as a random, spatially continous variable. Geostatistics is the branch of statistics which studies and describes random variables which are spatially correlated. A random variable is a variable which describes a spatially and/or temporally varying phenomena (Delhomme, 1978) such as spatially varying permeability. Spatial correlation of a random variable means that values of the variable are more similar at two points located near one another than at two points located further apart (Isaaks and Srivastava, 1990).

Geostatistical simulation techniques require a mathematical description of the correlation structure of hydraulic conductivity permeability as input. The correlation structure of a random variable is summarized by the experimental semi-variogram. Put simply, the variogram graphically expresses the similarity between data values as a function of separation distances in space. The procedure by which the experimental semi-variogram

is calculated is summarized in **Figure 1**. As shown, the set of mean squared difference of the random variable at a given lag distance are summed and divided by twice the number of data pairs separated by that lag; this procedure is repeated at all chosen lags. These mean square differences are then plotted against their respective lags, thereby forming a curve. A mathematical function is then fit to this curve which desribes the spatial correlation of the sample population.

The range of a semivariogram refers to the lag separation distance at and above which values of the mean squared distance no longer increase. The sill of a variogram refers to the maximum value of the mean squared difference attained when the variogram reaches the range (Isaaks and Srivastava, 1990). It is important to note here that a variogram will only exhibit a sill and a range if the variance is finite; otherwise, a monotonically increasing variogram is obtained indicating that the difference in the data values continues to increase with increasing spatial separation. A linear variogram can represent "self-similar" behavior. The reader is referred to the work of Wheatcraft and Tyler (1988) and Burroughs (1988) for a discussion of fractal fields.

Commonly used geostatistical simulation methods include the turning bands technique (Montaglou and Wilson, 1982) and the fast fourier transform technique (Gutjhar, 1989). Both these techniques produce realizations of random fields that have spatial correlation structures with a specified variogram.

As discussed above, these geostatistical simulation techniques require input of the permeability correlation structure of the aquifer. The hydrologist can characterize the

Variogram Estimator

$$\gamma(s) = \sum_{n=1}^{N} \frac{[k(x+s) - k(x)]^2}{2N}$$

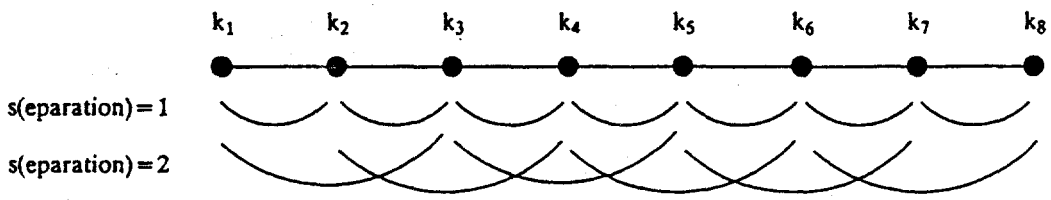

s = 1	s = 2
$d_1 = k_2 - k_1$	$d_1 = k_3 - k_1$
$d_2 = k_3 - k_2$	$d_2 = k_4 - k_2$
$d_3 = k_4 - k_3$	$d_3 = k_5 - k_3$
$d_4 = k_5 - k_4$	$d_4 = k_6 - k_4$
$d_5 = k_6 - k_5$	$d_5 = k_7 - k_5$
$d_6 = k_7 - k_6$	$d_6 = k_8 - k_6$
$d_7 = k_8 - k_7$	N = 6
N = 7	

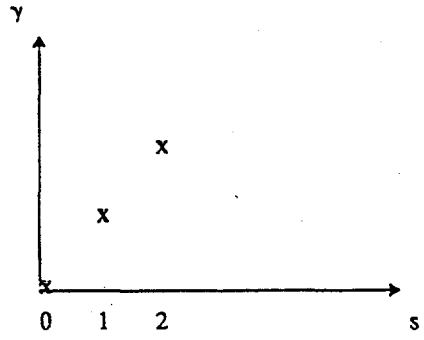

Figure 1: Illustration of experimental semi-variogram estimation procedure

permeability correlation structure by direct or indirect methods. The direct method involves direct quantification of the permeability distribution within an aquifer via variogram analysis of permeability measurements of hundreds of core samples collected by drilling in the aquifer. An alternate approach is to carry out aquifer tests (i.e. aquifer pump tests, tracer tests or flow impeller tests) at many locations in space to determine the spatial distribution of the aquifer's hydraulic conductivity. Examples of such direct aquifer permeability characterization techniques include work done at the Borden Site (Robin et al, 1991), the Cape Cod Site (LaBlanc et al, 1991; Wolf et al, 1990), and the Columbus Air Force Base in Mississippi (Herweijer and Young, 1990). While these aquifer tests do provide valuable information regarding aquifer parameters, they are generally time and cost intensive and provide only limited information about the detailed permeability structure of the subsurface.

The indirect method of permeability structure estimation involves first estimating the correlation structure of hydrologically distinct geologic units within the aquifer. Hydrologically distinct geologic units are those which are characterized by distinctly different permeability characteristics. Once the correlation structure of these hydrologically distinct geologic units has been established, the geology is then correlated to permeability, yielding a permeability correlation structure for the aquifer.

While more straightforward than direct characterization of the permeability structure, accurate description of the three-dimensional lithologic architecture of a groundwater aquifer is no small task. The primary problem which the hydrogeologist faces is that he/she must construct a three-dimensional view of subsurface geologic geometries based on one-dimensional borehole data. To do this, the geologist must first make a rough inference of

the depositional environment of the subsurface sediments. Rough inference of the depositional environment is achieved by reviewing regional geologic literature, and comparing the vertical facies successions in the boreholes to standard depositional type models.

Once the general depositional environment of the site has been established, the geologist then seeks out information in the geologic literature regarding typical lithologic geometries associated with the particular depositional environment. This type of information stems from two sources: 1) studies of contemporary processes and their associated deposits; and 2) outcrop studies which document the 3-d alluvial architecture of geologic deposits whose depostional environment is relatively well understood.

Examples of contemporary studies include the work of Picard and High (1977) in their study of the sedimentary structures associated with ephemeral stream deposits and the work of Mckee et al (1967) in their study of flood deposits of the Bijou Creek, Colorado. These studies and others like them provide valuable information regarding the type of sedimentary structures and geometries associated with specific depostional processes, but provide little information about what type of geologic features are actually preserved in the rock record.

Outcrop studies of geologic deposits provide insight not only into the three-dimensional geometry of sedimentary deposits associated with specific depositional processes, but also into what features are actually preserved in the rock record. Outcrop studies of alluvial/fluvial sedimentary environments are of particular interest to hydrogeologists due to the large number of groundwater contamination sites that are located in alluvial sedimentary

environments (Johnson and Dreiss, 1989). Likewise, fluvial deposits pose a special problem to contaminant hydrologists due to the sensitivity of flow on the interconnectedness of the fluvial sand bodies (Fogg, 1989).

Many workers have studied two-dimensional and three-dimensional outcrops of fluvial deposits. For a review of examples of these outcrop studies see Miall (1988) Most of these studies do an excellent job of qualitatively describing the geometry of the deposits, but only a handful of these outcrop studies have actually attempted to quantify the structure of these deposits. Zeito (1965) uses standard statistical tools to determine the probability that shale layers in deltaic and fluvial outcrops would converge. Ravenne et al (1989) quantify the proportions of sandstone and shaley sandstone in a 300-m long outcrop of fluvio-deltaic deposits by plotting the cumulative proportion of each facies versus vertical height and horizontal position in the outcrop.

Estimating the spatial correlation structure of the geology is achieved via geostatistical analysis of the geologic data. In other words the aquifer is discretize in space. Each data point contains information regarding the geologic unit at that point in space. The correlation structure of this data can then be analyzed via variogram analysis as described above.

Linking the geology to the permeability is the final step of the indirect approach. This link is based on the findings of recent work which suggests that permeability varies distinctly between different geologic units. Nearly all this research takes the form of outcrop studies in which hundreds to thousands of permeability measurements (either insitu or on cores collected from the outcrop) are made at different locations on the outcrop. The permeability distribution is then analyzed and compared to the geologic features observed in

outcrop. Examples of such outcrop studies include the work of Davis (1991), Goggin et al (1988), Kittridge and Lake (1989), Stalkup and Ebanks (1986), Dreyer & Scheie (1991), and Jones et al (1988). The results of these studies all point to the fact that, while it may be difficult to rigorously quantify, a relationship nonetheless exists between observed geologic structures and the permeability distribution.

1.2 Research Objective: A Quantitative Outcrop Study

Ideally, in order to quantify the permeability distribution at a given site, a geologist requires an outcrop study of deposits of similar origin which quantitatively describes the geologic geometries, as well as provides a quantitative relationship between the geologic and permeability structure. This kind of information will require numerous geologic outcrop studies which follow a three step process: 1) describe and quantify the spatial relationships between hydrologically distinct geologic units "with emphasis on how different depositional processes affect these spatial patterns" (Davis, 1990); 2) quantify the permeability patterns within the geologic units; and 3) correlate the geologic and permeability patterns. This quantified relationship can then be used to simulate permeability fields and study flow the system.

The objective of this study is is to perform the first step of this characterization process, namely an investigation aimed at describing and quantifying the lithologic structure found in an outcrop of fluvial deposits. Geostatistical techniques are used to quantify the geologic geometries. The second and third steps of the investigation are not within the scope of this work, but are ongoing at New Mexico Tech by other students involved in the same

research project.

The field site chosen for this investigation is an outcrop of the Sierra Ladrones Formation near Belen, N.M. This outcrop is 10,000 m^2 in areal extent and 25 m in vertical extent. The outcrop includes the 60m wide by 25m high outcrop studied by Davis (1990). The research effort entailed extensive mapping of the deposits at a variety of scales, inference of the depositional environment of the deposits and quantification of the observed lithologic geometries using statistical and geostatistical tools. The quantified geometries are then discussed in the context the inferred depositional environment.

CHAPTER 2: SITE GEOLOGY

This chapter describes the field site and its location within the Albuquerque Basin. This is followed by a discussion of the previous work done on the geology of the upper Sierra Ladrones Formation as this information serves as the reference point for the depositional environment analysis portion of this thesis.

2.1 Site Location and Description

The field site is located in Valencia County in the south-central portion of the Albuquerque Basin, approximately 60 km south of Albuquerque, NM. It is bounded by north latitudes 33'40" and 33'55" and west longitudes 48'05" and 48'20". The Veguita 7.5" quadrangle map provides topographic coverage of the area at a scale of 1:24,000.

Figure 2 illustrates the location of the field site. As shown, the site is just west of Bosque, New Mexico, and is part of a north-south trending escarpment of the Llano de Albuquerque. The Llano is a geomorphic surface which represents the culmination of basin aggradation during the Pleistocene (Lozinsky et al., 1991).

The Bosque Site is a peninsula-like geomorphic feature which extends eastward from the escarpment adjacent to the Llano. The site is connected to the escarpment by a narrow neck. This site was chosen for study due to its excellent three-dimensional exposure of the sediments.

The sediments exposed at the field site and along the escarpment consist of alluvial-fluvial deposits of the upper Sierra Ladrones Formation. The Sierra Ladrones Formation makes up the upper basin fill and the Popotosa Formation makes up the lower basin fill. Together, the Sierra Ladrones Formation and the Popotosa Formation form the Santa Fe Group (Machette,

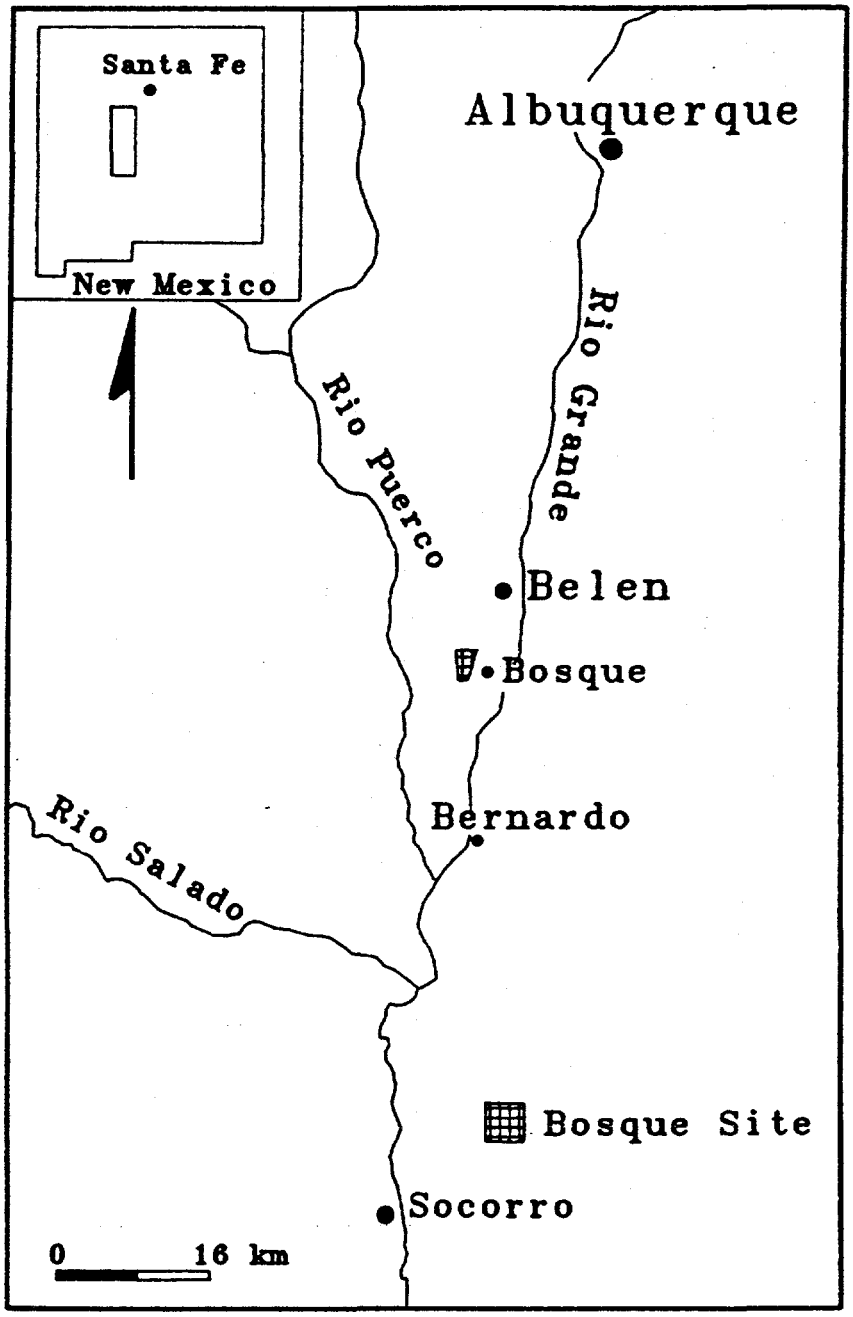

Figure 2: Site Location Map

1978).

The Albuquerque Basin is an approximately 1000 km long, 30-50 km wide structural basin. It is one of several en echelon basins which formed due to extension along the Rio Grande Rift. The basin is bounded to the west by the Lucero and Ladron uplifts, to the north by the San Felipe fault belt, to the east by the Manzano-Los Pinos uplift, and to the south by the Joyita uplift near San Acacia, NM. Structurally, the basin is composed of a series of half grabens which are eastward tillted in the northern half of the basin and westward tilted in the southern half (Lozinsky, 1988).

The Rio Grande and its tributaries have largely shaped the geomorphic features seen in the Albuquerque Basin today. Tributaries to the Rio Grande in the vicinity of the field site include the Rio Puerco, the Rio Salado, and several smaller arroyos which feed these rivers. Incision by the Rio Grande on the east side of the basin coupled with incision by the Rio Puerco on the west side has formed the southward narrowing tableland topped by the Llano de Albuquerque (Lozinsky et al, 1991). The gently sloping basin margins are largely a result of the many alluvial fans and associated arroyos which flank the Albuquerque Basin margins.

The Rio Grande is the largest river to traverse the Albuquerque Basin. The Rio Grande flows from its headwaters in the San Juan Mountains in southern Colorado southward through the central axis of the Albuquerque Basin to its final destination, the Gulf of Mexico. The Rio Grande is a perrenial river which exhibits a meandering character in its northern reaches, and a more braided character in the Albuquerque Basin region. The river carries predominantly sand and gravel; overbank deposits of the Rio Grande consist of fine sands, silt and clay.

The main channel of the Rio Puerco drains the west side of the San Pedro and

Naciemento Mountains near Cuba, New Mexico. The channel flows south to its confluence with the Rio Grande near Bernardo, NM. Several ephemeral rivers contribute flow to the Rio Puerco, including the Arroyo Chico which drains the north side of Mt. Taylor, and the Rio San Jose which drains the area west of Laguna, including the northern side of the Zuni Mountains west of the Continental Divide and the southern flank of Mt. Taylor. The Rio Salado originates in the mountains near Datil, NM, flowing thru the Lemitar and Ladron Mountains, and merges with the Rio Grande near San Acacia, just south of the Rio Puerco-Rio Grande confluence. The Rio Salado is an ephemeral braided river which flows only 30-40 days a year (Stephens et al, 1988).

2.2 *Basin-Filling History of the Albuquerque Basin*

Two episodes of rifting appear to have opened the basin to its current structural configuration (Chapin & Seager, 1975; Seager et al, 1984). The first episode occurred between the late Oligocene (30 Ma) and the early Miocene (approximately 18 Ma), and the second in the late Miocene (5-10 Ma).

Between the initiation of basin rifting and 5 Ma, the Albuquerque Basin remained a series of closed basins (Lozinsky, 1988). The Popotosa Formation records deposition during this time period. Analysis of Popotosa sediments in outcrop and from boreholes suggests that the three primary mechanisms of deposition during this time period were alluvial fans carrying detrital matter off the rising basin margins, playa deposits in the basin center, and eolian processes (Lozinsky, 1988).

The closed basins coalesced and the Rio Grande developed a through-flowing river

system approximately 5 Ma (Lozinsky et al, 1991). Between this time and approximately 0.5 Ma (Pleistocene), the Rio Grande and its associated tributaries were largely aggrading and filling the Albuquerque Basin. The Pliocene-Pleistocene deposits of the Rio Grande and its tributaries comprise the fluvial fcies of the Sierra Ladrones Formation.

2.3 Previous Geologic Study of the Upper Sierra Ladrones Formation

Young (1982), Lozinsky (1988), and Davis et al (1991) have all done geologic studies of the upper Sierra Ladrones Formation in the vicinity of the Bosque Site. Young (1982) measured geologic secctions and performed pebble counts in the vicinity of the site, and concluded that the upper Sierra Ladrones Formation was depostied primarily by a fluvial source flowing from the northwest. Lozinsky (1988) also measured a geologic section in the vicinty, and performed pebble counts of the sediments. **Figure 3** summarizes the hypothesized drainage system which Lozinsky et al (1991) propose laid down the upper Sierra Ladrones Formation.

Davis (1990) was the first to do geologic investigation at the Bosque Site. This study is essentially an extension of the original work by Davis (1990); therefore, a relatively detailed description is given below of his work. The bulk of his work went into mapping the geologic units along a 65m wide by 25m high two-dimensional face at the site which he refered to as Outcrop 1. Davis also performed in-situ permeability measurements at the Bosque Site; the reader is referred to Davis (1990) or Davis et al (1991) for more information regarding the permeability sampling at the Bosque site.

For the geological portion of his work, Davis began by mapping the geologic facies along the outcrop. Davis employed the fluvial facies classification scheme of Miall (1978) to identify

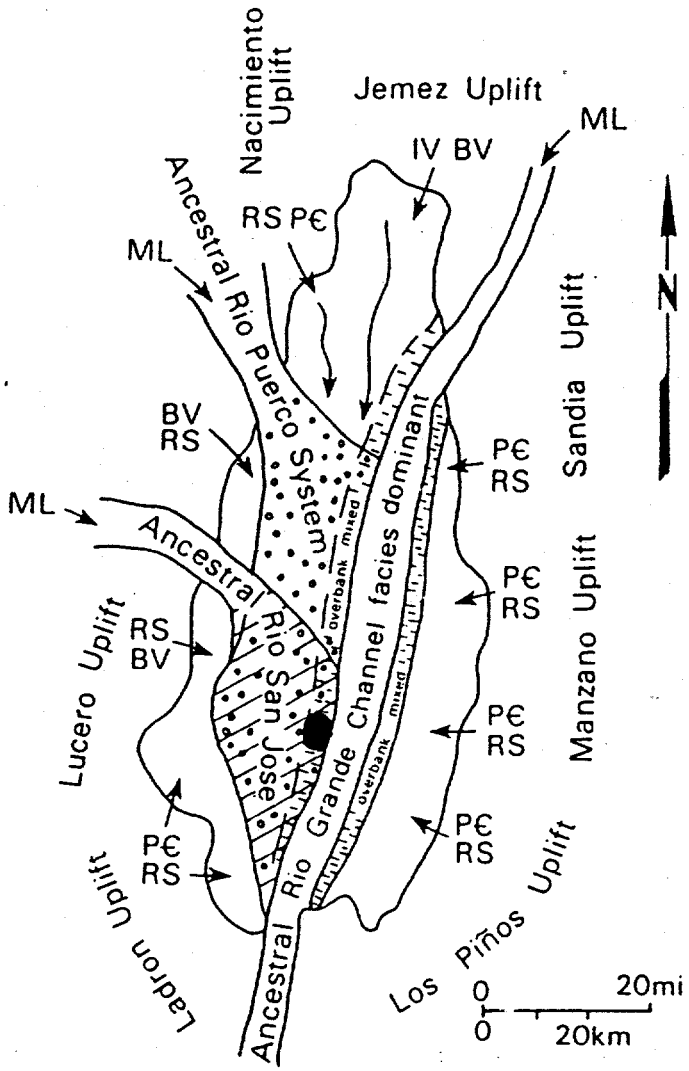

Figure 3: Hypothesized geometry of Albuquerque Drainage Basin during deposition of upper Sierra Ladronnes Formation by Lozinsky (1988). Arrows indicate source areas and clast types derived from those areas. PC=Precambrian, RS=reworked sedimentary rocks, IV=intermediate volcanic rocks, BV=mafic volcanic rocks, ML=mixed lithologies. Approximate location of Bosque Site is shown by black circle.

geologic facies at the field site. A few facies not specified by Miall (1978) were added to the classification in order to accommodate the deposits observed at the field site. This modified classification scheme is shown in **Table I.**

Davis then grouped these facies into genetically related assemblages which he called "architectural elements." The term "architectural element" was used by Allen (1983) in his study of the Devonian Brownstones of the Welsh Borders. His study subdivided the Brownstones into genetically related sedimentation units related by facies and/or paleocurrent direction which he called architectural elements.

The term "architectural element" was further defined by Miall (1985) in his analysis of fluvial deposits. Miall (1985) began using this term in response to the inadequacy of vertical facies analysis in terms of understanding the three-dimensional relationships of sedimentary deposits within a basin. According to his early work (Miall, 1985), all fluvial deposits are composed of a combination of eight architectural elements which he defines as sedimentary packages identified by their "grain size, bedform composition, internal sequence and, most critically, by external geometry." **Figure 4** illustrates these eight basic architectural elements.

In his later work, Miall (1988) refined the definition of an architectural element to mean "a lithosome characterized by its geometry, facies composition and scale [that] represents a particular process or suite of processes occuring within a depositional system." A lithosome is defined as a body of sediment deposited under uniform physiochemical conditions (Bates and Jackson, 1984). In the context of his six-fold hierarchy of fluvial bounding surfaces (Miall, 1988), an architectural element is defined as a fluvial sedimentary unit bounded by a fourth or higher order surface.

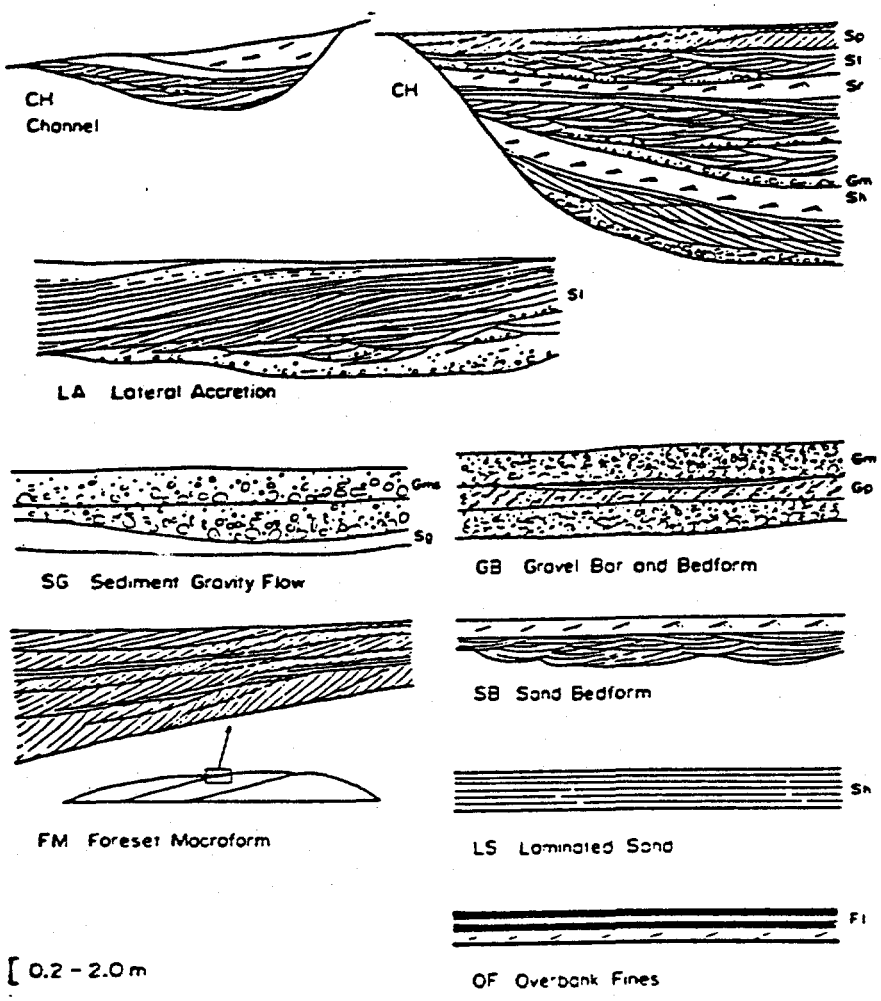

Figure 4: The eight major architectural elements as defined by Miall (1985).

Davis utilized Miall's (1988) definition of an architectural element when mapping at the Bosque Site. He grouped together facies into elements so as to delineate genetically related groups of sediment. The facies grouping employed by Davis (1990) is shown in Table II.

Table II

Facies Groupings for Definition of Architectural Elements at Bosque Site
Modified from Davis (1990)

Element Code	Facies Present	Description/Comments
CH-I	Gm, Gt, Sp, St, Sl, Sgm	Channel element consists dominantly gravelly and coarse sand facies.
CH-2	Gms, St, Sp, Sfl, Sh, Sl, Smb, Fl, Fm, Fsc	Sand and snad size clay clasts dominate with local lag gravel deposits.
P	P, Sm, Fsc	Soils and stacked soils
OF	Fr, Fm, Fsc, P	Overbank fines

Figure 5 is the architectural element map of Outcrop 1 prepared by Davis (1990). This map illustrates the four primary architectural elements identified by Davis at the Bosque Site: 1) medium to coarse sand and gravels (CH-I); 2) fine to medium sands with abundant interbedded clay and silt (CH-II); 3) interbedded clays, silts and thin paleosols (OF); and 4) paleosols (P).

Comparison of Table II and Figure 4 shows that Davis (1990) slightly modified the architectural element facies groupings defined by Miall (1985). The element Davis (1990) called a high energy channel element (CH-1), Miall (1985) would call a channel element (CH) and/or a gravel bar and bedform element (GB). The element Davis (1990) calls a low energy channel

Table I

Facies Classification Scheme employed by Davis (1990)

Facies Code	Facies Description	Sedimentary structures
Gms	massive, matrix supported gravel	none
Gm	massive or crudely bedded gravel	horizontal bedding, imbrication
Gt	stratified gravel	trough crossbeds
St	sand, medium to v. coarse, may be pebbly	solitary (theta) or grouped (pi) trough crossbeds
Sr	sand, v. fine to coarse	ripple marks of all types
Sh	sand, v. fine to v. coarse, may be pebbly	horiz lamination, parting or streaming lineation
Sp	sand, medium to v. coarse, may be pebbly	solitary (alpha) or grouped (omikron) planar crossbeds
Sl	sand, fine	low angle (< 10) crossbeds
Smb	fine to medium sand with mudballs	crude crossbedding
Sfl	sand, v. fine to coarse	fining upward sequence
Sm	sand, v. fine to v. coarse, may be pebbly	none
Sgm	sand, fine to v. coarse, pebbly	none
Fl	sand, silt, mud	fine lamination, very small ripples
Fsc	silt, mud	laminated to massive
Fm	mud, silt	massive, desiccation cracks
Fr	silt, mud	rootlets
P	carbonate	pedogenic features

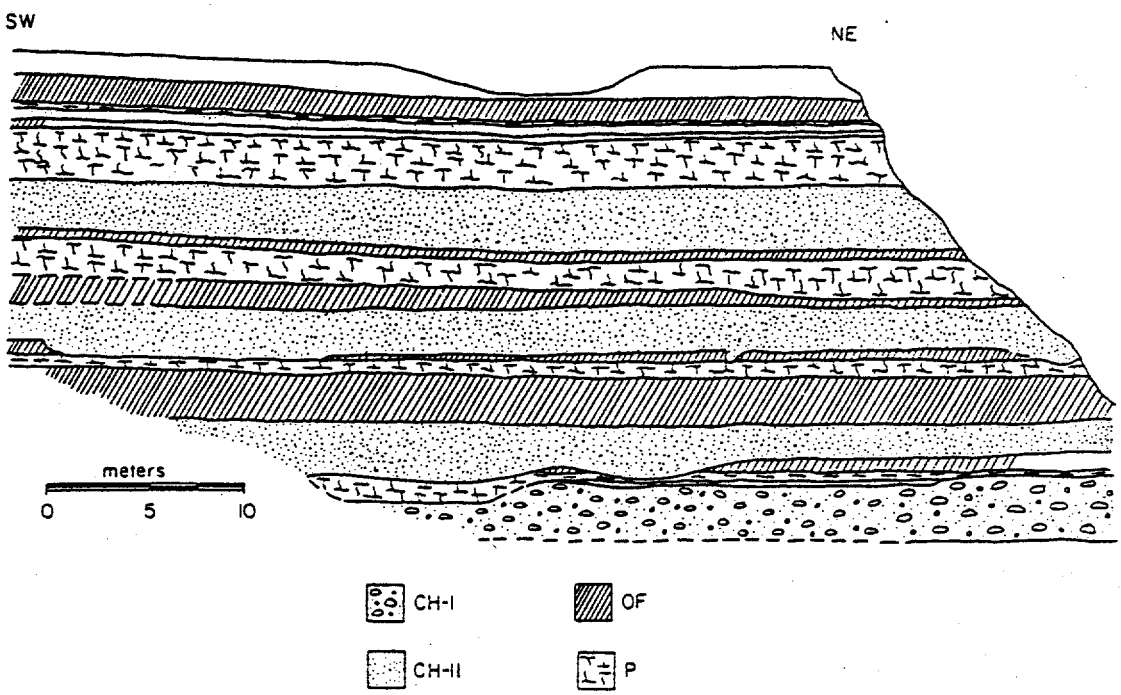

Figure 5: Architectural Element Map of Outcrop 1; map prepared by Davis (1990)

element (CH-2) would most likely be classifed as laminated flood sands (LS) or overbank fines (OF) by Miall (1985). The three paleosols (Ps, Pc, and Pgs) as well as the clay-silt element (OF) delineated by Davis (1990) all would be classified by Miall (1985) as part of the overbank fines element (OF).

Davis mapped the paleosols as genetically independent units due to their different hydrologic properties and their utility in terms of depositional environment analysis. Paleosols are defined as "a buried soil; a soil of the past" (Bates and Jackson, 1983). A body of sediment (the parent material) is altered into a soil by physical and chemical processes known collectively as pedogenesis (**Figure 6**). In essence, a body of sediment will be altered by pedogenesis into a soil if it is in an area of the landscape which is deprived of a significant source of sediment influx and/or erosion of an extended period of time. In an arid to semi-arid climate, the amount of time required for the formation of a mature soil is on the order of 10,000 to 100,000 years (Birkeland, 1984).

Based on his work, Davis hypothesized that the flow events which deposited much of the geologic units within the upper Sierra Ladronnes Formation were intermittent, suggesting that ephemeral/tributary type rivers may have dominated the depositional environment. Moreover, the abundance of paleosols and overbank fines in the section led Davis to the conclusion that river channels periodically moved away from the vicinity of the site, leaving the area deprived of sediment influx.

SOIL FORMING PROCESSES

Pedology, weathering, and geomorphological

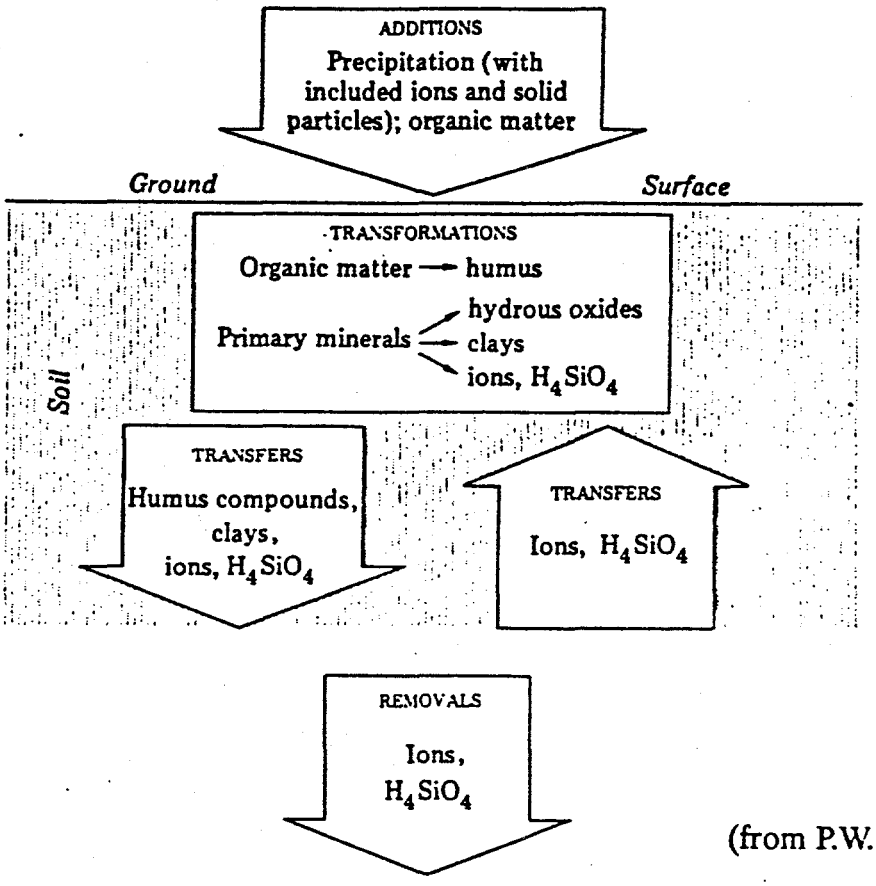

(from P.W. Birkeland, 1984)

Figure 6: Schematic illustrating the process of Soil Formation (Pedogensis)

CHAPTER 3: METHODOLOGY

As discussed in Chapter 1, in order to reconstruct subsurface geologic architecture, outcrop studies are required which quantitatively describe the three-dimensional geometry of deposits from a variety of depositional environments. The work of Davis (1990) was a start in this direction, but it was limited to two dimensions. Therefore, the goal of this research was to extend the mapping to three dimensions, and to quantify the three dimensional alluvial architecture following a four step methodology: 1) map the geologic deposits at a variety of spatial scales; 2) infer the depositional environment of the outcrop; 3) quantify the geologic structure using statistical and geostatistical tools; and 4) relate the observed geologic structure to the quantified depositional environment.

3.1 Geologic Mapping

The primary scale of mapping carried out for this thesis involved defining and tracing larger-scale lithosomes called "architectural elements" around the outcrop. A limited amount of mapping was also carried out at a smaller scale. This smaller scale mapping, heretoforth referred to as facies-scale mapping, involved observing the sedimentary structure and facies within the sand-dominated architectural elements. Taken together, these two scales of mapping produce a level of detail sufficient to allow both a solid understanding of the three-dimensional geometries of the deposits as well as inference of the depositional environment of the Bosque Site.

3.1.1 Architectural Element-Scale Mapping

The bulk of the mapping effort for this research went into defining and laterally tracing architectural elements around the perimeter of the outcrop. Element mapping for this thesis essentially follows the element delineation of Davis (1990) with two minor changes. First, the paleosol element was subdivided by parent material into sandy paleosols (Ps), clay-rich paleosol (Pc), and gravel-sand palesols (Pgs). Secondly, in many cases the sand dominated element (Ch-2) graded laterally into a silt and clay dominated element (OF). Therefore, the CH-2 elements are identified as containing less than 40% silt and clay, while the OF elements contain greater than 40% silt and clay.

The first step in the mapping effort was to prepare a topographic base map of the field site. This was necessary because the scale of study is considerably smaller than the scale of the USGS quadrangle of the area.

This base map was prepared using a Leitz theodolite and survey rod. In order to cover the entire areal extent of the outcrop, the theodolite was set up at twenty-two survey stations around the outcrop. From these stations, over 1000 points were surveyed. The survey points are located so as to delineate lithologic contacts, and topographically important features such as gulleys, knobs, and alcoves.

Raw survey data consists of the distance and angle (horizontal and vertical) between a survey point and the survey station from which it was shot. This distance-angle data is then converted into a data set containing the north coordinate, east coordinate, and elevation of each survey point (meters). The coordinates of each survey point are relative to the coordinates of the first survey station established in August 1989. This station was assigned

an arbitrary north, east position of (0,0) and an elevation of 1519.4 m (4985 ft) based on the careful analysis of the USGS topography map. An estimated measurement error of between 30 and 60 cm across the approximately 112,000 square meter area was determined when normalizing the data set.

The topographic base map was constructed by plotting the x-y coordinates of the 1000 survey points with their associated elevations onto a of 34" X 22" paper using the USGS computer package GSMAP and a Hewlett Packard 7540B pen plotter. The corresponding elevation (z) of each point was plotted adjacent to each point to allow hand contouring of the topography in 10 foot intervals. The final base map was visually checked for accuracy in the field. The hand contoured lines were then digitized using a Summagraphics digitizing table and GSMAP. The purpose of digitizing is to allow reproduction of the contour maps at any chosen scale.

The architectural element map of the Bosque site was recorded following a three-step procedure. The first step is to prepare a base geologic map. This is accomplished by superimposing the geologic contacts recorded by the survey data onto the topographic base map. Nearly 75% of the survey points record geologic contacts, and therefore provide excellent vertical and lateral control on the location of the elements on the outcrop.

The second step involves filling in the "gaps" of geologic information on the map. This is achieved by measuring numerous vertical sections up the outcrop. The locations of these sections are determined by careful comparison of the surrounding topographic and geologic features on the base map and those visible in the field. Elements are also traced laterally around the outcrop by again carefully comparing feature visible in the field and on

the geologic/topographic base map.

Videotapes and photographs of the outcrop provided additional sources of information for filling in the geologic map. The location of each survey point was audiovisually recorded with a Sony Sports Camcorder during the surveying process. Photographs of the outcrop were also helpful when filling in the base map. These photographs allowed one to sit at a distance from the outcrop and trace visually observable elements directly onto the scaled photographs. This information was then transferred by hand onto the base map.

The final color Architectural Element Map of the Bosque Site was prepared by digitizing the hand-drawn elements as separate polygons. These digitized polygons were then plotted in ink using GSMAP and the HP 7580 plotter. The digitized topographic contours were then plotted on top of the element map. Details of the geologic geometries are not readily apparent when the elements are plotted on the contour map. For this reason, three cross sections were prepared of the site. The three cross sections, sections A-A', B-B' and C-C' essentially follow the perimeter of the outcrop.

3.1.2 Qualitative Studies of Sedimentary Structures

All six types of architectural elements identified at the Bosque Site were studied in detail at selected locations across the site in order to construct a type description of each element. These studies involved looking at the elements more closely with the objective of preparing an element type description. Features noted in these studies include grain size, angularity and sorting (Canadian Geological Society Classification Scheme), as well as color and in the case of soils, the degree of pedogenesis (McGrath and Hawley, 1987).

In the case of the sand-dominated elements CH-2, actual cleared outcrops were prepared using a shovel and trowel, and upon drying, were brushed with a paintbrush to bring out the sedimentary structures. The outcrop are generally 1-3 meters wide and 1-2 meters high, and cover the entire thickness of the element. These outcrops were then photographed, and the spatial distribution of the above parameters was recorded on the photographs.

3.2 Inference of Depositional Environment

The depositional environment of the Bosque site sediments was inferred by close analysis of the vertical sequences of sediments, the three dimensional geometries of the deposits. Comparison of the architecture of the mapped deposits with the alluvial models of Allen (1974) and Kraus and Bown (1987) allowed inference of the allocyclic and autocyclic controls on deposition.

This inferred depositional environment was refined using a source terrain analysis performed by Harris (1991). This analysis consisted of collecting a total of thirty samples of the sediments within selected CH-2 elements at the Bosque Site, and from the river terraces of the ancestral Rio Grande, the ancestral Rio Puerco, and the ancestral Rio San Jose. The sample locations are shown in **Figure 7**. Harris (1991) prepared the unconsolidated samples for standard thin section analysis by first sieving the samples to the 1 phi size, and then impregnating them with epoxy. The thin sections were double stained to allow resolution of the feldspars. Harris (1991) constructed ternary diagrams based on 200 point grain counts of the thin sections.

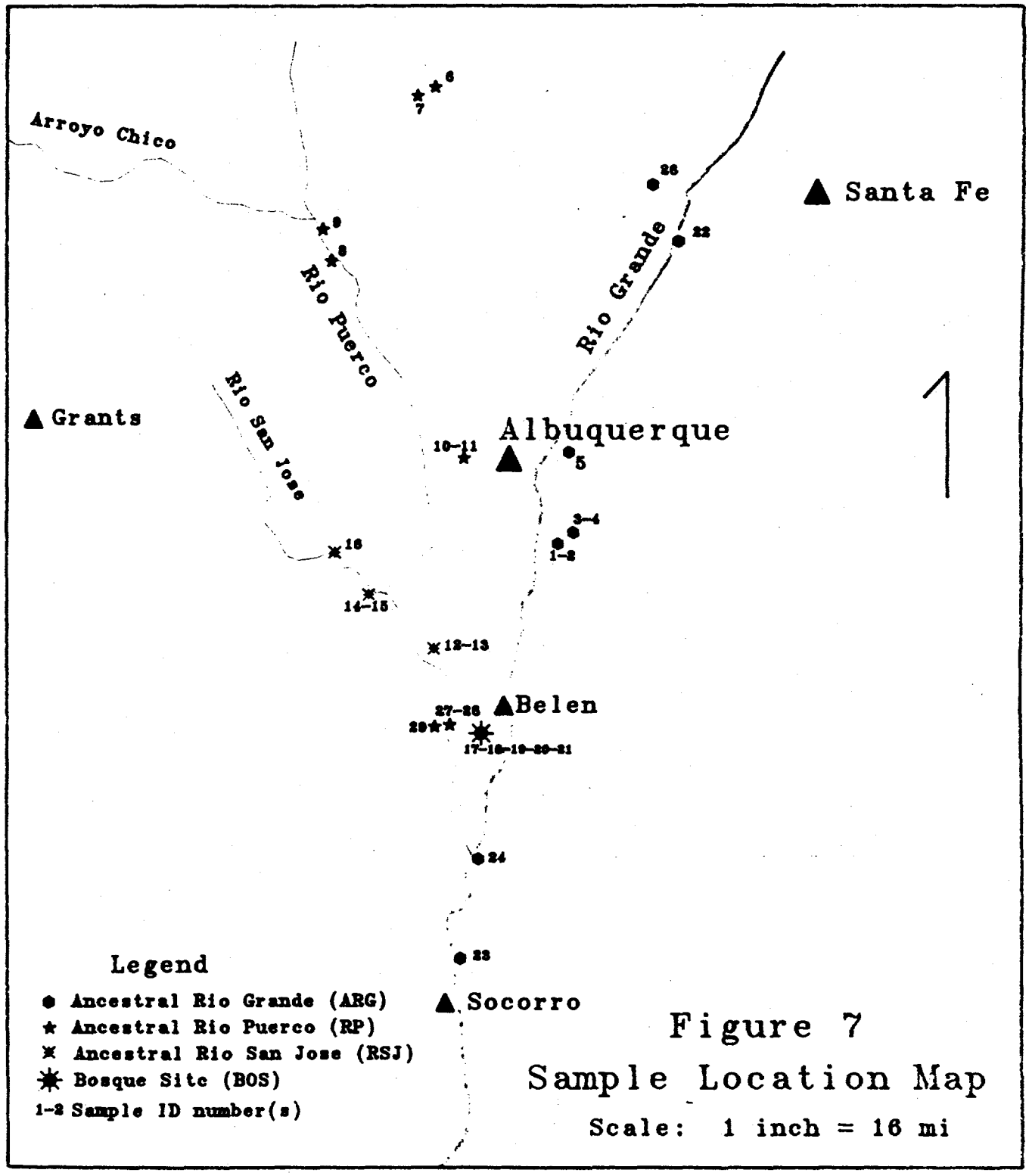

Figure 7
Sample Location Map
Scale: 1 inch = 16 mi

3.3 Quantification of Geologic Architecture

The geologic geometries mapped at the Bosque Site are quantified using geostatistical variogram analysis. The variable chosen for analysis is mean log k (darcies). Five data sets were constructed: two 3-dimensional data sets based on the architectural element map (AEM), one containing 1,454 samples and another containing 54,402 samples, and three 2-dimensional data sets based on the geologic cross sections. Horizontal and vertical variograms were then estimated for these five data sets. As a final step, an analysis of the sensitivity of the variograms to various input parameters was performed.

3.3.1 Preparation of Data Sets

The smaller of the two AEM data sets is based on the 75 semi-vertical stratigraphic sections shown on the AEM (Plate 1). The (x,y) location of the basal contact of each element in the stratigraphic sections was recorded using the digitizing table, and the elevation (z) of each contact and the code for the element was manually entered during the digitizing process. The original digitized data which recorded the location of the basal contact of each element was transformed into a data set recording the centroid of each element using linear interpolation. This data set was supplemented with the (x,y,z) locations of all element pinchouts. These pinchouts are recorded as locations on the map where the thickness of the pinched out element is entered as 0. A mean log k (darcies) value was assigned to each element based on permeability estimates of Freeze and Cherry (1979; p. 29), and essentially follow the classification scheme used by Davis (1990) for his numerical experiment. Table V illustrates the values of log k assigned to each of the six architectural elements.

Table III

Assigned Log k (darcies) Values for Small AEM Data Set

Element Type	Assigned Log K value (darcies)
Gravel Element (CH-1)	3
Sand Element (CH-2)	1
Gravel Sand Paleosol (Pgs)	0
Sand Paleosol (Ps)	-1
Clay-Silt (OF) and Clay Paleosol (Pc)	-3

Following the completion of variogram analysis of the small AEM data set, it was determined that a larger and more exhaustive data was required for geostatistical characterization of the Bosque Site. As such, the large AEM data set containing 54,402 data points was prepared. This larger set was prepared by first overlaying a dense grid of test points (one point every meter in the x and the y direction) over the architectural element map. The grid was generated using the fortran program TESTPT which is included in **Appendix A.**

The (x,y) coordinates of the test points as well as the coordinates of the digitized element polygons and associated element codes were then introduced into a computer program designed to determine within which element (represented as a polygon) each test point lies. The program prepared for this purpose is called PTPOLY and is included in Appendix A. A program called DATAPREP (Appendix A) was used to format the GSMAP data file for the PTPOLY.

PTPOLY outputs (x,y,element code) for each test point found to be inside an element polygon. The data set is not complete, however, without the elevation (z) of the test points determined to be inside an element polygon. In order to determine the z value, another computer program was prepared called FITPLANE (Appendix B) which accepts as input the (x,y,z) coordinates of the digitized elevation contour lines (shown on Plate 1) and the (x,y,element code) output from PTPOLY. FITPLANE fits a plane to the nearest three digitized contour points with z values greater and less then the test point. In other words, the program performs a simple three-dimensional interpolation of the z value of the test point.

Instead of assigning log (k) values to the architectural elements based on Freeze and Cherry (1979) as was done for the small AEM data set, actual measured permeability values collected at the Bosque Site by Davis (1991) were used in order to make the large AEM data set more representative of the conditions at the Bosque Site. A single value of mean log (k) was assigned to each mapped element type based on the results of in-situ air permeability sampling of the CH-1, CH-2, Ps and Pgs elements carried out at the Bosque Site by Davis (1991), and laboratory analysis of a sample of the OF element. Davis (1991) collected six-hundred spatially located air-permeability measurements within the CH-1, CH-2, Ps, and the Pgs elements. The mean of each of these sets of measurements was used as input for the variogram analyses. A falling head permeability test was conducted on an intact clay sample from the OF element. The measured permeability is approximately 10^{-6} darcies. Given this uncertainty, the variograms were run for log k = -6 and log k = -4, and log k = -2 in order to test the sensitivity of the variograms to the assigned clay permeability. **Table IV** contains

the best estimates of log permeability assigned to each of the six architectural elements.

Table IV

Assigned Mean Log k (darcies) for large AEM data set
and Cross Section Data Sets

Architectural Elements	Mean Log k (darcies)
Gravel element (CH-2)	1.24
Sand element (CH-1)	0.70
Sand and Gravel-Sand Paleosols (Ps,Pgs)	0.42
Clay elements (OF, Pc)	-6.0

The three 2-d data sets of the geologic cross sections were created using the above described computer programs. For the purpose of analysis, the cross sections were viewed as (x,y) data all with a z value equal to zero. The x direction was taken as horizontal in the variogram analyses, and the y direction as vertical. Mean log k values were assigned to the elements based on Table IV.

3.3.2 Variogram Analysis of Data Sets

Two horizontal variograms were estimated for the small AEM data set, one in a direction orientated parrallel to the inferred paleoflow direction (N30W), and another orientated perpendicular to inferred paleoflow direction (N60E). A variogram was not estimated in the vertical direction due to the insufficient number of pairs in the vertical direction. Two horizontal variograms, one orientated N30W and the other N60E, and one vertical variogram were estimated for the large AEM data set. Finally, a single horizontal and vertical variogram was estimated for each of the three cross section data sets.

The computer code utilized to compute both the two-dimensional and the three-dimensional variograms is a 3-dimensional variogram code called GAM3V (Deutsch and Journel, 1991). This code is included in **Appendix B.** GAM3V allows the user to specify not only the direction for sampling, but also the horizontal and vertical angle tolerances. The code was also modified to allow the user to specify a maximum vertical search range. The purpose of this maximum vertical search range is to maintain a specified horizontal search window over large horizontal distance. **Figure 8** illustrates the directional and angle tolerances, as well as the values of these parameters used in estimation of the variograms for this study.

3.3.3 Sensitivity Analysis

Sensitivity analysis was performed on the horizontal variograms estimated from the large AEM data set for four input parameters: 1) the value of the low k units; 2) the horizontal search direction; 3) the horizontal angle tolerance; and 4) the maximum vertical search distance tolerance. The sensitivity of the variograms to the value of the low k units was assessed due to the lack of sufficient permeability data on the clay units. The variograms were tested for directional sensitivity to assess the impact of the search windows and distances on the resultant variograms. These four sensitivity parameters are summarized in **Table V.**

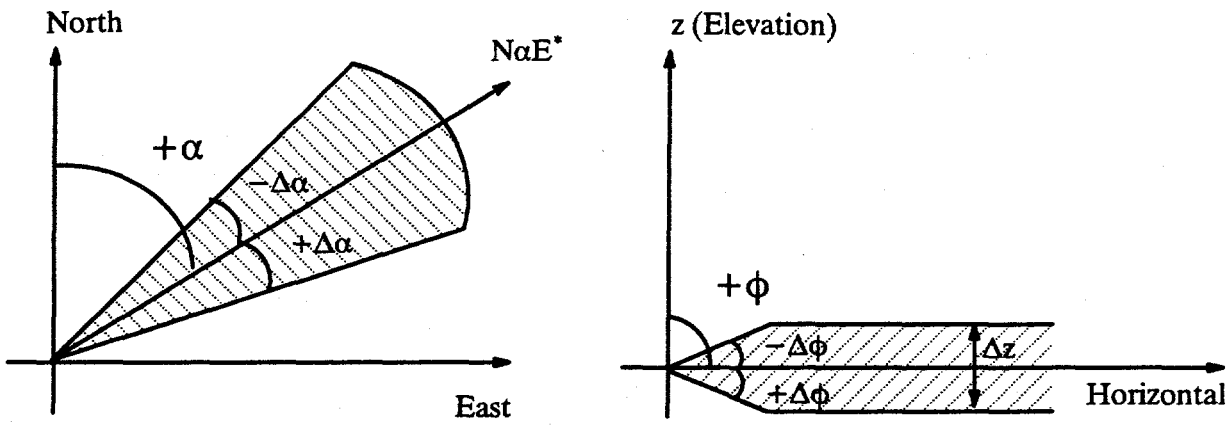

(a) Plan view (b) Cross−section view

* Horizontal variogram directions NαE and NαW correspond to $+\alpha$ and $-\alpha$, respectively.

Data Set	Direction (α)	Horz. Angle Tolerance (Δα)	Vertical Direction (ϕ)	Vert. Angle Tolerance (Δϕ)	Vert. Distance Tol. (ΔZ [m])	Figure
Small AEM	N30W	30	90	10	0.1	20
	N60E	30	90	10	0.1	20
Large AEM	N30W	30	90	10	0.25	21
	N60E	30	90	10	0.25	21
	Vertical	180	0	50	N/A	21
A−A'	Horizontal	30	90	0	0.25	22
	Vertical	30	90	0	N/A	22
B−B'	Horizontal	30	90	0	0.25	23
	Vertical	30	90	0	N/A	23
C−C'	Horizontal	30	90	0	0.25	24
	Vertical	30	90	0	N/A	24

Figure 8. Illustration of variogram search window parameters for a) horizontal direction and b) vertical direction; and summary of values used for variogram estimates in this study.

Table V

Horizontal Variogram Sensitivity Analysis Parameters

Parameter	Trial 1	Trial 2	Trial 3
Value of clay units[1]	log(k) = -6	log(k) = -4	log(k) = -2
Horiz. Direction[2]	N45W/N45E	N30W/N60E	N-S/N90E
Horiz. Angle Tol.[3]	10 degrees	30 degrees	50 degrees
Vertical Distance Tol.[4]	0.10 m	0.25 m	1.0 m

1. Horizontal angle tolerance = 30 degrees; vertical distance tol. = 0.25 m
2. Horizontal direction = N60E / N30W; vertical distance tol. = 0.25 m
3. Horizontal direction = N60E / N30W; horizontal angle tol. = 30 degrees
4. Horizontal direction = N60E/ N30W; horizontal angle tol.; vertical distance tol. = 0.25 m

CHAPTER 4: GEOLOGICAL RESULTS AND INTERPRETATION

This chapter presents the results of the geologic mapping at the Bosque Site. The chapter begins with a discussion of the internal characteristics of the six architectural elements, and what these internal characteristics suggest about the predominant depositional processes. This is followed by an analysis of the three-dimensional geometry of the elements. Finally, the allocyclic and autocyclic controls on deposition are evaluated by comparing the Bosque Site alluvial architecture to alluvial models found in the geologic literature.

4.1 Descriptions and Interpretations of Architectural Elements

The Architectural Element Map (**Plate 1**) and the three cross sections A-A', B-B' and C-C' (**Figures 9, 10** and **11,** respectively) show the relative positions of the six element types identified at the Bosque Site. As discussed in Chapter 2, these six elements were identified due to their apparently different genetic origin, as well as their different internal lithologies and geometries.

Gravel Element CH-1

The gravel element is dominated by light to dark grey poorly sorted coarse sand to gravel. Coarse gravel lag deposits and trough cross bedding structures are common at the base of this element type. The deposits often fine upward into horizontally laminated clean sands. Clay interbeds and clay rip-up clasts are rare in the gravel

See Next Page

Figure 9: Bosque Site Cross Section A-A'

A

NE

CROSS SECTION
N55E

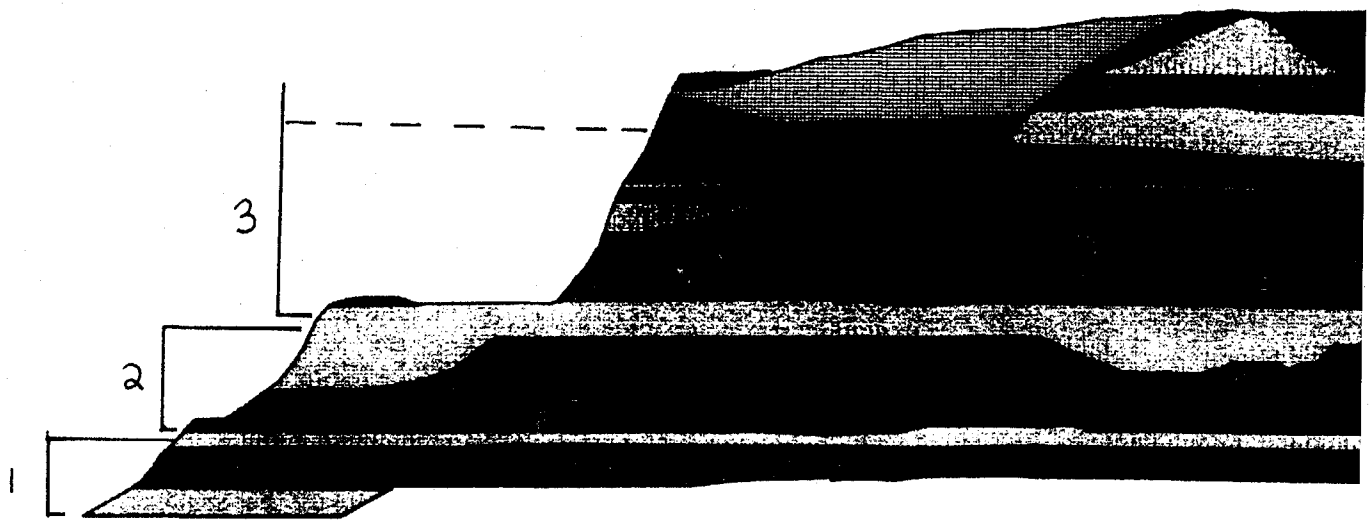

Sand Gravel Clay Paleosol

See Next Page

Figure 10: Bosque Site Cross Section B-B'

B

CROSS SECTION B
N35W

SE

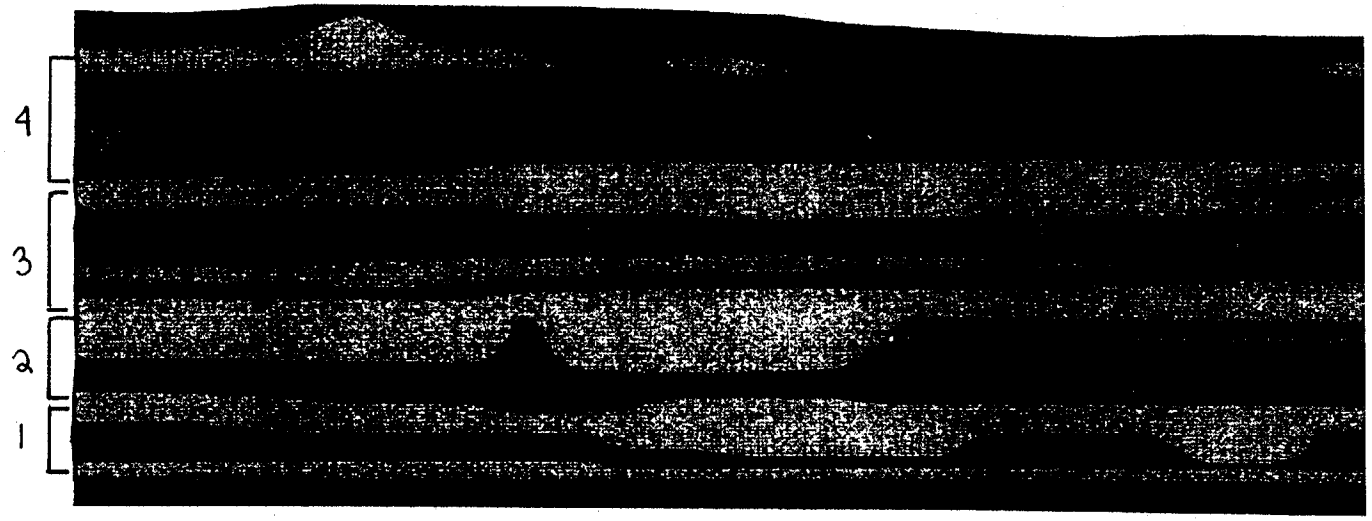

Sand Gravel Clay Paleosols

See Next Page

Figure 11: Bosque Site Cross Section C-C'

C

CROSS SECTION C–C'

SW

N70W

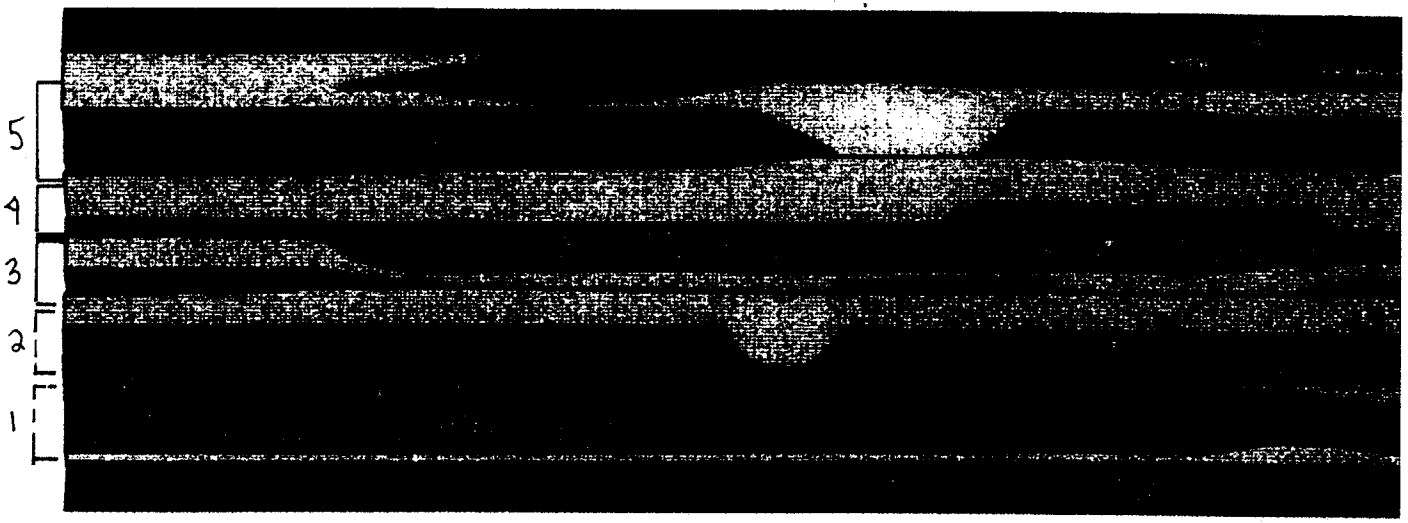

Sand Gravel Clay Paleosols

elements. As shown on the Architectural Element map, only two notable gravel elements are mapped at the site: one at the base of the mapped section, and the other at the top. The gravel element at the top of the section consists of generally coarser material, and is strongly cemented with calcite cement. The thickness of the two mapped gravel elements ranges across the field site from 2 to 6 meters. An intact obsidian cobble area was found in one of the two upper gravel elements. This cobble is believed to be derived from Mt. Taylor, which was last active 3 Ma (Lipman & Mehnert, 1980), and lies within the drainage basin of the Rio San Jose. Gravel elements become more common in the region above the mapped section and the top of the Llano de Albuquerque.

In order to infer the flow regime which prevailed during deposition of this element type, it is helpful to see what type of sedimentary structures develop under different conditions. This relationship between bedding type and flow regime conditions is illustrated in **Figure 12.** The flow regime of a depositional system is defined by its Froude number. Systems characterized by froude numbers less than one are dominated by lower energy conditions and are hence part of the lower flow regime. Systems characterized by Froude numbers greater than 1.0 are part of the upper flow regime (Davis, 1983). Figure 12 shows that for trough cross-bedding to form in coarse to very coarse sands, these sands must be flowing in the upper flow regime. Moreover, pebbles or cobbles larger than one inch are generally transported only in the upper flow regime (Harms and Fahnestock, 1965). Figure 12 suggests that the horizontally laminated coarse sands in the basal and middle portions of the gravel elements were deposited by upper flow regime conditions, as opposed to the horizontally fine to medium sands in the upper sections which may represent waning flow

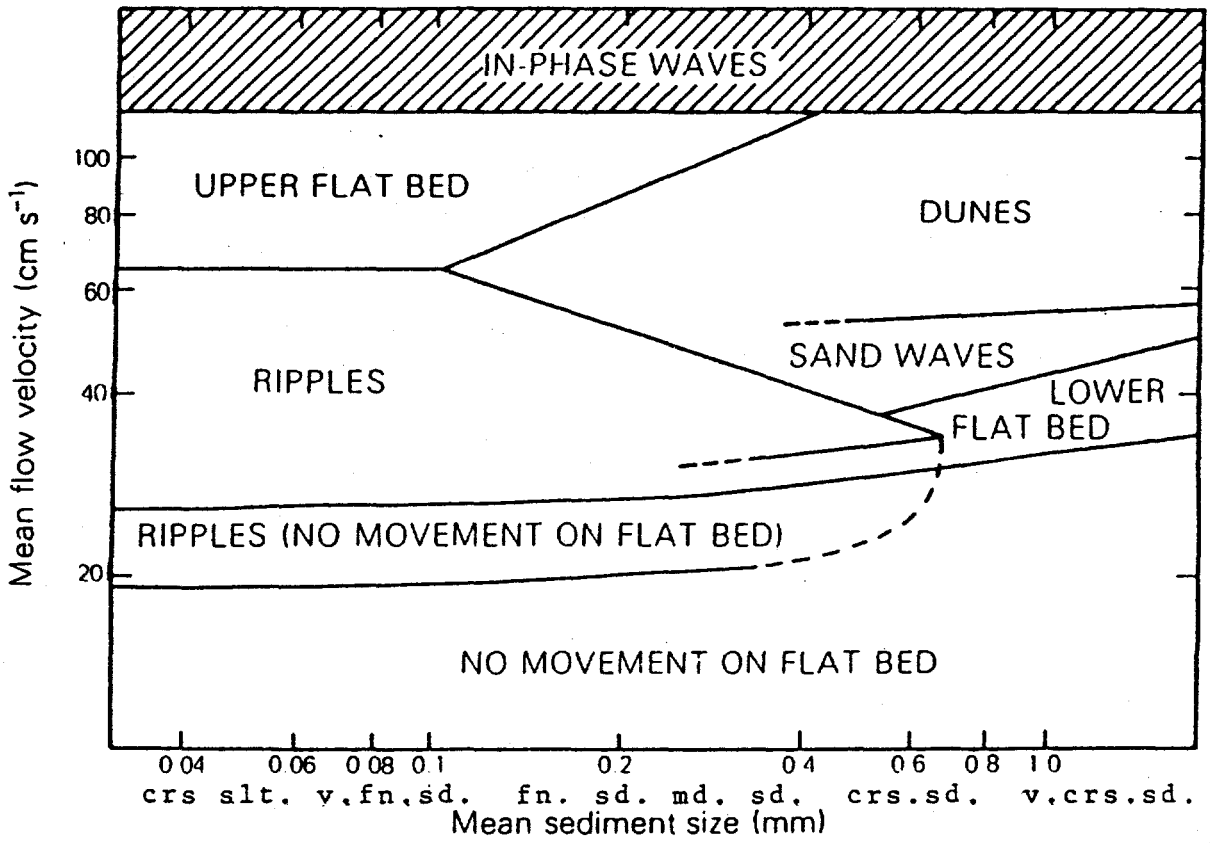

Figure 12: Relationship between different bedforms, flow velocity and grain size for a mean flow depth of 20 cm. (modified from Collinson and Thompson, 1982)

lower flow regime conditions. Therefore, the gravel element CH-1 mapped at the Bosque site appear to be axial deposits of a fast-moving competent river.

As discussed previously, a study of the provenance of these gravel elements was carried out by Harris (1991). The point count results for the samples from the Bosque site, the ancestral Rio Grande, the ancestral Rio Puerco and the ancestral Rio San Jose are plotted on a ternary diagram (**Figure 13**). **Table VI** summarizes the average quartz, feldspar and lithic fragment fraction of the four groups.

Table VI
Average Point Count Data

Source	Quartz [%]	Feldspar [%]	Lithic Fragment [%]
Rio Grande	43.91	26.01	29.93
Rio Puerco	54.32	21.82	29.71
Rio San Jose	65.58	10.84	23.48
Bosque Site	57.07	15.56	27.29

As Figure 13 and Table VI illustrate, the Bosque Site sediments bear similarity to all three river populations. This would suggest that the Bosque Site sediments received input from all three rivers, the Rio Grande, the Rio Puerco and its tributary the Rio San Jose. Three possibilities exist for such a scenario: 1) the confluence of the Rio Puerco and the Rio Grande was located to the north of the Bosque Site, and consequently, the Bosque Site sediments record only Rio Grande floodplain deposits; 2) the Rio Puerco was located to the west of the Bosque Site and the Rio Grande to the east (much like the modern-day configuration), and the Bosque Site sediments record deposition by both the Rio Grande and

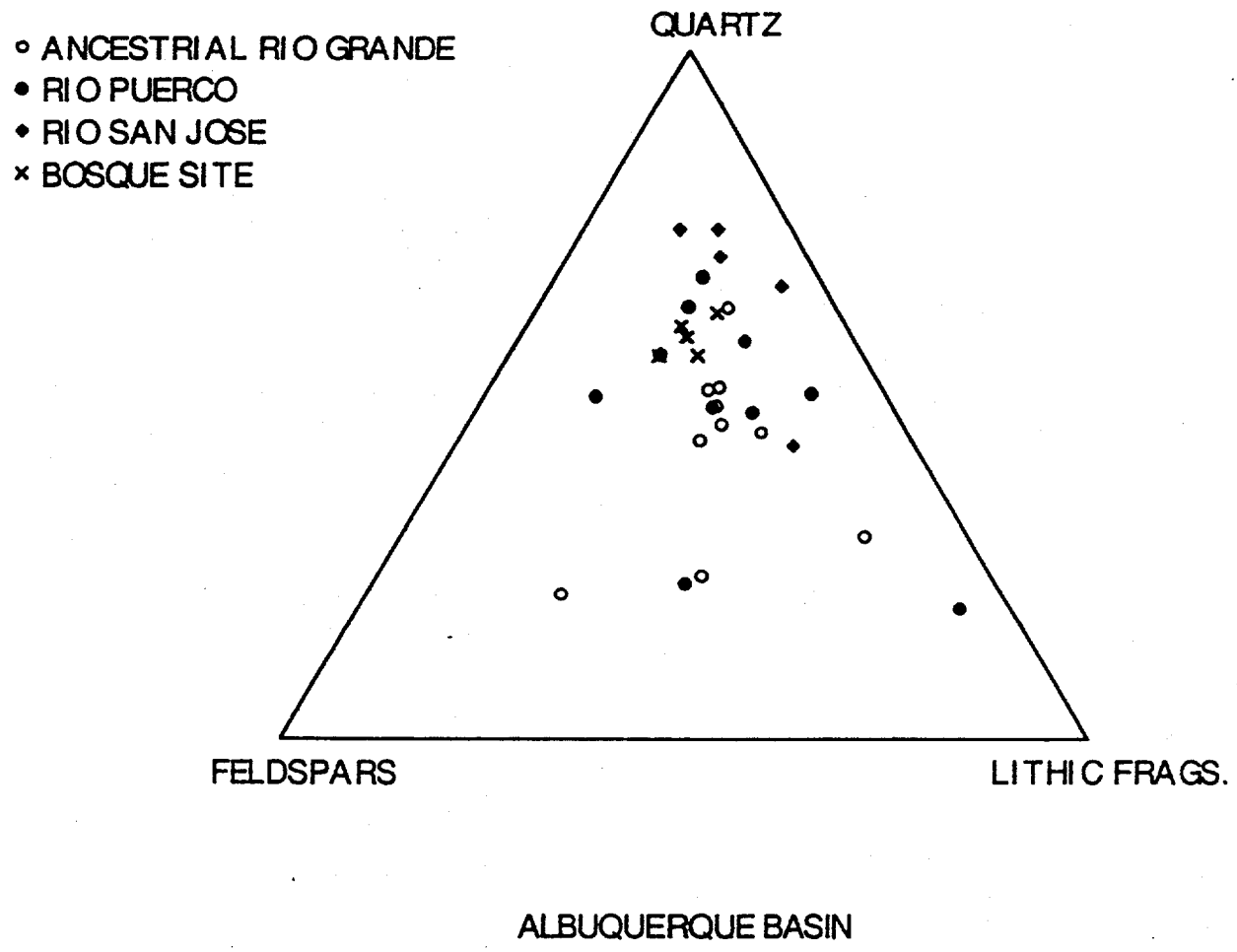

Figure 13: Ternary Diagram of point count analysis of Harris (1991)

the Rio Puerco; and 3) the confluence of the Rio Grande and the Rio Puerco was located to the south of the Bosque site, but both rivers were located to the east.

Distinguishing which of these three possibilities is most likely is difficult with the current data. However, the fact that several of the sand elements pinch out to the west, coupled with the mean sand scour orientation of N30W would suggest that the second scenario may be the most likely.

Sand Element CH-2

Tan to light gray, very fine to medium sand (1/16 mm to 1/2 mm in diameter) with locally abundant 0.5 cm to 1.5 cm thick clay drapes characterize this element. The sand deposits consist of moderately to well sorted, subangular to subrounded sand grains. Sand-sized clay clasts are commonly observed in these deposits. The base of elements of this type are horizontal to concave upwards, with little to no observable gravel lag. Armored mud balls are common at the base of these deposits, ranging from 2 to 60 cm in diameter. CH-2 elements are largely unconsolidated and range in thickness from 0.5 m to 9.0 m.

Common sedimentary structures within this element type include continuous and discontinuous horizontal laminated medium sands, foresets of incline planar cross bedding within fine to medium sands, ripple cross laminated fine to medium sands, and climbing ripple stratification in very fine to fine sands. Clay drapes interbedded with very fine sand and laminated clay and silt are common towards the top of these elements.

Figures 14 and **15** are photographs of two different CH-2 elements at the Bosque site. Figure 14 shows a typical vertical succession of sedimentary structures within CH-2

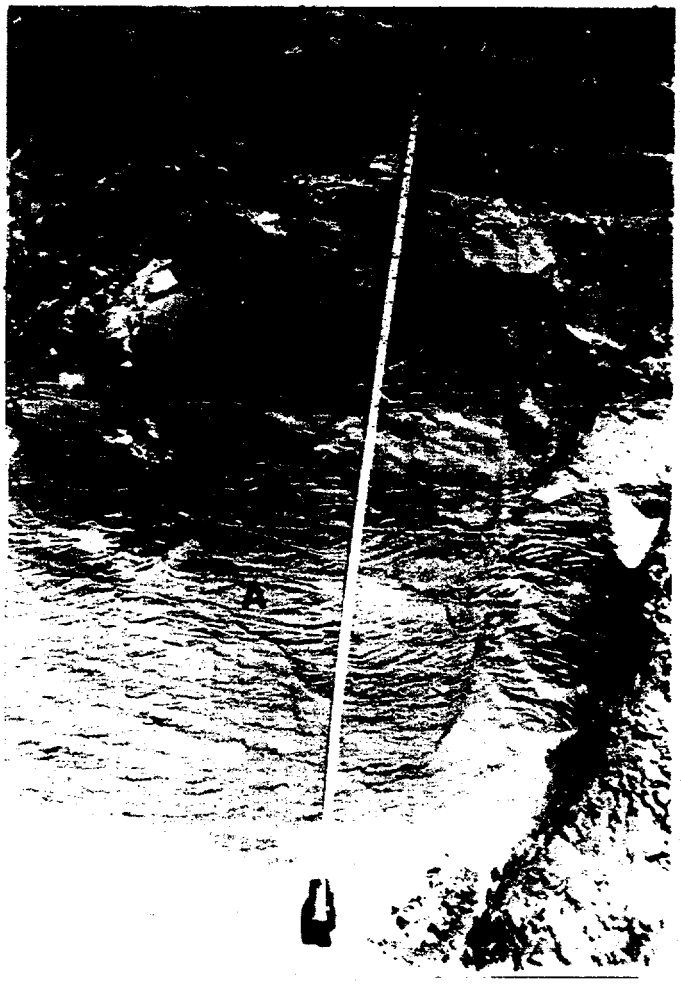

Figure 14: Photo #1 of vertical sequence within CH-2 element; see text for discussion of letters. The tape measure is extended 1 m. Outcrop is viewed from the south looking north.

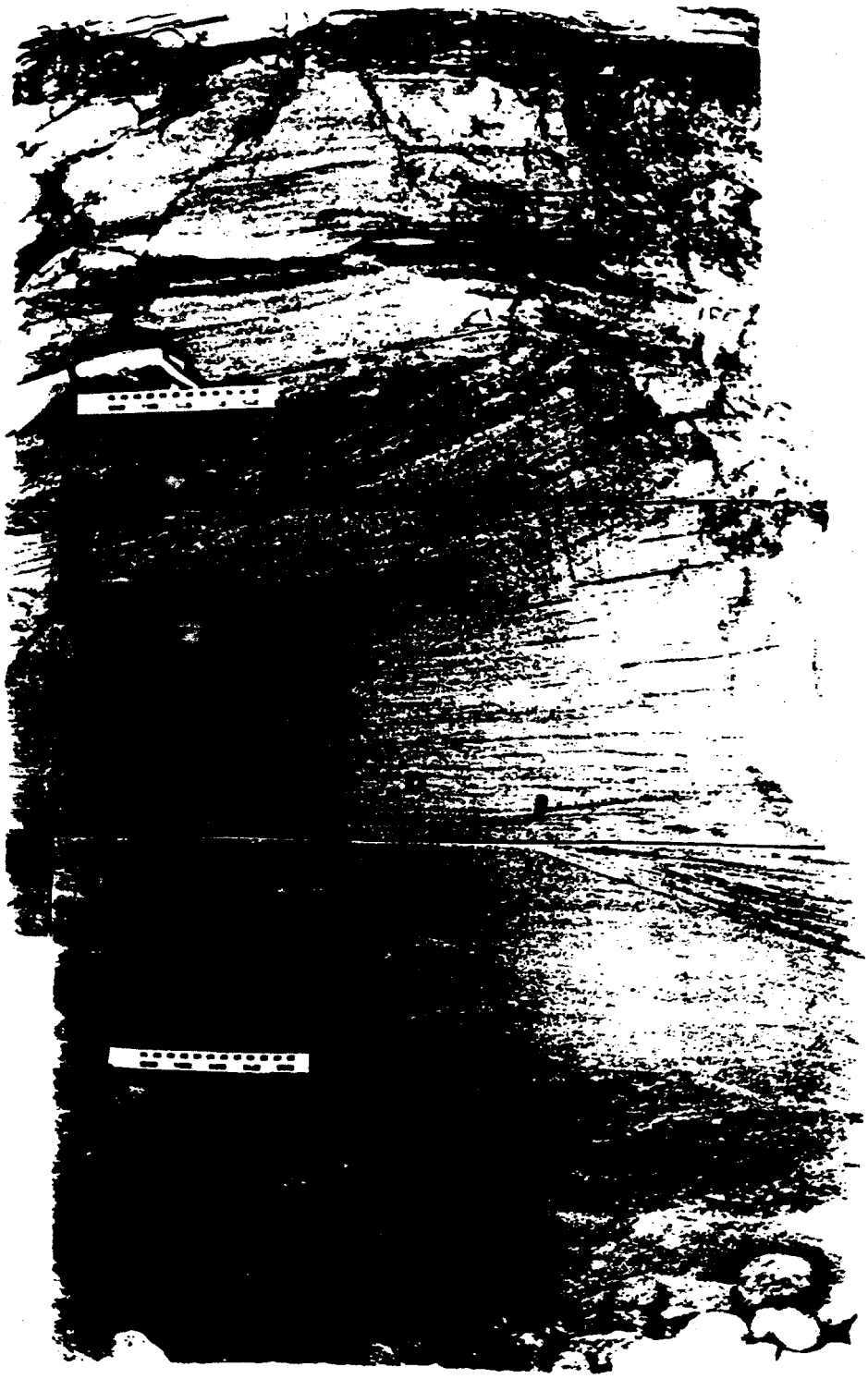

Figure 15: Photo #2 of vertical sequence within CH-2 element: see text for explanation of letters.

elements. The tape measure is located approximately 0.5 m above the base of the element. Letter A is located within a 0.5 m thick package of southwest dipping climbing ripple laminated fine sand. These climbing ripple sands are separated from the overlying horizontally laminated fine sands (B) by a nearly horizontal reactivation surface. The reactivation surface indicates that a second flow event with different flow conditions moved across the top of the land surface in this area, depositing a new package of sand. The top of this element is marked by a thick clay drape (C), indicating that flow subsided altogether, leaving ponded water on the land surface.

Figure 15 illustrates a vertical sequence viewed in another CH-2 element at the site. Numerous reactivation surfaces are present within this element, which suggests that this element is the product of multiple shallow flow events. The abundance and variable size of mudballs which are often present at the base of these elements is shown in this photo (A). The small-scale trough cross stratification (B) at the base is interpreted as the result of ripple migration in the lower part of the lower flow regime (Harms and Fahnestock, 1965). Ripple laminated fine to medium sands (C) are found higher in this element, with a pronounced reactivation surface underlying a lense of clay-clast rich sand (D). Finally, a thick clay drape is seen at the top of this element (E) which is typical for the CH-2 elements.

Several characteristics of the CH-2 elements suggest that with the exception of a few of the mapped CH-2 elements, these elements are primarily proximal flood plain sands. Firstly, the elements are largely non-erosive at their base as shown by the absence of gravel lag. Secondly, the vertical succession of sedimentary structures indicate that flow conditions

changed over time from initially either fast moving upper flow conditions or shallow lower flow regime conditions to more slowly moving waters as the flood waters waned. The horizontally laminated mediums sands which are common at the base of CH-2 elements are probably the result of either upper flow regime plane bed or lower flow regime plane bed conditions (Figure 12). The transition upwards into ripple laminated fine sands probably represent decreasing flow velocities.

The presence of abundant climbing ripple lamination is another good indicator of a floodplain environment. Climbing ripples are formed in environments where an abundance of sediment was being deposited from suspension in slowly moving waters (McKee, 1966). Such flow conditions occur during the waning phases of a large flood (McKee, 1967), and in natural levee environments adjacent to the axial channel. The abundance of clay drapes interbedded with fine sand and silt near the top of CH-2 elements mark the repeated cessation and reactivation of small flow events such as would be recorded on a fluvial floodplain. A final indicator that many of the CH-2 sands are actually flood plain sands is the fact that these elements commonly grade laterally into stacked clays and silts (OF element).

As mentioned above, there are areas at the field site where the CH-2 elements take on more of an axial channel character. These areas are shown on the cross sections by marked vertical scours of the yellow (CH-2) into the underlying elements, in places up to 5 meters deep. Scours of this size may be indicators of the presence of the actual axial channel or of large flood events which produced deep scouring adjacent to the axial channel on the floodplain. These deep scours are commonly infilled by multiple flow events as evidenced by the presence of several upward fining cycles, each of which is capped by a clay layer.

Clay-Silt Element OF

This element is composed of dark brown clay locally interbedded with tan silt and thin immature sand and clay paleosols. The most common sedimentary structure is parallel stratification between clay and silt. Interbeds of immature paleosols become especially common higher in the section. Lower in the section, this element is often a massive dark brown clay with red-brown sand filled polygonal cracks. Elements of this type are very common in the mapped section, and range from 1 to 7 meters thick.

Elements of this type are interpreted as representing the portions of the flood plain where the primary mode of sedimentation is from the slow settling of clay and silt-sized materials from suspension. This may be either the distal portion of the flood plain during the large flood events or relatively proximal portions of the flood plain during small flood events. The relative abundance, thickness, and lateral continuity of these clay-silt elements suggests that the alluvial plain on which the river(s) flowed may have been relatively wide and flat (Mack and Seager, 1990). A wide flat alluvial plain would cause individual flood events to easily overtop its banks, and spread a sheet of fine sand near the channel (McKee, 1967) and laterally continuous layers of clay and silt at more proximal distance from the channel.

Paleosol Elements Ps, Pc, and Pgs

Three different types of paleosol elements were identified at the Bosque Site Site: sandy paleosols Ps, clay paleosols Pc, and gravel-sand paleosols Pgs. The paleosols at the Bosque site were identifed on the basis of their pedogenic characteristics.

In arid to semiarid climates, calcium carbonate tends to accumulate in the C horizon due to high rates of evapotranspiration, shallow depths of leaching and the input of airborne calcium ions. The $CaC0_3$ builds up at depths where lower $C0_2$ pressures and a rise in pH favor the precipitation of $CaC0_3$ (Birkeland, 1984). The longer a soil is exposed at the land surface (before it is either buried or eroded), the stronger the $CaC0_3$ development will be. McGrath and Hawley (1987) have developed a five-stage classification scheme for arid soils based on the degree of $CaC0_3$ accumulation of the soil. A stage I soil exhibits the weakest degree of $CaC0_3$ accumulation, with $CaC0_3$ being present only as thin discontinous coating on clasts or ped surfaces. On the other hand, a stage V soil is nearly completely indurated with $CaC0_3$. The calcic soil which tops the Llano de Albuquerque would be classified as a stage IV soil. The equivalent soil in the Hatch-Rincon Valley exhibits a greater degree of $CaC0_3$ accumulation, and is therefore classsified as a Stage V soil.

Paleosols are also recognized in outcrop on the basis of the near absence of sedimentary structures. The physical and chemical processes which make up pedogenesis effectively destroy the original sedimentary structure within the parent material.

The strong orange color was another quality which allowed identification of the paleosols at the Bosque site. Desert soils commonly exhibit a strong red to orange color (hues 2.5 YR and 5 YR). According to Gile et al (1981), "hues of the Bt horizon become redder and chromas higher with increasing age." The source of the red color in desert soils is the conversion of ferrihydrite to hematite (Walker, 1967; Torrent et al, 1980).

The presence of eluviated clays in the soil matrix is another pedogenic feature used to identify paleosols in an alluvial sequence. The clays are moved downwards in the soil zone

by mechanical and chemical processes collectively known as eluviation (Scholle, 1979). In immature soils, the clay is seen as coatings on the individual grains. In more mature soils, a clay matrix develops around the grains.

Sand Paleosol Element Ps

This Ps element exhibits an orange-red soil color of 5 YR 6/5 to 5YR 6/6 (Munsell Soil Color Chart) and is composed of moderately to well-sorted, very fine to fine sand. The sand grains are subangular to rounded, depending on the sampling location. Few if any sedimentary structures remain in the upper 2/3 of these elements, although weak horizontal stratification is visible in the lower third in some of these paleosols. Many of these sand paleosols exhibit a marked zone of white $CaC0_3$ accumulation. The most mature of the sand paleosols at the site would be classified as a stage I by McGrath and Hawley (1987).

Ps elements range in thickness from 0.5 m to 3 m, the thickest of which are characterized by weak sedimentary structures and textures in the lower one-third of the elements. The geometry of these elements is generally tabular, although in some places they take on a distinctly lense-like character, thinning from over 3 meters to only 0.3 meters in the span of only 3 m horizontally (see Cross Sections B-B' and C-C').

This element is interpreted as a combination of fluvial and eolian sands which were left exposed on the floodplain, free of sedimentation for thousands of years. The tabular elements are commonly composed of well-sorted, well-rounded quartz grains, indicating a possible eolian origin. The more lense-shaped Ps elements may represent fluvial sands abandoned by the channel which received an eolian sand influx at the surface as pedogenesis

progressed.

Clay Paleosol Element Pc

The clay paleosol element is a red-brown (2.5 YR, 4/6) paleosol consisting of clay and sandy clay. This element was differentiated from the clay-silt (OF) element of on the basis of its red-brown color, its lack of original sedimentary structures, and its blocky texture. Only one notable element of this type was mapped at the Bosque site (purple on the Architectural Element Map and cross sections). The thickness of this element is variable, ranging from 0.3 meters to 1.5 meters. It grades into a clay-silt element in the southwestern portion of the field site (see Cross section C-C'). In actuality, thin clay paleosol layers (1-3 cm) exist within some of the clay-silt elements, but they were lumped into the OF element for the sake of simplicity.

This clay paleosol is interpreted as a floodplain mud which was left deprived of sediment for an extended period of time, probably due to the rapid movement of the fluvial channel away from the floodplain. The fact that this element grades into an OF element to the southwest suggests that the fluvial channel may have been located further to the southwest at this time.

Gravel-Sand Paleosol Pgs

Only one element of this type was mapped at the Bosque Site. It is red/pink in color (2.5 YR, 6/6), and is composed of pebble and cobble-sized fragments in a matrix of sandy material. Preliminary analysis of this element in thin section shows that the grains in the

matrix are very fine to fine sand, and are very angular. The thin sections show that many of the grains are coated with clay, which is evidence of eluviation in the soil profile. No original sedimentary structures remain in this largely calcite-cemented deposit.

Cross Sections A-A' and B-B' illustrate the interesting geometry of this element. The element is thickest along a nearly east-west axis (up to 3.5 m), and thins rapidly to the north. A lack of outcrop to the north prevented a complete definition of the geometry of this deposit. The chaotic appearance of this matrix-supported deposit suggests that these sediments may been the product of gradual infilling of a deep depression. The coarse gravel underlying the Pgs element suggests that this depression was a scour that developed rapidly, probably as a result of some kind of flood event. After the flood event, sedimentation within this depression may have taken the form of occasion fluvial deposition, eolian input, and slumping of the surrounding sediments into the oversteepened banks. As long as these modes of sedimentation were intermittent, pedogenesis could have worked on these deposits, producing the chaotic deposit seen in outcrop today.

4.2 Overall Architecture of Elements

The unique three-dimensional exposure offered by the Bosque site allows two different ways of evaluating the overall architecture of the sediments: 1) vertical sequences sequence analysis of the two-dimensional cross sections; and 2) analysis of overall element geometries on the three-dimensional architectural element maps.

Several sedimentary cycles are delineated on the cross sections of the Bosque site (Figures 9, 10 and 11). A sedimentary cycle is here used to describe the vertical sequence

of sediments deposited by a river as it moves away from and returns to its original position. As discussed above, the sand elements (CH-2) mark the nearby presence of a river channel. Clay and silt elements (OF) signify that the river has moved some distance away, leaving fine-grained flood plain deposits in its wake. The paleosols (Ps, Pc and Pgs) are indicative of a region deprived of sediment influx, and therefore suggest that the river channel is at a large distance from the area.

Different types of sedimentary cycles can yield information about the types of river movement which occurred in the vicinity of the Bosque Site during the time of deposition. A river channel that moved gradually away from and then returned to its original position will tend to produce a vertical sequence elements as follows: CH-OF-P-OF-CH, where CH can be either a sand element (CH-2) or a gravel element (CH-1), and P can be a paleosol of any parent material. On the other hand, if a river moved gradually away but returned abruptly, the resulting vertical sedimentary sequence would tend to be CH-OF-P-CH. Finally, a channel that moved abruptly away and returned abruptly to its original location will deposit the simple vertical element sequence of CH-P-CH.

On Cross section A-A', the lowermost sedimentary cycle records the gradual departure and return of the river from its original location. The second cycle shows nearly the same pattern except that on the northeast side, the uppermost clay element is missing. The third cycle is more complicated, showing that the river remained at some distance from the site for a long period of time, and then returned abruptly. This is shown by the thick stack of clay and soil elements with a sand element directly on top of them. This cycle is interrupted on the northeast side of the cross section by a CH-1/Pgs sequence. The third

cycle is further complicated by the fact that some of the sand elements pinch out to the west. This suggests that the fluvial system associated with these sands may have been situated to the east (assuming south and/or southwest flow).

The sedimentary cycles delineated on cross section B-B' are similar to those on A-A' with the exception that scours in the sand element are more visible from this angle, especially in the lower half of the section. An interesting feature to notice on section B-B' is the abrupt thickening of the Ps element located at an elevation of around 5030 feet.

Cross section C-C' again illustrates that some of the sand elements pinch out to the west, as seen in cycle 1 in the lower northeast portion of the section. Cross section C-C' differs slightly from the other two sections in that more pronounced scours within the sand elements are visible from the angle, especially at the higher elevations. The effect of these scours on this side of the outcrop is to produce a stacking of sand elements at several locations across the hillside. The gradation of the clay paleosol element into a clay-silt element is seen within the fourth sedimentary cycle on this cross section.

Analysis of the three-dimensional geometry of the elements was accomplished by correlating the sand scours across the field site on the Architectural Element Map (Plate 1). **Figure 16** summarizes the correlated sand scour directions across the Bosque Site. As shown, the orientation of the correlated scours ranges from N10E to N70W, with a weighted average flow direction of N30W. This suggests that the primary axis of deposition in this system was approximately N30W.

Analysis of the Architectural Element Map also shows that, on average, the sand

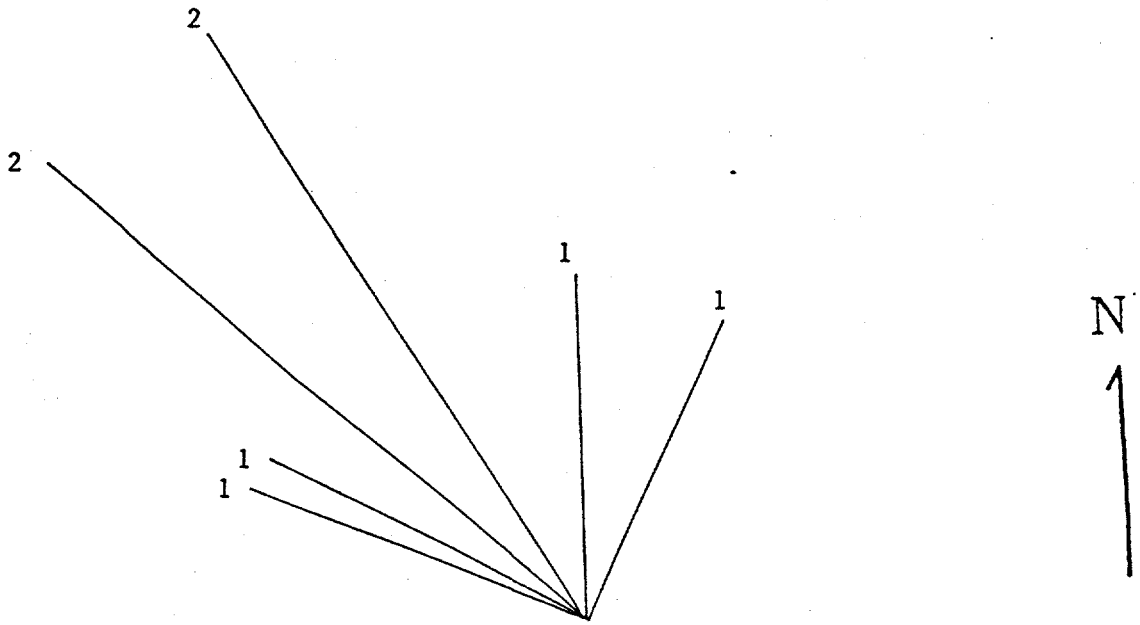

Figure 16: Summary of orientations of sand element (Ch-2) and gravel element (CH-1) scours correlated across the Bosque Site. The numbers at top of each line refer to the number of scours correlated with this orientation.

elements pinch out in a westerly direction. While more information is required before any firm conclusions can be drawn, this preliminary analyis would suggest that the axis of the channel which deposited these sands lay to the east of the Bosque Site. In general, the abundance of laterally continuous sands with occasional scours suggests that during large flood events, the flood waters overtopped the banks, and moved across the floodplain in sheetlike flow in some areas, and in channelized flow in others. As discussed above, not all the sand elements at the site are necessarily floodplain deposits, as some of the deeper scours may represent axial river deposits.

4.3 Allocyclic and Autocyclic Controls on Deposition

While the gross depositional environment of the upper Sierra Ladrones Formation is relatively well understood, the details of the allocyclic and autocyclic controls on deposition in the vicinity of the site are unknown. **Figure 17** shows the components of autocyclic and allocyclic depositional controls. Autocyclic controls on river movement are the result of changes in energy within the sedimentary basin, and result in channel avulsion, crevassing and channel migration and cut-off. Allocyclic controls, on the other hand, originate in energy changes outside the sedimentary basin such as shifts in the climatic and tectonic regimes. Changes in the allocyclic controls of deposition result in overall changes in the discharge, load and slope of the river, which in turn can produce the above-referenced channel avulsion, crevassing and migration and cut-off.

Inference of the autocyclic and allocyclic controls which prevailed during deposition in the vicinity of the Bosque site is achieved by comparing the sedimentary geometries observed at the site to the geometries predicted by alluvial models of J.R.L. Allen (1974) and

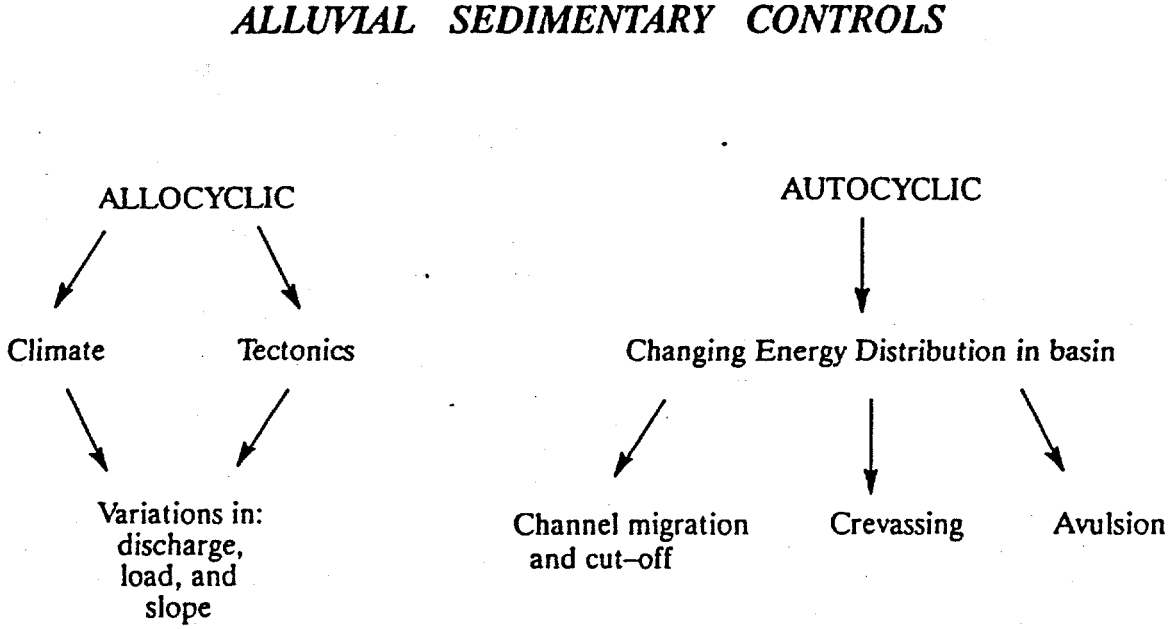

Figure 17: Autocyclic and Allocyclic Controls on Deposition

M.J. Kraus and T.M. Bown (1987).

Allen (1974) developed six conceptual models of alluvial architecture containing paleosols and associated fluvial and alluvial deposits in an effort to determine the alluvial sedimentary controls responsible for deposition of the Lower Old Red Sandstone (LORSS). The six models conceptually evaluate how autocyclic and allocyclic controls on river movement affect the patterns of sedimentation at the scale of tens of kilometers horizontally, and tens of meters vertically.

The first of the six models is controlled by purely allocyclic controls, namely extreme climatic fluctuations. The second, third and fourth models are purely autocyclic models, which differ only by the dominant pattern of river movement. The fifth and sixth models are controlled by both autocyclic and allocyclic controls.

The element geometries at the Bosque Site most closely resemble Allen's third and fourth models. Allen's two models are shown in **Figure 18.** The upper model illustrates the deposits which result from a single river avulsing in small lateral steps across an alluvial plain. A vertical section through this model yields a vertical sedimentary cycles of CH-OF-P-OF-CH. The controls on this type of river movement are purely autocyclic. The lower model in Figure 18 illustrates the deposits which would result from a single river moving in large avulsive steps across an alluvial plain. Vertical sections through this model are often truncated due to large avulsive steps of the river, yielding sedimentary cycles of CH-OF-P-CH and CH-P-OF-CH.

The similarity between the sedimentary cycles marked on the cross sections of the Bosque Site and the sedimentary cycles in these two models is the basis for comparison

River Avulsions

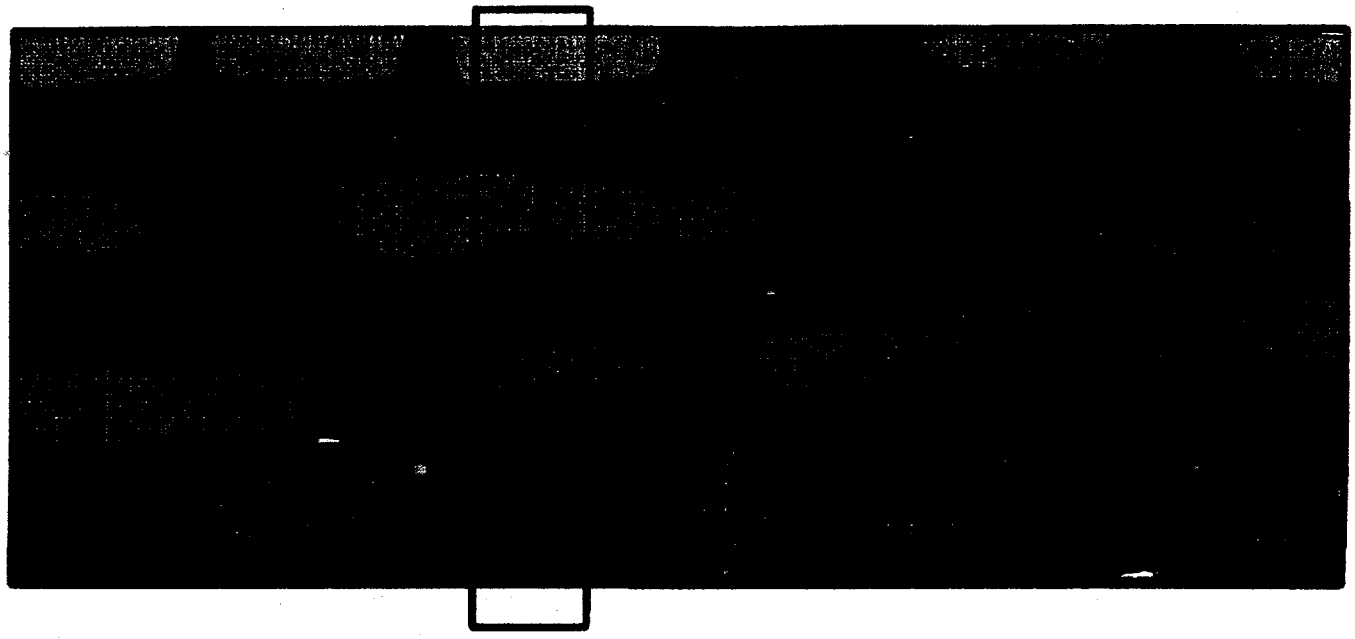

Large-Scale River Avulsions

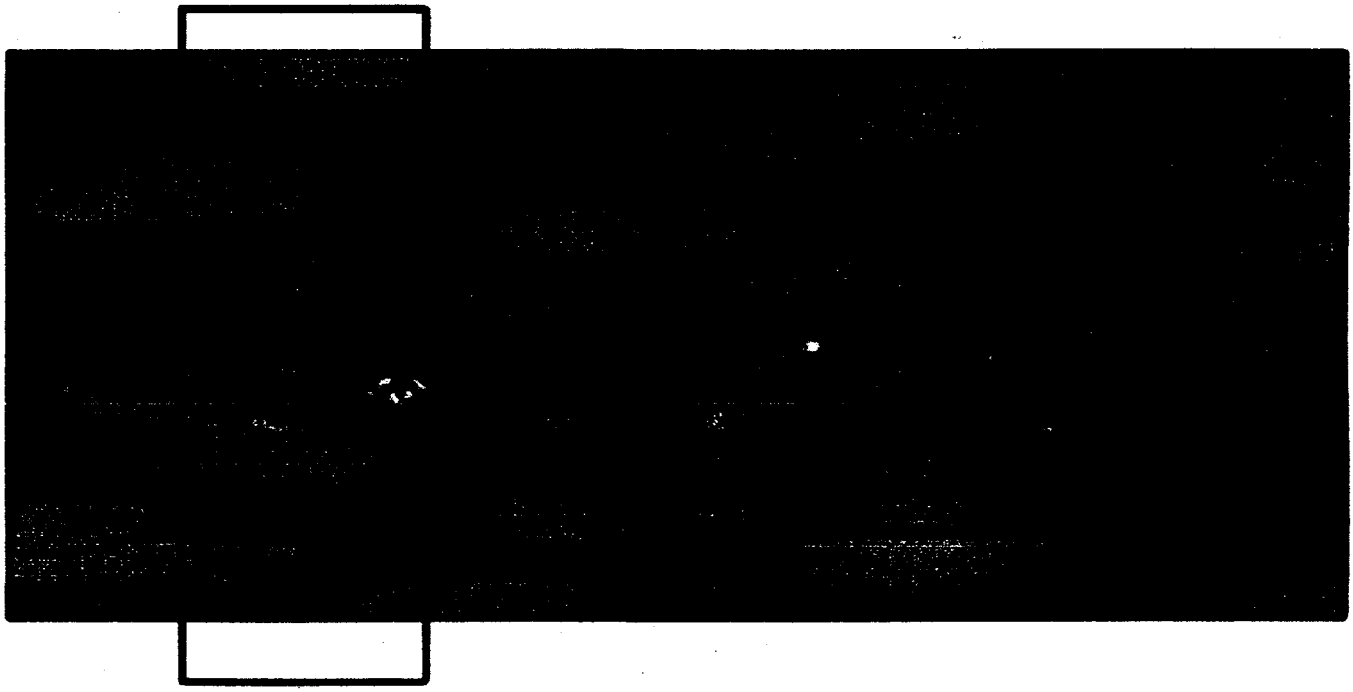

Floodplain Deposits (mudstones)

Channel Sandstones

Pedogenic Carbonate Units

Approximate Scale of Site Cross Sections

between the two models in Figure 18 and the element geometries at the Bosque Site. This similarity suggests that the autocyclic controls on deposition in the vicinity of the Bosque site were river(s) moving across a wide alluvial plain in small and large avulsive steps.

The paleosol model of Kraus and Bown (1987) is founded on a concept they call "pedofacies." Pedofacies are defined as "laterally contiguous bodies of sedimentary rock that differ in their contained laterally continuous paleosols as a result of their distance (during formation) from areas of relatively high sediment accumulation" (Kraus and Bown, 1987). In this model, the area of high sediment accumulation is the channel belt. **Figure 19** illustrates the five pedofacies stages. In essence, the sand content decreases and the degree of pedogenesis increases in the pedofacies with increasing distance from the channel.

Kraus (1987) defines vertical sections of alluvial sequences which contain these different pedofacies as compound pedofacies sequences. According to the model, observation of these sequences and overall trends within these sequences can yield information about the autocyclic and allocyclic controls on deposition. Packages of compound pedofacies sequences are referred to as pedofacies megasequences. Pedofacies megasequences allow inference of the larger scale allocyclic controls on deposition. In essence, Bown and Kraus argue that an overall change in the maturity of paleosols within an alluvial section yield information about the sedimentation rate and correspondingly, the allocyclic controls on deposition such as tectonics and climate.

The sedimentary cycles delineated on the cross sections of the Bosque Site can be interpreted as compound pedofacies sequences. Taken together, they can be viewed as a portion of what Kraus and Bown call a pedofacies megasequence. In general, the maturity of

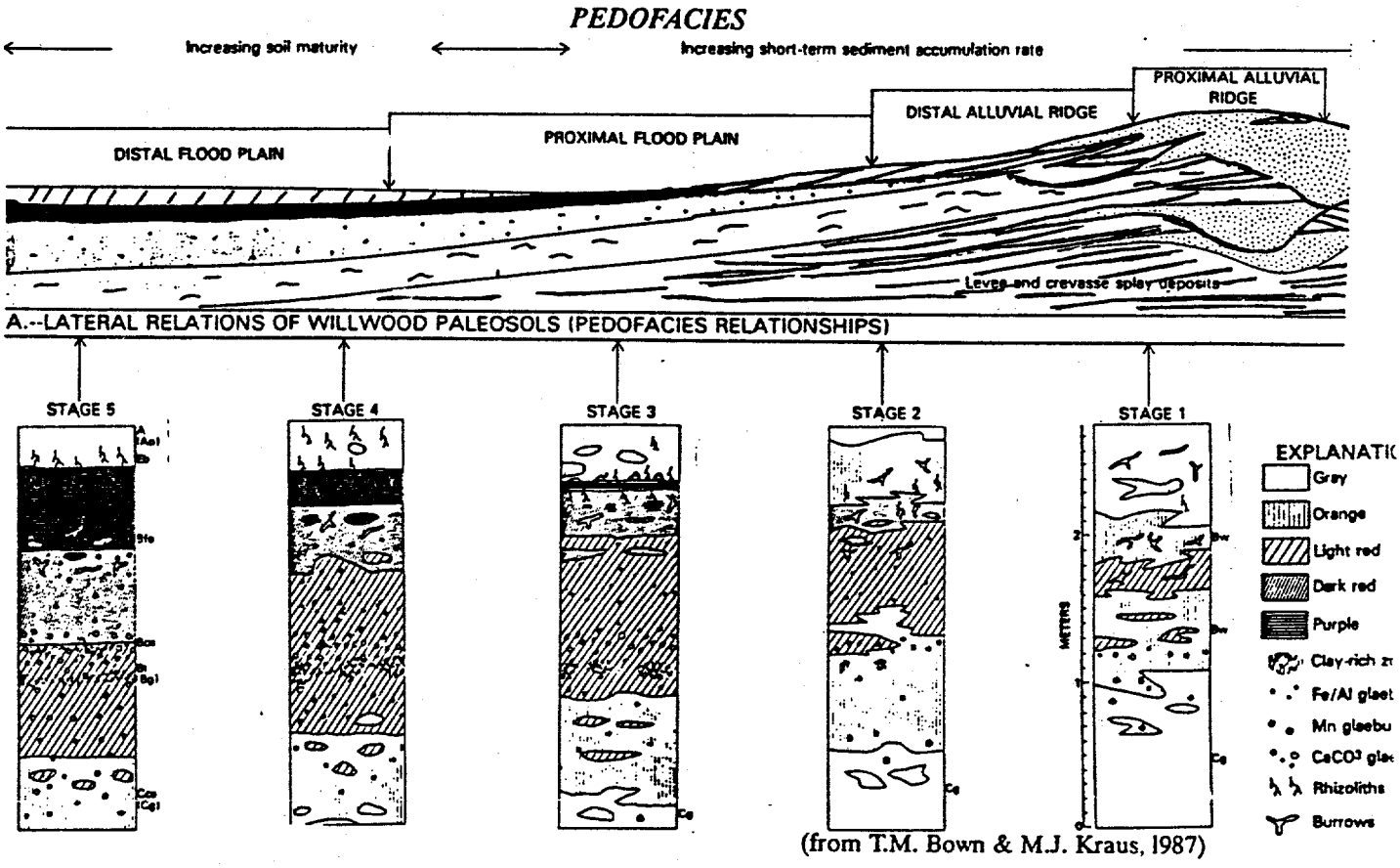

Figure 19: Five pedofacies stages as defined by Kraus and Bown (1987).

the paleosols at the Bosque Site decreases upwards in the section. The most mature and thickest paleosol is found in the midsection of the outcrop. This paleosol, shown as the three meter thick paleosol element in the middle of the outcrop, exhibits a strong orange color and a pronounced white-colored zone of calcium carbonate accumulation. The least mature paleosols are found within the thick clay-silt sequences (OF) near the top of the section. Paleosols and clay/silt elements are almost totally absent above the mapped section, with coarse sands and gravels being the predominant facies.

Invoking Bown and Kraus's concept of pedofacies megasequences, this overall upwards decrease in pedofacies maturity suggests that sedimentation rates were increasing with time. One possible reason for this apparent increase in sedimentation rate is the onset of a wetter climate. The abundance of gravels higher in the section also supports this as they suggest a significant increase in river competence. A second possible reason for the absence of paleosols higher in the section is that basin subsidence, which may have been relatively rapid during deposition of the lower and middle portions of the section, slowed during deposition of the upper units. Such a slowing of subsidence would result in very little net aggradation, with river deposits reworking the soils and overbank deposits.

CHAPTER 5: GEOSTATISTICAL ANALYSES AND INTERPRETATION

This chapter presents the results of the geostatistical analyses of the architectural element map and the cross sections. As discussed in Chapter 2, a total of five data sets were prepared for variogram analysis: a small 3-dimensional data set (1454 points) of the Architectural Element Map (AEM) consisting of samples separated by 10-20 meters in the horizontal direction and 1-2 meters in the vertical direction; a large 3-dimensional data set (54,402 points) made by sampling the AEM every meter in the horizontal direction, and approximately every 0.2 m in the vertical direction; and finally, three 2-dimensional data sets of the geologic cross sections sampled every 1.5 m in the horizontal direction, and every 0.3 m in the vertical direction. Analysis of these five data sets sheds light on the correlation structure of the deposits at the Bosque Site, as well as on the relationship between sampling density and the estimated spatial correlation structure.

5.1 Architectural Element Map Analyses

Table VII illustrates the relative percentages of the four log (k) groupings as well as the mean and variance for the large and the small AEM data sets.

Table VII
Distribution Statistics of Small and Large AEM Data Sets

Data Set	OF & Pc	Ps & Pgs	CH-2	CH-1	Mean log (k)	Variance
Large AEM	35.9%	6.81%	55.71%	1.58%	-1.59	10.12
Small AEM	34.14	18.4%	38.34%	9.11%	-1.72	10.29

As shown, the two data sets contain roughly the same percentage of clay elements (OF and Pc),

but the large data set has a larger relative amount of sand (CH-2), and a smaller relative amount of soils and gravels.

The two horizontal variograms estimated for the small AEM data set are shown in **Figure 20.** The variogram estimated in the N30W direction is linear, rising with a slope of .004 from a nugget of 1.4. The variogram estimated in the N60E direction is also linear with a nugget of 0.85, but appears to reach a sill at a lag separation distance of about 150 m.

Isaaks and Srivasta (1990) define a linear variogram as one that increases linearly with the lag separation distance. Burroughs (1983) investigates the causes of such a linear variogram model. According to Burroughs (1983), a random variable Z(x) can be decomposed into the weighted sum of a series of random functions (RFs), where each RF takes on a constant value over a given range r. In the case of soils, these RFs are the spatial processes which affect soil formation such as worm activity, geological formation, topographic relief, localized climate, etc. In the case of geologic deposits, these RFs represent the average dimensions of the lithologic units. Burroughs' (1983) nested model is expressed as follows:

$$Z(x) = B_0 RF_0 + B_1 RF_1 + ... B_q RF_q$$

In this model, the effects of each RF are nested within the range of the next, producing a linear variogram. Burroughs refers to small-scale spatial variability of Z(x) as short-range RFs, and large-scale spatial variability as long-range RFs. Burroughs shows that a large nugget effect in a variogram may simply denote that the sampling interval is larger than the short-range RF scale. Likewise, a horizontal sill will only be attained if the sampling interval is large enough to capture the scale of the long-range RFs.

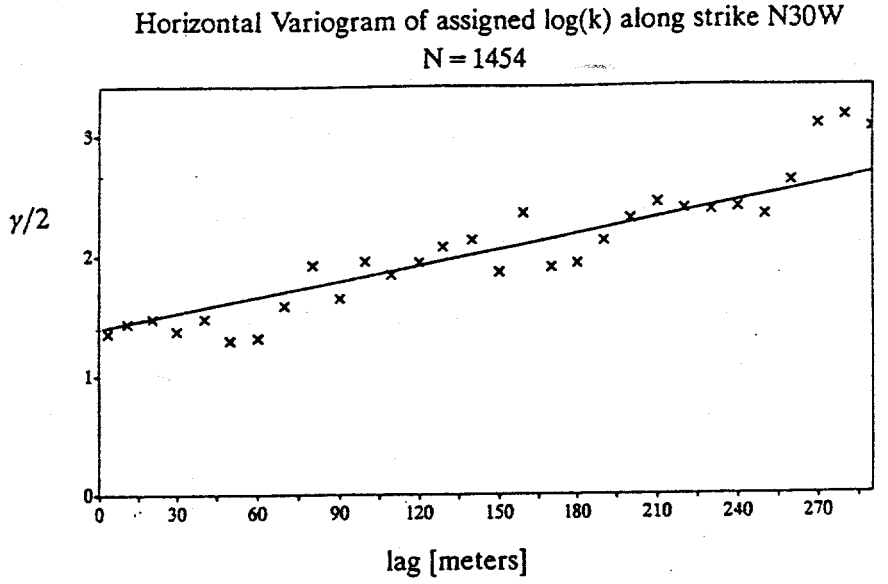

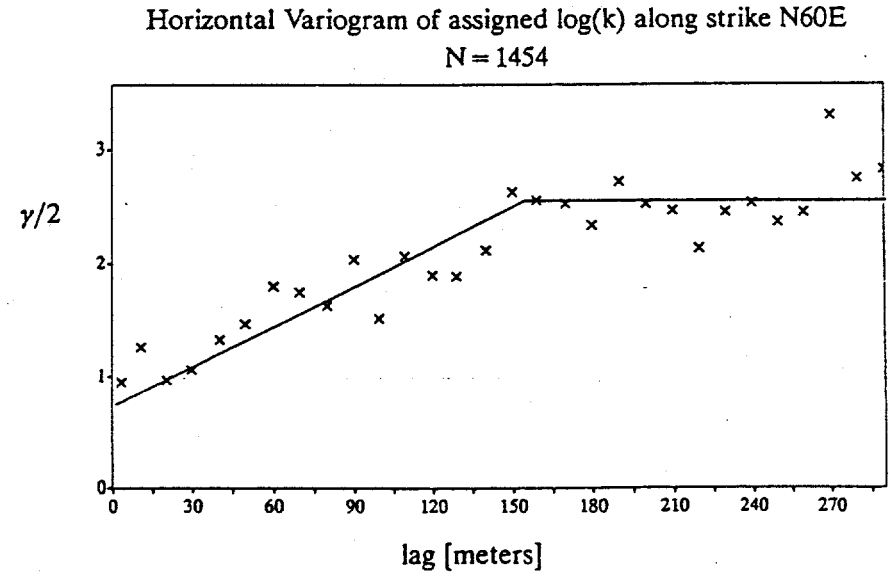

Figure 20: Variograms estimated in the horizontal directions N30W and N60E for the small AEM data set.

Utilizing the nested model of Burroughs (1983), the single slope line shown in the N30W variogram suggests that the 400 m sampling range represents a larger scale of variability in this direction than the mapped region. Since the data consists of assigned values without measurement error, the large nugget seen in this variogram suggests that variability may exist at scales smaller than the 10-20 m sampling interval of this data set.

In the N60E variogram, the maximum variance is achieved at a lag separation distance of 150 m. The presence of a nugget in this direction is another indicator that variability may exist at scales smaller than the smallest lag (5 m). Another reason that the variance is high for small lag spacings in this small AEM data set is that the only vertical sections located close to one another were deliberately placed there in order to sample scours. Hence, the short lag spacings in the small AEM data set are biased towards higher variability.

The larger AEM data set was created in order to more accurately assess the smaller scale variability at the Bosque Site. The two horizontal variograms and the vertical variogram estimated for the large data set are shown in **Figure 21**. As shown, the horizontal variogram estimated parallel to the inferred paleoflow direction (N30W) exhibits a nested exponential/linear behavior. The variogram appears exponential with a range of approximately 20 m for lags up to 40 m. For lag separations larger than 40 m, the variogram is approximately linear rising with a slope of approximately 0.001. The source of the small-scale correlation range of 20 m is uncertain, but appears to correspond with the average scour width seen on all three cross sections. The fact that the small AEM N30W variogram exhibits a nugget for small lags shows that the sample spacing of the small data set was too large to capture this small-scale exponential behavior. The linear behavior of the N30W variogram for large lags suggests that when

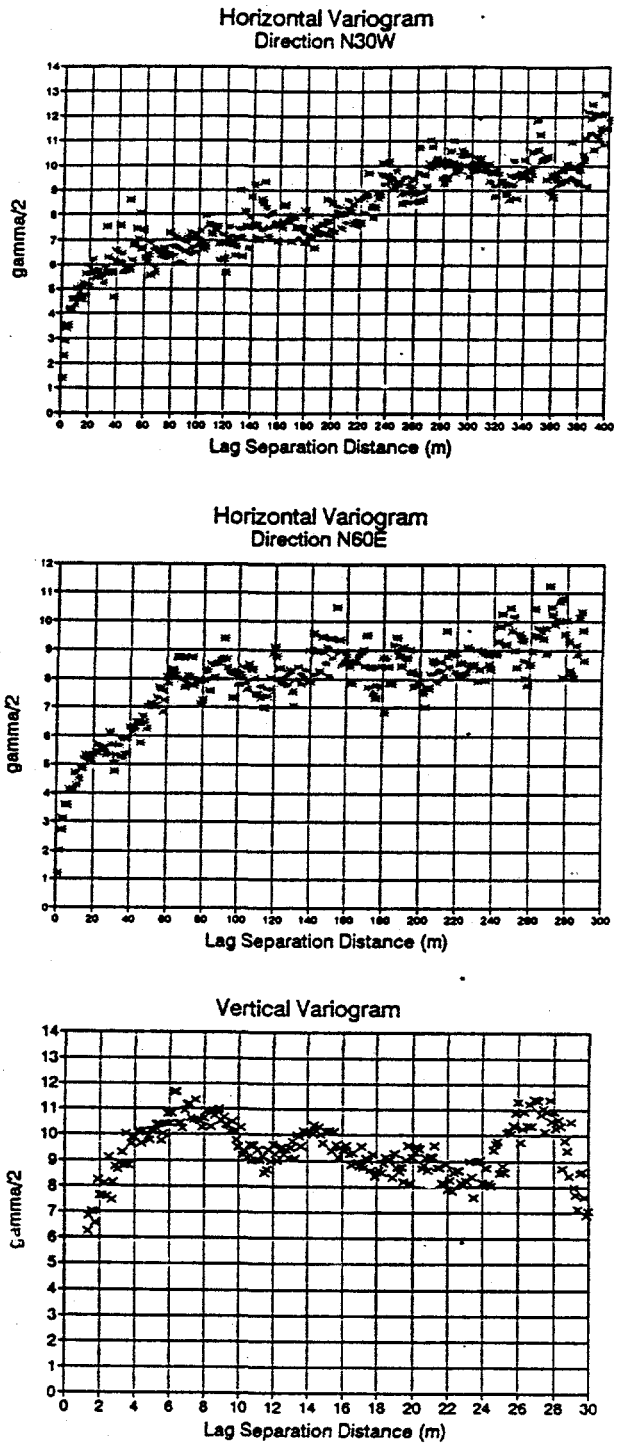

Figure 21: Horizontal and Vertical Variograms estimated for large AEM data set.

sampled parallel to the paleoflow direction, the maximum scale of variability is not attained for the largest sample spacings. This is consistent with the fact that the average dimension of the elements exceeds 300 m when sampled along the N30W orientation.

The horizontal variogram of the large data set estimated perpendicular to the inferred paleoflow direction (N60E--Figure 21) displays a nested exponential behavior. The small-scale exponential reaches a sill at approximately 20 m, and the larger scale exponential reaches a sill at approximately 75 m. It is believed that the 20 m correlation length again corresponds to the average scour dimension across the Bosque Site. The maximum scale of variability is attained at a leg separation distance of 75 m. The exact cause of this 75 m correlation length is again difficult to ascertain, but it appears to correspond to an average dimension of the elements when sampled along the N60E direction. Examination of Cross section A-A' (Figure 9) which is orientated N55E shows that several of the elements are in fact approximately 75 m long. However, it must be remembered that the large AEM N60E variogram represents sampling along many transects orientated in this direction, not just one, and is therefore displaying the average behavior of all such transects. Direct comparison to the small AEM N60E variogram is difficult due to different log (k) assignments. However, both the large and the small AEM N60E variograms do exhibit a finite correlation range as evidenced by the fact that they both reach a sill.

The vertical variogram for the large AEM data is strongly periodic as one would expect for a discrete layered system. A pronounced hole effect is evident at a lag separation of 11 m. This distance is interpreted as the average vertical repeatability of elements across the Bosque Site.

5.2 Geologic Cross Section Analyses

Analysis of the variograms estimated of the cross section data sets provides insight into the correlation ranges observed in the AEM variograms. **Table VIII** illustrates the relative percentages of the four log (k) groupings as well as the mean and variance for the three cross section data sets.

Table VIII
Distribution Statistics of Geologic Cross Section Data Sets

Data Set	OF/Pc	Ps/Pgs	CH-2	CH-1	Mean log (k)	Variance
A-A'	39.54%	19.22%	31.58%	9.64%	-1.95	10.76
B-B'	33.52%	14.95%	40.29%	11.22%	-1.53	10.13
C-C'	21.18%	20.82%	39.18%	18.81%	-0.68	7.68

Table VIII shows that the sample populations of the data sets from cross sections A-A' and B-B' are quite similar, but that the data set of cross section C-C' exhibits a higher mean and lower variance. The higher mean and lower variance is attributed to the larger percentage of gravels and lower percent of clay elements. This decrease in the amount of clay-silt elements is attributed to the large sand and gravel scours in section C-C'.

The horizontal and vertical variograms for cross sections A-A' (orientated N55E) and B-B' (N35W) are shown in **Figures 22** and **23**. As shown, the horizontal variograms for Cross Sections A-A' and B-B' are linear. The fact that these variograms rise linearly and do not reach a sill suggests that the maximum scale of horizontal variability is not reached in these two cross sections. This hypothesis is supported by the fact that the variograms rise to a variance equal to only about half the total variance of the data sets (Table VIII). In essence, the

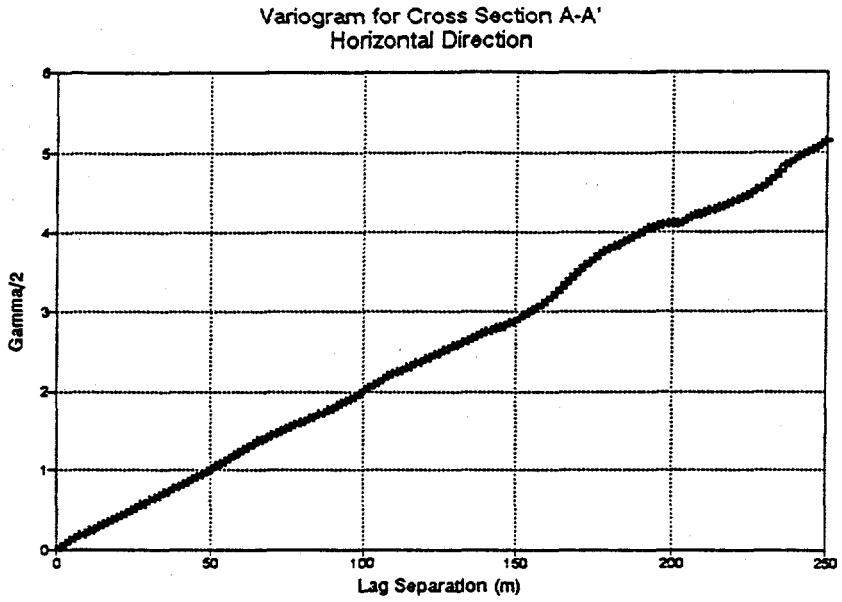

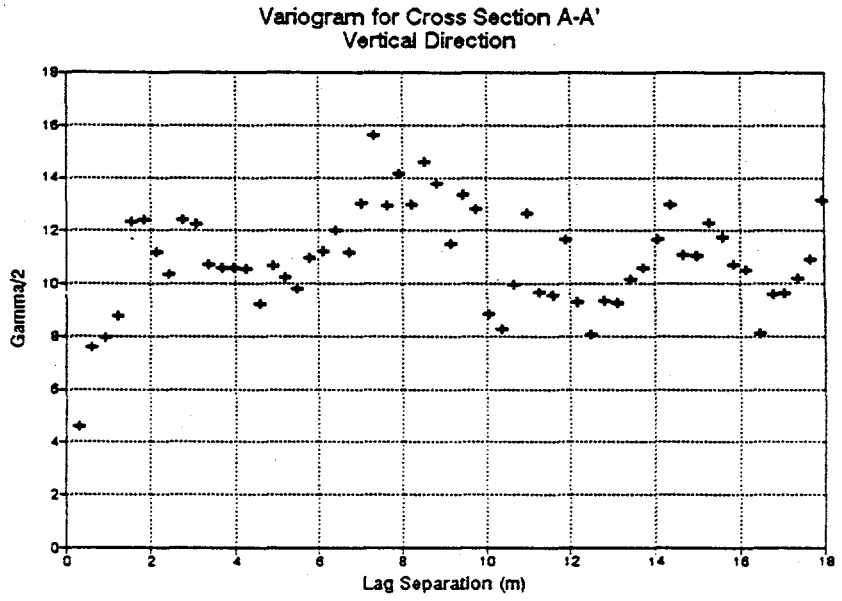

Figure 22: Horizontal and Vertical Variograms for Cross Section A-A'

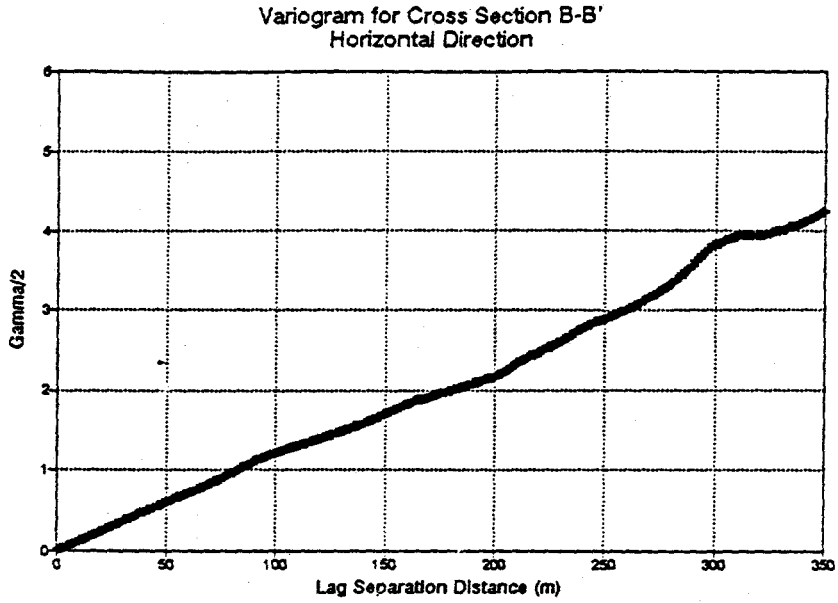

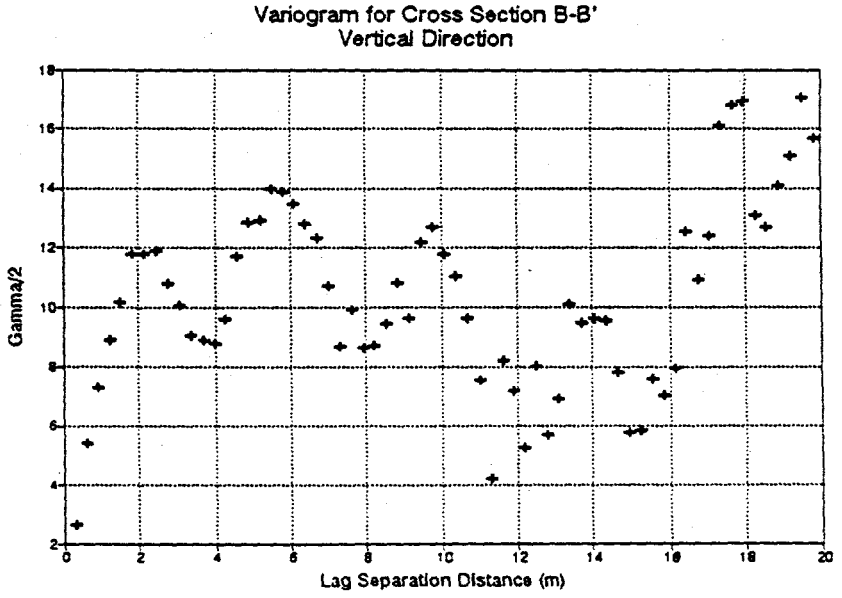

Figure 23: Horizontal and Vertical Variograms for Cross Section B-B'

average dimensions of the elements exceed the actual size of the domains.

The vertical variograms for cross sections A-A' and B-B' are very similar to one another. Both are strongly periodic with a hole effect for lag separations between 4 and 5 m. Examination of cross sections A-A' and B-B' shows that the elements repeat themselves in the vertical direction approximately every 4 to 5 m.

Figure 24 illustrates the horizontal and vertical variograms estimated for cross section C-C' (N70W). Like the horizontal variograms for sections A-A' and B-B', the horizontal variogram for section C-C' rises linearly from zero. However, it differs from the others in that it reaches a sill at a range of approximately 175 m. Visual inspection of cross section C-C' shows that the lateral continuity of elements which is so common in sections A-A' and B-B' is absent on section C-C' due to the increased size and abundance of scours by the CH-2 elements. Thus, it appears that the larger number of scours and scoured elements seen on cross section C-C' may be responsible for the observed sill.

Comparison of the variogram and the total variance of the data set (Table VII) shows that the sill is reached at a variance less than one-third of the overall variance of the data set. Thus it appears that the correlation structure for this cross section probably consists of nested scales of variability, and the sill seen in Figure 24 represents but one of these nested scales.

The vertical variogram estimated along cross section C-C' also exhibits periodic behavior with a hole effect at a lag separation distance of 12 m. This distance of 12 m reflects the fact that several deep scours are present on this section which disrupt the simple cyclic vertical sequences witnessed on Sections A-A' and B-B'. The fact that the vertical variogram for the large AEM data set exhibits a strong hole at approximately 11 meters suggests that the scouring

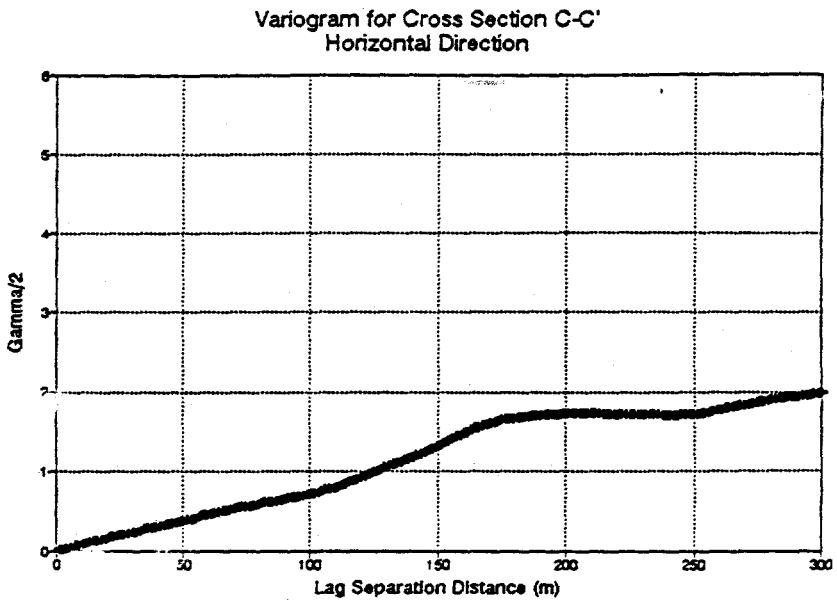

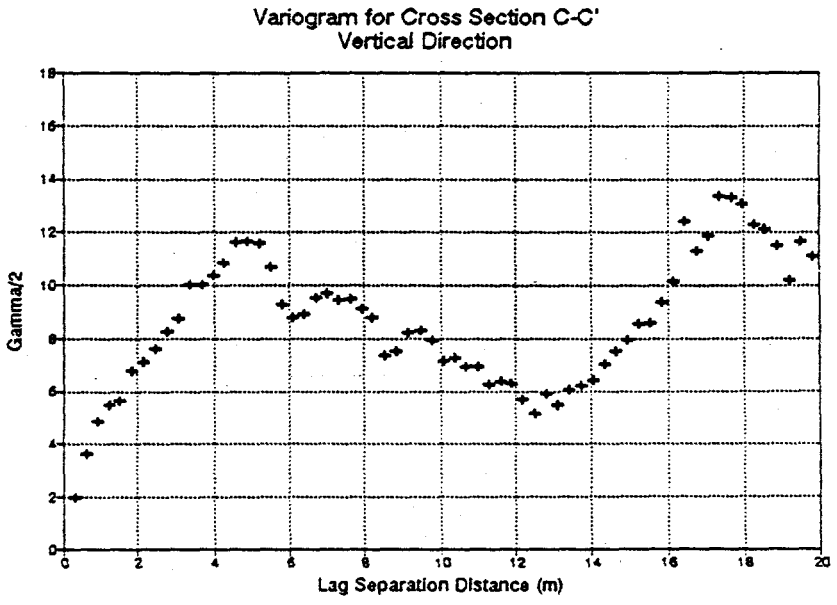

Figure 24: Horizontal and vertical variograms for cross section C-C'

effect observed in cross section C-C' may dominate the vertical variogram for the entire site.

5.3 Variogram Sensitivity Analysis

Due to the inherent uncertainty in the permeability of the clay elements (OF and Pc) at the Bosque Site, a sensitivity analysis was performed by estimating the horizontal variograms for the large AEM data set with a variety of different assigned mean log (k) values. The results of this analysis for the horizontal variogram estimated in the N30W direction are shown in **Figure 25.** As shown, varying the mean log(k) values of the clay elements affects only the overall variance of the variogram, not the actual shape of the variogram. This same result is found for the horizontal variograms estimated in the N60E direction (Appendix C). A regression analysis was performed on the linear portions of the variograms in an effort to correlate the slope of the lines with the changing values of log(k). The results of this regression analysis (Figure 25) show that the slope of the linear portion of the variogram becomes steeper with decreasing values of log(k). Additional variograms for different log(k) values would need to be estimated in order to more quantitatively define this relationship.

The sensitivity of the horizontal variogram to changing window geometries was assessed by estimating the variogram for a variety of different parameters, and then analyzing the similarity or lack therefore between the variograms. The three window geometry parameters examined include: 1) the search direction; 2) the horizontal angle tolerance; and 3) the vertical distance tolerance.

Figures 26 illustrates the sensitivity of the horizontal variogram to variations in the

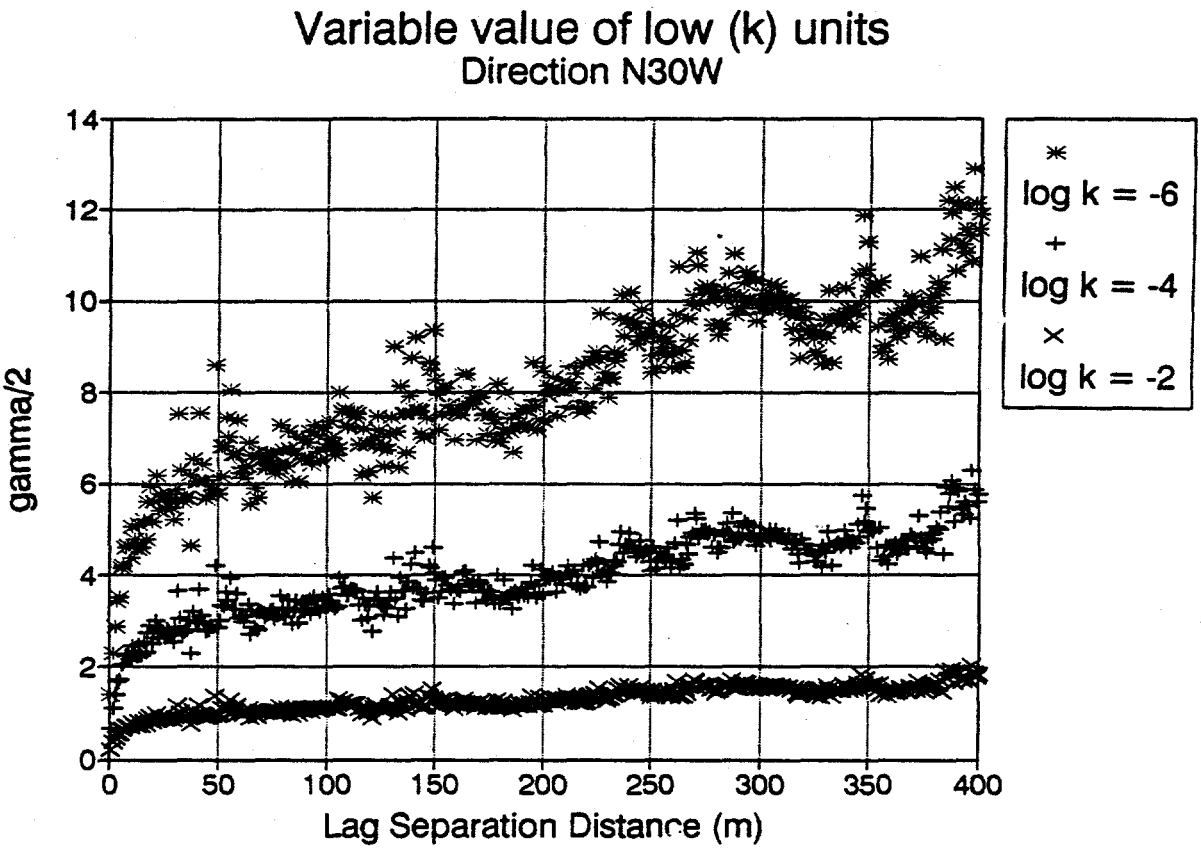

Results of Regression Analysis on Log(k) Variograms

log(k)	y intercept	slope	r squared
-6	5.63	0.0136	0.7915
-4	2.77	0.0063	0.7877
-2	0.92	0.0020	0.7734

Figure 25: Sensitivity Analysis of horizontal variograms to variations in the log(k) value of the clay elements.

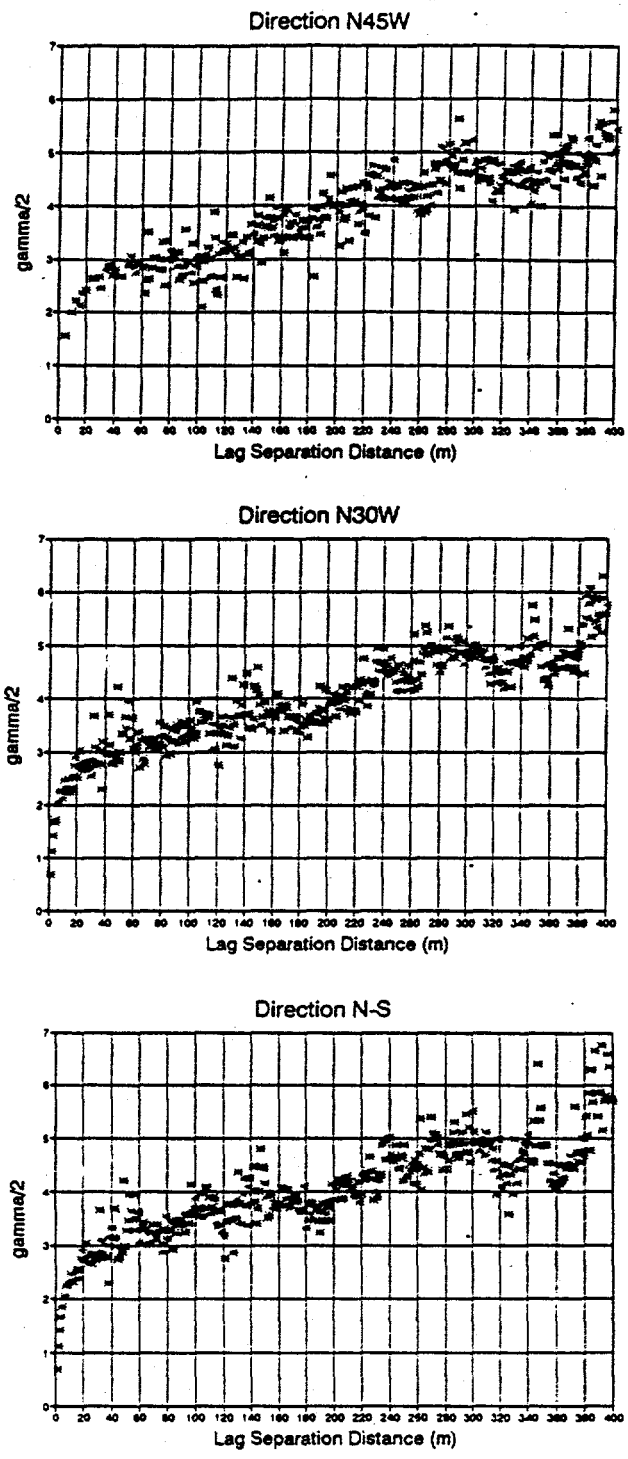

Figure 26: Sensitivity Analysis of horizontal variograms to different sampling directions.

direction of sampling. Three directions were chosen for sampling: N45W, N30W, and N-S. As shown, the shape of the three variograms is relatively similar. This is probably due to the fact that all three of these orientations coincide with correlated scour orientations (Figure 16), and are therefore all reflecting the control exerted by the overall paleoflow direction on the permeability structure. The only notable differences between the three are that the variogram estimated in the N45W direction shows less correlation for small lags, and that the variogram estimated in the N30W direction exhibits the least amount of scatter. The reason that the N45W variogram does not detect the small-scale exponential behavior seems to be due to the relatively small number of pairs for small lags in this direction. The fact that N30W is the average paleoflow direction may account for the small amount of scatter in the N30W variogram. The same sensitivity analysis was performed for variograms estimated in the directions N45E, N60E and N90E with similar results, and are included in Appendix C.

Sensitivity analysis was also performed on the response of the horizontal variogram to changes in the horizontal angle tolerance and the vertical distance tolerance (**Figures 27** and **28**, respectively). These two figures illustrate that increasing either the horizontal angle tolerance or the vertical distance tolerance has the effect of decreasing the overall variance. When the horizontal search angle becomes quite small (10 degrees), the number of pairs is greatly reduced for many lag distances, especially the small lags. This results in increased scatter of the variogram and a lack of detection of the small-scale exponential behavior. The variogram appears to be less sensitive to the vertical distance tolerance, as the small scale exponential behavior is detected for even the smallest vertical distance tolerance tested.

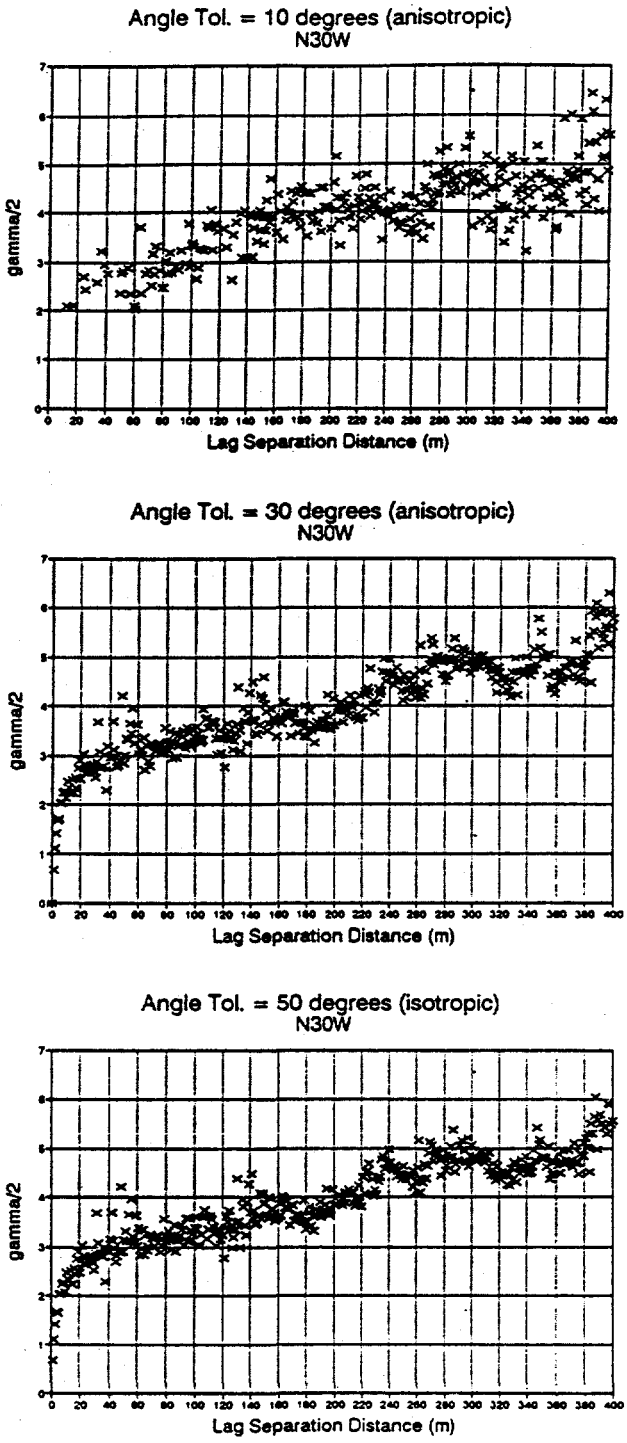

Figure 27: Sensitivity Analysis of horizontal variograms (N30W) for large AEM data set to horizontal angle tolerance.

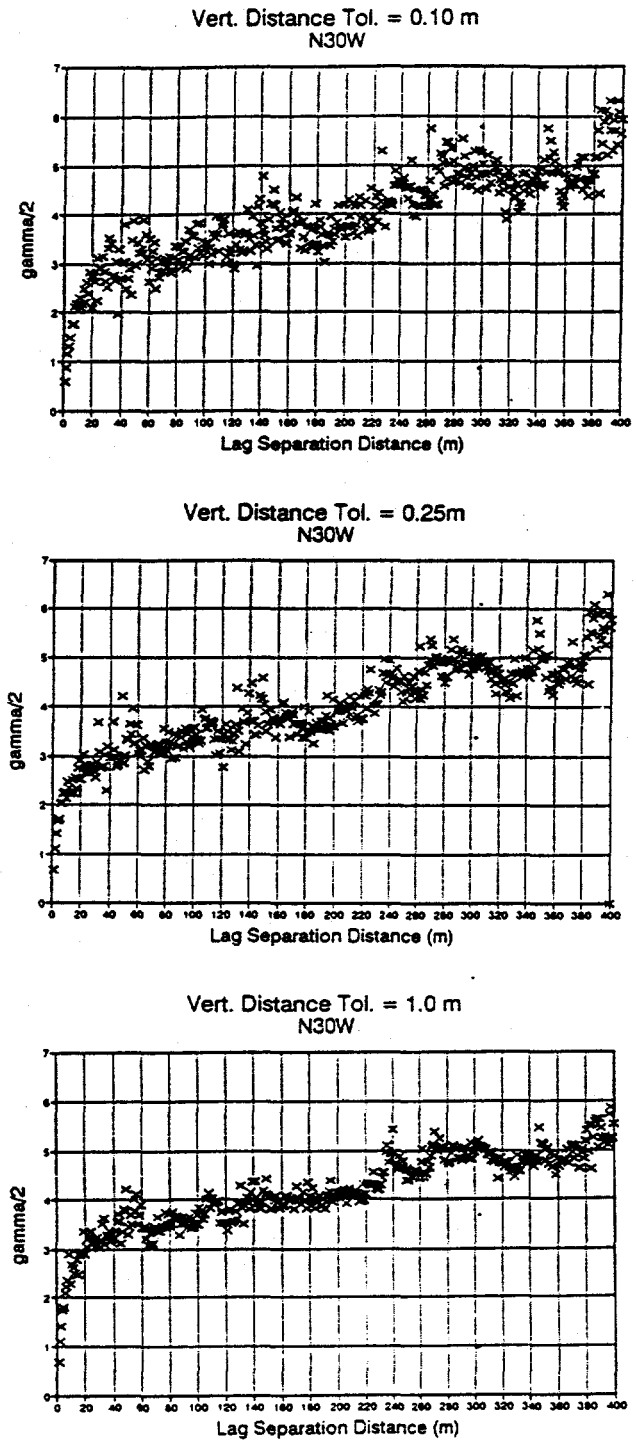

Figure 28: Sensitivity Analysis of horizontal variograms (N30W) for large AEM data set to Vertical Distance Tolerance.

CHAPTER 6: DISCUSSION AND CONCLUSIONS

6.1 Discussion

The results of the depositional environment analysis support and refine the previously understood depositional environment of the upper Sierra Ladrones Formation in the south-central Albuquerque Basin region. Taken as a whole, the analyses of the sedimentary cycles, the three-dimensional element geometries, and the comparisons between the overall alluvial architecture with the alluvial models of Allen (1974) and Kraus and Bown (1987) suggest that the Bosque site records axial and floodplain deposition by the Rio Puerco, its tributary (Rio San Jose) and the Rio Grande. **Figure 29** illustrates the overall interpretation of the depositional environment of the Bosque Site sediments.

The abundance of overbank clays, silts and paleosols suggests that the Bosque site was a distance from axial fluvial channels for a large portion of the time recorded by these deposits. Moreover, the sands themselves (CH-2) are characterized by predominantly lower flow regime sedimentary structures and a fine grain size, both of which indicate deposition in shallow, slow moving waters such as would be found on a floodplain.

Several lines of evidence point to the fact that the Rio Puerco, its tributary the Rio San Jose and the Rio Grande all contributed sediment to the CH-1 elements at the Bosque site. For one, the presence of the Grants obsidian cobble in the gravel underlying the Pgs element indicates that these deposits were derived from the Mt. Taylor area. At the present time, the Rio San Jose drains this area. Moreover, the provenance analysis of Harris (1991) points to a similarity between the Bosque site gravels and deposits of the ancestral Rio Puerco, Rio San Jose, as well as the ancestral Rio Grande. The fact that several sand

Proposed Depositional Environment

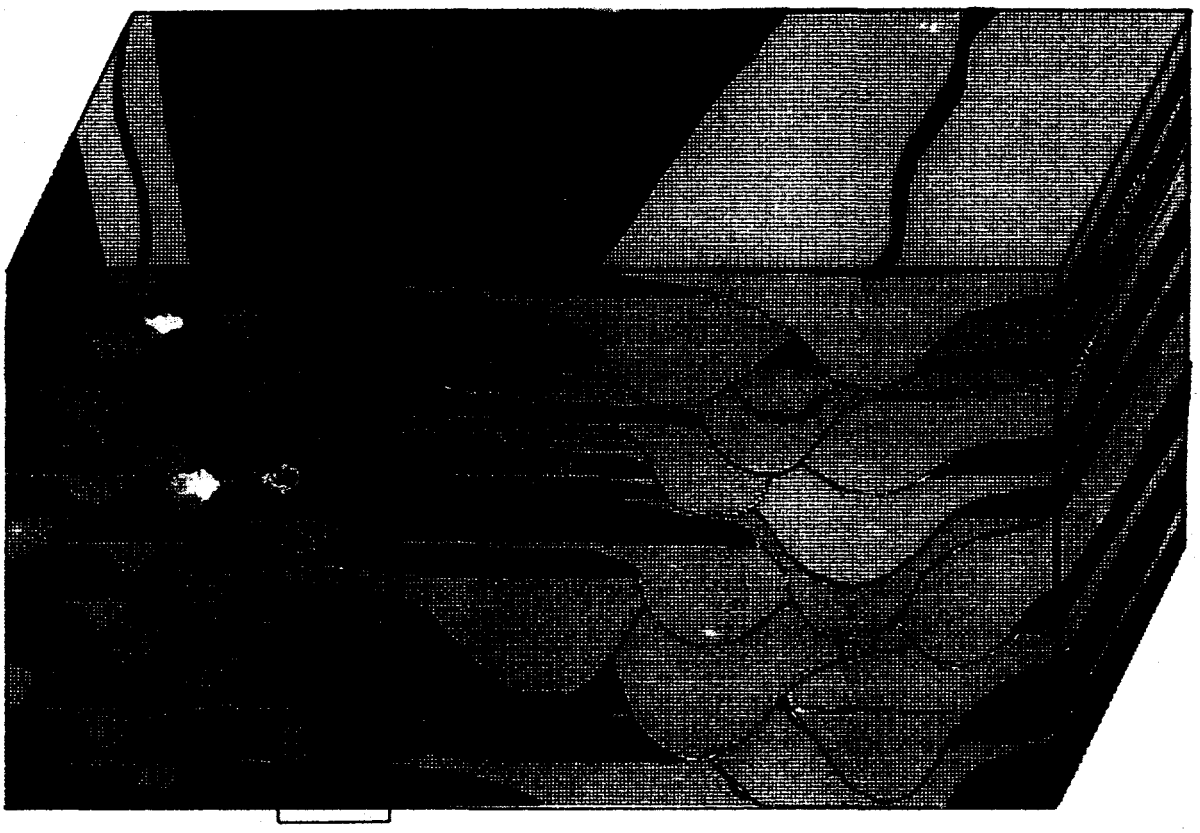

Floodplain Deposits (mudstones)

Channel Sandstones

Pedogenic Carbonate Units

Approximate Site Location

elements (CH-2) thin and grade into clay-silt elements (OF) in a westerly direction indicates that the source of sedimentation for these sand elements lay to the east. According to the hypothesized paleo basin geometries outlined by by Lozinsky et al (1991) shown in Figure 3, this source of sedimentation was most likely the Rio Grande. Provenance analysis studies such as those done by Harris (1991) on the gravels will need to performed on the sand elements (CH-2) in order to better define the fluvial source of these sands.

The relative position of the Bosque Site to the confluence of the Rio Grande and its tributaries the Rio Puerco and the Rio San Jose cannot be determined with the current data. Continued mapping to the north and south of the Bosque Site coupled with more provenance analyses in these locations will need to be done in order to address this question.

As a final point, the vertical sequence of sediments suggest that a wetter climate may have set in during deposition of the upper portion of the mapped section. Continued mapping higher in the section needs to done in order to substantiate this hypothesis. This type of information could be very useful in aquifer characterization, as it could help identify the zones of higher permeability.

The results of the variogram analyses of the three-dimensional data sets show that the system is statistically anisotropic, and that the causes of this anisotropy are most likely the depositional processes. For one, the strongly periodic character of the vertical variograms accurately detects the discrete layered nature of the deposits. Moreover, the variograms estimated in the horizontal directions support the geologic interpretation that the inferred axis of deposition in the system was orientated N30W.

Variograms estimated parallel to the inferred axis of deposition all display a linearly

rising variogram model with no visible horizontal sill. This indicates that the dimensions of the outcrop itself are smaller than the average dimensions of the architectural elements when viewed parallel to the paleoflow direction. By contrast, the variograms estimated perpendicular to this inferred axis exhibit a finite correlation scale suggesting that at least one scale of variability is captured when sampling in this direction.

When the sample spacing is small enough, the three-dimensional variograms also detect a small-scale exponential correlation structure in all the sampling directions. The 20 m range of this correlation structure appears to correspond with the average width of the scours across the field site.

The nested exponential behavior of the horizontal variograms estimated perpendicular to the paleoflow direction shows that multiple scales of variability are present at the Bosque Site. As discussed above, the smallest of these scales appears to be the average dimension of the scours themselves. The next largest dimension may correspond to the average dimension of the scoured elements. Larger scales of variability are not captured in this analysis due to the limiting size of the outcrop itself, but it is assumed that the next larger scale of variability may be the average dimensions of the elements as a whole.

Continued mapping should provide additional information about these larger scales of variability. If the paleoflow direction is indeed in a south-southeasterly direction, than a great deal of information regarding the geometries of these elements probably lies both to east and to west of the Bosque Site. Unfortunately, the incision of the Rio Grande has removed any outcrops of the upper Sierra Ladrones Formation to the west, and the presence of the Llano de Albuquerque prevents continuous mapping to the east. Thus, further mapping will necessarily

be parrallel and/or subparrallel to the inferred axis of deposition.

The results of the variogram analysis of the three cross sections shed some interesting light on the relationship between two-dimensional and three-dimensional variograms. As noted above, for small lags, the three-dimensional variograms consistently display exponential behavior while the two-dimensional variograms are always linear. The precise cause of this relationship is unknown, but it is hypothesized that while the two-dimensional linear variograms represent sampling along one plane within the outcrop, the three-dimensional variograms are the average expression of sampling along many such planes.

An exponential variogram model, by definition, describes data whose correlation decreases rapidly with increasing lag separation distance. The fact that variograms of the AEM data set display this type of behavior is a surprising result for geologic deposits with as much visible lateral continuity as is seen at the Bosque Site. It is hypothesized that this exponential behavior may be the result of the discrete nature of the field. That is, as lag separation distance increases and new element boundaries are crossed, the variance increases rapidly due to the distinctly different log(k) values between the elements.

The fact that the variogram shape is insensitive to the value of the log(k) of the clay elements is important, especially given the inherent difficulties in actually measuring the permeability of these units. This finding means that for future studies, the shape of the permeability correlation structure can be assessed, even if the exact value of the clay elements if uncertain.

As discussed above, the Bosque Site deposits are statistically anisotropic, showing that the variograms are sensitive to the sampling direction. However, as the directional sensitivity

analysis shows, as long as the sampling is within +/- 30 degrees of the principal direction of anisotropy, the general shape of the variogram for the principal direction will still be evident. Moreover, the variograms appear to be relatively insensitive to horizontal angle tolerance and the vertical distance tolerance.

For an exercise such as this one where the geology is documented in detail, variogram analysis essentially supports the information visually seen on the maps. But for cases where the geology is not well documented such as in aquifers, random sampling in a variety of orientations is likely to produce a variogram with little to no meaning. This is where a relatively detailed understanding of the depositional environment of the aquifer is useful. Knowledge of the depositional environment can provide insight into the primary axes of anisotropy in the system, such as the inferred axis of deposition in this case. This information can then be used to guide in analysis of the data.

6.2 Conclusions

This study is an effort to produce a quantitative three-dimensional description of geologic deposits coupled with a detailed description of the depositional environment. As discussed in Chapter 1, this combination of information is critical to the process of indirect permeability structure characterization. The results of this study show that outcrop studies such as this one can provide detailed information about the three-dimensional structure of the geologic deposits associated with a given depositional environment.

The small-scale mapping at the Bosque site allowed for a relatively detailed analysis of the depositional environment of the sediments. The Bosque Site deposits are the result of largely

fluvial and interfluvial processes. The deposits record the presence of least one and possibly two or three rivers which moved in avulsive steps across the floodplain. The geometry of the sediments as well as a provenance analysis (Harris, 1991) suggest that these sediments were deposited by a combination of the Rio Puerco, the Rio San Jose and the Rio Grande. The sediments record a possible onset of a wetter climate near the top mapped section.

Several conclusions can be drawn from the the variogram analysis of the Bosque Site Architectural Element Map (AEM) and the geologic cross sections. For one, the three-dimensional variograms appear to reflect the depositional processes which formed the deposits. The primary axis of deposition in the system is detected in that the variograms estimated perpendicular to this direction exhibit a maximum range of correlation, whereas the variograms estimated parallel to this direction do not.

Secondly, nested scales of variability may be present at the Bosque Site, as evidenced by the nested exponential behavior of the three-dimensional horizontal variogram estimated perpendicular to the paleoflow direction. In order of increasing scale, these nested scales are hypothesized to correspond to the average width of the scours, the average dimensions of the scoured elements, and finally the average dimensions of the elements themselves. Only the first two scales of variability are seen in the variograms estimated for the Bosque Site.

Thirdly, the shapes of the variograms reflect only the overall geometry of the elements, not the absolute values of permeability assigned to these units. This is evident by the results of the sensitivity analysis of the variograms to the assigned permeability value of the clay elements. Only the variance changes when the permeabilities are changed, not the shape of the variograms themselves.

Fourthly, a linear variogram appears to indicate that the average dimensions of the geologic units exceeds the dimensions of the sample domain. Moreover, the exponential behavior of the variograms is a surprising outcome for a field with as much apparent lateral continuity as the Bosque Site, and is tentatively attributed to the assignment of single values of permeabilty to a field of discrete geologic units.

In general, this study is an analysis of discrete, single-valued units, and does not represent the total variability of the permeability within the Bosque Site deposits. For this information to be examined, instead of assigning mean log(k) values to the elements, the within-element permeability variability must be superimposed on the elements. Information regarding the within-element permeability variations can only be assessed by further outcrop sampling such as the work of Davis (1990).

The results of this study should provide useful quantitative geologic information for hydrogeologists working in aquifers produced by similar depositional environments. In order for this type of information to be most useful for aquifer characterization, more attention needs to be devoted to determining the within-element permeability structure, as well as the optimum method of synthesizing these various forms of information.

REFERENCES

Allen, J.R.L. 1974. Studies in fluviatile sedimentation: Implication of pedogenic carbonate units, Lower Old Red Sandstone, Anglo-Welsh Outcrop, *Geol. Jour., v. 9,* p. 181-208.

Allen, J.R.L., 1986, Pedogenic calcretes in the Old Red Sandstone Facies (Late Silurian-early Carboniferous) of the Anglo-Welsh Area, Southern Britain, *in* P.V. Wright (ed), Paleosols: Their Recognition and Interpretation, Princeton University Press, Princeton, New Jersey.

Bates, R.L and J.A. Jackson, 1984, Dictionary of Geological Terms, 3rd ed., The American Geological Institute, Doubleday, New York, 571 p.

Birkeland, P.W., 1984, Soils and Geomorphology, Oxford University Press, London.

Burroughs, P.A., 1983, Multiscale sources of spatial variation in soil II: A non-Brownian fractal model and its application in soil survey, *Jour. Soil Sci., v. 34,* p. 599-620.

Chapin C.E. and W.R. Seager, 1975, Evolution of the Rio Grande rift in Socorro and Las Cruces areas, New Mexico Geological Society Guidebook 26, p. 297-321.

Collinson J.D. and D.B. Thompson, 1982, Sedimentary Structures, George Allen & Unwin, Boston, 194 p.

Davis, J.M. 1990, An Approach for the Characterization of Spatial Variability of Permeability in the Sierra Ladrones Formation, Albuquerque Basin, Central New Mexico: M.S. Thesis. New Mexico Institute of Mining and Technology, Socorro. 128p.

Davis, J.M., S.J. Colarullo, F.M. Phillips and R.C. Lohmann, 1991, Alluvial aquifer heterogeneities in the Rio Grande valley: Implications for groundwater contamination, New Mexico Water Resources Research Institute Technical Completion Report, Project Number 1345681, iii p.

Delhomme, J.P., 1978, Kriging in the hydrosciences, *Adv. Water Resour., v. 1,* p. 251-266.

Deutsch, C.V. and A.G. Journel, in press, GSLIB: Geostatistical Software Library User's Guide, Oxford University Press, New York.

Desbarats, A.J., 1990, Macrodispersion in sand-shale sequences, *Water Resour. Res., vol. 26.,* p. 153-164.

Dreyer, T., A. Scheie, and O. Walderhaug, 1990, Minipermeameter-based study of permeability trends in channel sand bodies, *Amer. Assoc. Petrol. Geol. Bull., v. 74,* p.

359-374.

Fogg, G.E., 1989, Stochastic analysis of aquifer interconnectedness: Wilcox Group, Trawick Area, East Texas, Bureau of Economic Geology, The University of Texas at Austin, Report of Investigations No. 189, 68 p.

Freeze, R.A. and J.A. Cherry, 1979, Groundwater, Prentice-Hall, Inc., Englewood Cliffs, N.J, 604 p.

Gile, L.H., J.W. Hawley, and Grossman, R.B., 1981. Soils and geomorphology in the Basin and range area of southern New Mexico--Guidebook to the Desert Project. New Mexico Bureau of Mines & Mineral Resources, Memoir 39., 222 p.

Goggin, D.J., M.A. Chandler, G. Kocurek, and L.W. Lake, 1988, Patterns of permeability in eolian deposits: Page Sandstone (Jurassic), Northeastern Arizona, *Soc. Petrol. Eng. Form. Eval.,v. 3,* p. 297-306.

Gutjahr, A.L., 1989, Fast Fourier Transforms for random field generation, Project Report for Los Alamos National Labs Grant to New Mexico Tech, Contract Number 4-R58-2690R, 106 p.

Harms, J.C. and R.K. Fahnestock, 1965, Stratification, bedforms, and flow phenomena (with an example from the Rio Grande), pp.84-115, in G.V. Middleton (ed.), Primary Sedimentary Structures and their Hydrodynamic Interpretation, Soc. Econ. Paleontologists and Mineralogists Spec. Publ. 12, 264 p.

Harris, J., 1991, Provenance analysis of upper Sierra Ladrones Formation near Bosque, New Mexico, unpublished data.

Herweijer, J.C. and S.C. Young, 1990, Use of detailed sedimentological information for the assessment of pumping and tracer tests in a shallow fluvial aquifer, in Proceedings of the 5th Canadian/American Conference on Hydrogeology "Parameter Identification and Estimation for Aquifer and Reservoir Characterization", Calgary, Canada, September 18-20

Hess, K.M., S.H. Wolf, M.A. Celia, and S.P. Garabedian, 1991, Macrodispersion and spatial variability of hydraulic conductivity in a sand and gravel aquifer, Cape Cod, Massachusetts, U.S. Environmental Protection Agency Environmental Research Brief EPA/600/M-91/005., 9 p.

Henriquez, A., K.J. Tyler, and A. Hurst, 1990, Characterization of fluvial sedimentology for reservoir simulation modeling, *Soc. Petrol. Eng. Form. Eval., v. 5,* p. 211-216.

Isaaks, E.H. and R.M. Srivastava, 1989, An Introduction to Applied Geostatistics, Oxford University Press, New York, 561 p.

Jones, J.R., A.J. Scott, and L.W. Lake, 1988, The geologic aspects of reservoir characterization for numerical simulation: Mesaverde meanderbelt sandstone, Northwestern Colorado, *Soc. Petrol. Eng. Form. Eval., v. 3,* p. 97-107.

Johnson, N.M. and S.J. Dreiss, 1989, Hydrostratigraphic interpretation using indicator geostatistics. *Water Resour. Res., v. 25,* p. 2501-2510.

Journel, A.G. and F.G. Alabert, 1988, Focusing on spatial connectivity of extreme-valued attributes: Stochastic indicator models of reservoir heterogeneities, *Soc. Petro. Eng. paper 18324,* presented at the 63rd Annual Technical Conference and Exhibition of the Society of Petroleum Engineers held in Houston, TX, October 2-5, 1988.

Kittridge, V.G. and L.W. Lake, 1989, Outcrop-subsurface comparisons of heterogeneity in the San Andres Formation, *Soc. Petrol. Eng. paper 19596,* presented at the 64th Annual Technical Conference and Exhibition of the Society of Petroleum Engineers, San Antonio, TX, Oct. 8-11.

Kraus, M.J. and T.M. Bown, 1987, Integration of channel and floodplain suites, I: Developmental sequence and lateral relations of alluvial paleosols, *Jour. Sed. Petrology, v. 57,* p. 587-601.

Kraus, M.J., 1987, Integration of channel and floodplain suites, II: Vertical relations of alluvial paleosols, *Jour. Sed. Petrology, v. 57,* p. 602-612.

LeBlanc, D.R., S.P. Garabedian, K.M. Hess, L.W. Gelhar, R.D.Quadri, K.G. Stollenwerk, and W.W. Wood, 1991, Large-scale natural gradient test in sand and gravel, Cape Cod, Massachusetts: 1. Experimental design and observed tracer movement, *Water Resour. Res., v. 27,* p. 895-910.

Lipman, P.W. and H.H. Mehnert, 1980, Potassium-argon ages from the Mount Taylor volcanic field, New Mexico: U.S. Geological Survey Professional Paper 1124-B, 8 p.

Love, D.W. and J.D. Young, 1983, Progress report on the Late Cenozoic evolution of the Lower Rio Puerco, New Mexico Geological Society Guidebook, 34th Field Conference, Socorro Region II, p. 277-284.

Love, D.W., 1986, A geological perspective of sediment storage and delivery along the Rio Puerco, central New Mexico, in Hadley R.F., (ed), Drainage basin sediment delivery, International Association of Hydrological Sciences, Publication 159, p. 305-322.

Lozinsky, R.P., 1988, Stratigraphy, sedimentology, and sand petrology of the Santa Fe Group

and pre-Santa Fe Tertiary deposits in the Albuquerque Basin, Central New Mexico: PhD Dissertation, New Mexico Institute of Mining and Technology, Socorro, New Mexico, 298p.

Lozinsky, R.P., J.W. Hawley, and D.W. Love, 1991, Geologic overview and Pliocene-Quaternary history of the Albuquerque Basin, Central New Mexico, *in* J.W. Hawley and D.W. Love (eds.), Quaternary and Neogene landscape evolution: A transect across the Colorado Plateau and Basin and Range provinces in West-Central and Central New Mexico, New Mexico Bureau of Mines and Mineral Resources Bulletin 137, p. 157-162.

Machette, M.N., 1978, Geologic map of the San Acacia quadrangle, Socorro County, New Mexico, U.S. Geological Survey Map GQ-1415, scale 1:24,000.

Mack, G.H. and W.R. Seager, 1990, Tectonic control on facies distribution of the Camp Rice and Palomas Formations (Pliocene-Pleistocene) in the southern Rio Grande rift, *Geol. Soc. Amer. Bull., v. 102*, p. 45-53.

McGrath, D.G. and J.W. Hawley, 1987, Geomorphic evolution and soil-geomorphic relationships in the Socorro area, Central NM, *in* Mclemore, V.T. and M.R. Bowie (eds), Guidebook to the Socorro Area, New Mexico, New Mexico Bureau of Mines and Mineral Resources, Socorro NM, pp. 55-67.

McKee, E.D., 1966, Significance of climbing-ripple structure, U.S. Geological Survey Professional Paper 550-D, p. D94-D103.

McKee, E.D., E.J. Crosby, and H.L. Berryhill Jr., 1967, Flood deposits, Bijou Creek, Colorado, June 1965, *J. Sed. Petrology, v. 37*, p. 829-851.

Miall, A.D., 1978, Lithofacies types and vertical profile models of braided river deposits: a summary *in* A.D. Miall (ed.), Fluvial Sedimentology, Can. Soc. Petrol. Geol. Mem. 5, p. 597-604.

Miall, A.D., 1985, Architectural element analysis: A new method of facies analysis applied to fluvial deposits, *Earth Sci. Rev., v. 22*, p. 261-308.

Miall, A.D., 1988, Facies Architecture in Clastic Sedimentary Basins, *in* K.L. Kleinsphen and C.Paola (eds.), New Perspectives in Basin Analysis, Springer-Verlag, New York, 452p.

Montoglou, A. and J.L. Wilson, 1982, The turning bands method for simulation of random fields using line generation by a spectral method, *Water Resour. Res., v. 18*, p. 1379-1394.

Neuman, S.P., 1990, Universal scaling of hydraulic conductivities and dispersivities in geologic media, *Water Resour. Res., v. 26*, p. 1749-1758.

Picard, M.D. and L.R. High, 1973, Developments in Sedimentology 17: Sedimentary Structures of Ephemeral Streams, Elsevier Scientific Publishing Co., New York, 223 p.

Poeter, E. and G.R. Gaylord, 1990, Influence of aquifer heterogeneity on contaminant transport at the Hanford Site. *Groundwater, v. 28,* p. 900-909.

Poeter, E. and P. Townsend, 1991, Multiple indicator conditional stochastic simulation of a section of the unconfined aquifer, Hanford Site, Washington, USA, In review for publication.

Polasek, T.L. and C.A. Hutchinson, Jr., 1967, Characterization of non-uniformities within a sandstone reservoir from a fluid mechanics standpoint, in Seventh World Petroleum Congress Mexico Proceedings, Elsevier Publishing Co., p. 397-408, 973 p.

Ravenne, C., R. Eschard, A. Galli, Y. Mathieu, L. Montadert, and J.L. Rudkiewicz, 1989, Heterogeneities and geometry of sedimentary bodies in a fluvio-deltaic reservoir, *Soc. Petrol. Eng. Form. Eval., v. 4,* p. 239-246.

Reading, H.G., 1986, Facies, *in* Reading, H.G. (ed.) Sedimentary Environments and Facies, 615 p.

Robin, M.J.L., E.A. Sudicky, R.W. Gillham, and R.G. Kachanoski, 1991, Spatial variability of strontium distribution coefficients and their correlation with hydraulic conductivity in the Canadian Forces Base Borden Aquifer, *Water Resour. Res., v. 27,* p. 2619-2632.

Rubin, D.M., 1987, Cross bedding, bedforms, and paleocurrents, Soc. Econ. Paleontologists and Mineralogists, Concepts in Sedimentology and Paleontology, v. 1, Tulsa, Oklahoma, 187 p.

Ruhe, R.V., 1965, Quaternary Paleopedology, *in* H.E. Wright and D.G. Frey (eds.) The Quaternary of the United States, Princeton University Press, Princeton, New Jersey, p. 755-764.

Scholle, P.A., 1979, A color illustrated guide to constituents, textures, cements, and porosities sandstones and associated rocks, Amer. Assoc. Petrol. Geol. Mem. 28.

Schwartz, F.W., 1977, Macrodispersion in porous media: The controlling factors, *Water Resour. Res., v. 13,* p. 743-752.

Seager, W.R., M. Shafiqullah, J.W. Hawley, and R. Marvin, 1984, New K-Ar dates from basalts and the evolution of the southern Rio Grande rift, *Geol. Soc. Amer. Bull., v. 95,* p. 87-99.

Silliman, S.E., and E.S. Simpson, 1987, Laboratory evidence of the scale effect in dispersion of solutes in porous media, *Water Resour. Res., v. 23,* p. 1667-1673.

Slavin, P.J., 1991, Summary of recent work on the geomorphology of the upper Rio Puerco, in J.W. Hawley and D.W. Love (eds.), Quaternary and Neogene landscape evolution: A transect across the Colorado Plateau and Basin and Range provinces in West-Central and Central New Mexico, New Mexico Bureau of Mines and Mineral Resources Bull. 137, p. 171-172.

Smith, L. and F.W. Schwartz, 1980, Mass Transport 1. A stochastic analysis of macroscopic dispersion, *Water Resour. Res., v. 16,* p. 303-313.

Smith, L. and F.W. Schwartz, 1981, Mass Transport 3. Role of hydraulic conductivity data in prediction, *Water Resour. Res., v. 17,* p. 1463-1479.

Stalkup, F.I and W.J. Ebanks Jr., 1986, Permeability variation in a sandstone barrier island-tidal channel-tidal delta complex, Ferron Sandstone (Lower Cretaceous), Central Utah, *Soc. Petol. Eng. Paper 15532* presented at the 61st Annual Technical Conference and Exhibition, New Orleans, October 5-8.

Stephens, D.B., W. Cox, and J. Havlena, 1988, Field Study of Ephemeral Stream Infiltration and Recharge, New Mexico Water Resources Research Institute Technical Completion Report, Project Numbers 1423655, 1423658, 188 p.

Sudicky, E.A., 1986, A natural gradient experiment on solute transport in a sand aquifer: Spatial variability of hydraulic conductivity and its role in the dispersion process, *Water Resour. Res., v. 22,* p. 2069-2082.

Torrent, J., V. Schwermann, and D.G. Schulve, 1980, Iron-oxide mineralogy of some soils of two river terrace sequences in Spain, *Geoderma, v. 23,* p. 191-284.

Van de Graaff, W.J., and P.J. Ealey, 1989, Geological modeling for simulation studies, *Amer. Assoc. Petrol. Geol. Bull., v. 73,* p. 1436-1444.

Walker, T.R., Formation of red beds in modern and ancient deserts, *Geol. Soc. Amer. Bull., v. 78,* p. 353-368.

Weber, K.J., 1980, Influence on fluid flow of common sedimentary structures in sand bodies, *Soc. Petrol. Eng. Paper 9247,* presented at 55th Annual Fall Technical Conference and Exhibition of the Society of Petroleum Engineers of AIME, Dallas, Texas, September 21-24.

Young, J.D., 1982, Late Cenozoic geology of the lower Rio Puerco, Valencia and Socorro Counties, New Mexico: M.S. Thesis, New Mexico Institute of Mining and Technology,

Socorro, 126 p.

Wheatcraft, S.W., and S.W. Tyler, 1988, An explanation of scale-dependent dispersivity in heterogeneous aquifers using concepts of fractal geometry, *Water Resour. Res., v. 24,* p. 566-578.

Wolf, S.H., M.A. Celia, and K.M. Hess, 1991, Evaluation of hydraulic conductivities calculated from multi-port-permeameter measurements, *Groundwater, v. 29,* p. 5166-525.

Wright, H.E., Jr., 1946, Tertiary and Quaternary geology of the lower Rio Puerco area, New Mexico, *Geol. Soc. Amer. Bull., v. 57,* p. 383-456.

Zeito, G.A., 1965, Interbedding of shale breaks and reservoir heterogeneities, *Jour. Petrol. Tech., v. 2,* p. 1223-1228.

APPENDIX A
Computer Programs used for Data Preparation

```
      program dataprep
C*************************************************************************
C     This program takes the gsmap digitized data file (converted
C     to an ascii file in the GSMUTIL program using option 2) and
C     outputs two data files which are used as input to the
C     ptpoly program.
C*************************************************************************
      integer code,total
      character*30 indat,outdat1,outdat2,title1,title2,outdat3

      write(*,*) 'Enter GSMAP ascii digitized data file'
      read(*,'(a)')indat
      write(*,*) 'Enter (x,y) data file for ptpoly program'
      read(*,'(a)')outdat1
      write(*,*) 'Enter polygon/code file for ptpoly program'
      read(*,'(a)')outdat2

C     The total number of polygons needs to read from the GSMAP ascii
C     file--just look at the last entry number and this is the total #.

      write(*,*)'Enter the total number of polygons'
      write(*,*)'you need to look at last entry # in GSMAP file'
      read(*,*)npoly

      write(*,*)'Enter the x multiplier to get (1 in = 1 ft)'
      read (*,*)xmult
      write(*,*)'Enter the y multiplier to get (1 in = 1 ft)'
      read(*,*)ymult
      write(*,*)'Enter the name of the min/max file'
      read(*,'(a)')outdat3

      open (unit=20,file=indat,status='old')
      open (unit=30,file=outdat1,status='unknown')
      open (unit=40,file=outdat2,status='unknown')
      open (unit=50,file=outdat3,status='unknown')

      read(20,'(a)')title1
      read(20,'(a)')title2
      read(20,*)dum1,dum2
      read(20,*)dum3,dum4
      read(20,*)dum5,dum6
      read(20,*)dum7,dum8

      write(40,*)npoly
      total = 0

         xmin=1000000
         xmax=-1000000
         ymin=1000000
         ymax=-1000000

      do 50 i=1,npoly

         read(20,*)entry,npts,code,p1,p2
         total = total + npts
         if(code.eq.402) code=2
         if(code.eq.403) code=3
         if(code.eq.404) code=4
         if(code.eq.405) code=5
         if(code.eq.406) code=6
         if(code.eq.407) code=7
         write(40,*)npts,code

         do 100 j=1,npts
            read(20,*)x,y
            x1 = x*xmult
            y1 = y*ymult
            write(30,*)x1,y1
            if (x1.gt.xmax) xmax = x1
            if (x1.lt.xmin) xmin = x1
            if (y1.gt.ymax) ymax = y1
            if (y1.lt.ymin) ymin = y1
100      continue
50    continue
      write(30,*)total
      write(*,*)'The total number of (x,y) pairs = ',total
```

```
      write(*,*)'(This number is at the bottom of x,y output'
      write(*,*)'file...YOU NEED TO MOVE THIS NO. TO THE TOP OF THE'
      write(*,*)'FILE!!!)'

     write(*,*)'Xmax=',xmax,' Xmin=',xmin
     write(*,*)'Ymax=',ymax,' Ymin=',ymin
     write(50,'(a)')'Min and Max data for file ',indat
     write(50,*)'xmax = ',xmax
     write(50,*)'xmin = ',xmin
     write(50,*)'ymax = ',ymax
     write(50,*)'ymin = ',ymin

      end
```

```
      program testpt
C*********************************************************************
C     This program generates a grid of points to be overlayed on a
C     2-D map of polygons.  The program allows the user to specify
C     the grid spacing, and then fits the grid to the minimum and
C     maximum coordinates of the polygons.
C*********************************************************************
C     maxpts = the maximum points in the test point grid
C     t(2,maxpts) = the array of grid test points
C     xmin, xmax = the min and max x coordinates of the polygons
C     ymin, ymax = the min and max y coordinates of the polygons
C*********************************************************************

      PARAMETER (MAXPTS=35000)

      INTEGER  t(2,MAXPTS),del,iend,xcount,ycount
      INTEGER  XMAX,XMIN,YMAX,YMIN
      character*30 fname

      WRITE(*,*)'ENTER XMIN OF THE TEST AREA'
      READ(*,*)XMIN
      WRITE(*,*)'ENTER XMAX OF THE TEST AREA'
      READ(*,*)XMAX
      WRITE(*,*)'ENTER YMIN OF THE TEST AREA'
      READ(*,*)YMIN
      WRITE(*,*)'ENTER YMAX OF THE TEST AREA'
      READ(*,*)YMAX

      write(*,*)'enter the test point output file'
      read(*,'(a)')fname

      open(unit=99,file=fname,status='new')

      write(*,*)'enter the desired distance between test pts'
      read(*,*)del

      iend=int((xmax-xmin)/del)+1
      jend=int((ymax-ymin)/del)+1
      write(99,*)iend*jend
      xcount=xmin
      do 150  i=1,iend
              t(1,i)=xcount
              xcount=xcount+del
              ycount=ymin
                     do 250 j=1,jend
                            t(2,j)=ycount
                            write(99,*)t(1,i),t(2,j)
                            ycount=ycount+del

250   continue
150   continue

      END
C*********************************************************************
```

```
      program fixcode
C*****************************************************************
C     This program simply changes the lithology code into an
C     assigned log k value.
C*****************************************************************

       real x,y,z
       integer code
       character*30 indat,outdat

       write(*,*)'Enter input (x,y,z,code) file'
       read(*,'(a)')indat
       write(*,*)'Enter output (x,y,z,logk) file'
       read(*,'(a)')outdat

       write(*,*)'Enter the total number of data points'
       read(*,*)npts

       open (unit=90,file=indat,status='old')
       open (unit=92,file=outdat,status='unknown')

       do 10 i=1,npts
          read(90,*)x,y,z,code
          if (code.eq.2) code=1
          if (code.eq.6) code=3
          if (code.eq.3) code=-3
          if (code.eq.4) code=-1
          if (code.eq.5) code=-3
          if (code.eq.7) code=0
          write (92,*)x,y,z,code
10     continue


       end
```

```
      program PTPOLY
C-----------------------------------------------------------------------
C     This program is designed to overlay a grid of test points over
C     a two-dimensional map of polygons.  The polygons consist of strings
C     of (x,y) pairs and their associated codes.  The test point grid is
C     generated by the program testpt.  The polygon date needs to be in
C     two files:  one file is a list of all the (x,y) pairs of the
C     polygons in the order they were digitized (i.e. polygon 1 points
C     followed by polygon 2 points and so on).  The other file explains
C     how many points per polygon and the code of the polygon.
C     The algorithm is based on the fundamental principle that if you
C     draw a horizontal line from the test point in question to the
C     right edge of the polygon map, if this horizontal line intersects
C     the segments of the polygon an even number of times, than the
C     test point is outside the polygon.  If the number of intersections
C     is an odd number, than the test point is inside the polygon.  There
C     is also a check built into the program in the case where the
C     horizontal line passes directly through a polygon point.
C     This algorithm is based on C psuedocode documented on pp. 347-356
C     in the book "Algorithms in C" by Robert Sedgewick, 1991.
C-----------------------------------------------------------------------


C-----------------------------------------------------------------------
C       maxpoly = maximum number of polygons to search
C       maxppol = maximum number of points on all of the polygons
C       maxpts  = maximum number of test points
C       x       = 1 denoting the first coordinate of the data point
C       y       = 2 denoting the second coordinate of the data point
C       nptspp  = array of the number of points on each polygon
C       check   = integer answer returned by the various functions
C       points  = contains the x and y coordinates for the points poly(x,y)
C       poly    = contains the integer list of points occuring on each poly
C-----------------------------------------------------------------------


        parameter (MAXPOLY=200,MAXPTS=210000,MIN=1,MAX=2)

        integer   check, Points(2,MAXPTS),XM(MAXPOLY,2),YM(MAXPOLY,2)
        integer   NPTSPP(MAXPOLY), NFIRST(MAXPOLY),INT_MAX,NPTS

        integer   xmin,xmax,ymin,ymax,x1,x2,y1,y2
        INTEGER   INSIDE,T(2,MAXPTS),code(maxpoly)

        character*80 fname

        common    int_max,NPTS,NPOLY,NPTSPP

        write(6,*)'enter the polygon (1,Y) PAIRS file name'
        read(5,'(a)')fname
        open(unit=99,file=fname,status='old')

        write(6,*)'enter the POLYGON/CODE file name'
        read(5,'(a)')fname
        open(unit=96,file=fname,status='old')

        write(6,*)'enter the input test point file name'
        read(5,'(a)')fname
        open(unit=95,file=fname,status='old')

        write(6,*)'Enter the X,Y,CODE output file-name'
        read(5,'(a)')fname
        open(unit=97,file=fname,status='unknown')

        write(6,*)'Enter the POINT,POLY output file-name'
        read(5,'(a)')fname
        open(unit=98,file=fname,status='unknown')

C     enter the x coordinate of the right side of polygon map

        WRITE(6,*) 'ENTER THE MAX X VALUE FOR TEST LINE'
        READ(5,*) INT_MAX


C:  read in the array of test points
```

```
      read(95,*)ntstpts
      WRITE(6,*)'THE NUMBER OF TEST POINTS IS ',NTSTPTS

      do 150  i=1,ntstpts
         read(95,*)t(1,i),t(2,i)
150   continue


C   read in the total number of (1,y) pairs on the polygons
      read(99,*)npts
      write(6,*)'Number of total points on the polygons = ',npts

c   read in the (1,y) pairs for the points on the polygons
      do 100 i=1,npts
         read(99,*)points(1,i),points(2,i)
100   continue

C   read in the total number of polygons
      read(96,*)npoly
      write(6,*)'Number of polygons = ',npoly

C read in the number o. points per polygon and the code of each
C     polygon

      kount = 0
      do 200 i=1,npoly
         read(96,*)nptspp(i),code(i)
         kk = kount + 1
         NFIRST(I) = kk

         do 300 j=1,nptspp(i)

            kount = kount + 1
300      continue
200   continue

C   determine the max and min coords of each polygon

      do 400 i=1,npoly
         istart = nfirst(i)
         iend = (nptspp(i)+istart-1)
         call minmax(istart,iend,points,xmin,xmax,ymin,ymax,i)
         XM(i,1)=XMIN
         XM(i,2)=XMAX
         YM(i,1)=YMIN
         YM(i,2)=YMAX

400   continue

C  NOW START CHECKING TEST POINTS AGAINST POLYGONS

      DO 600 I = 1, NTSTPTS
         IA= T(1,I)
         IB = T(2,I)


C   FIRST SEE IF POINT IS WITHIN POLY MIN AND MAX
C   IF IT IS, WRITE (1,Y,CODE) TO A FILE FOR POINTS IN POLYS

            DO 455 J=1,NPOLY
               istart = nfirst(j)
               iend = (nptspp(j)+istart-1)
               X1=XM(J,1)
               X2=XM(J,2)
               Y1=YM(J,1)
               Y2=YM(J,2)

C     IF THE TEST POINT IS INSIDE THE MIN AND MAX OF POLYGON J
C     THEN PROCEED TO SEE IF THE TEST POINT IS INSIDE POLYGON J

               IF ((IA.GT.X1).AND.(IA.LT.X2).AND.
     +             (IB.GT.Y1).AND.(IB.LT.Y2)) THEN

C     CALL SUBROUTINE INSIDE

                  CHECK = INSIDE(IA,IB,ISTART,IEND,POINTS,J,I)
```

```
C     IF THE TEST POINT IS INSIDE, WRITE TEST POINT NUMBER AND
C     POLY NUMBER TO A FILE

                  IF (CHECK.EQ.1) THEN
                        WRITE(98,*)I,J
                        WRITE(*,*)I,J
               C1=FLOAT(IA/1000)
               C2=FLOAT(IB/1000)

C     WRITE THE X,Y AND CODE OF POLGON IT IS INSIDE TO A FILE

                 WRITE(97,*)C1,C2,CODE(J)
                        GOTO  600
                   ENDIF
                ENDIF
455     CONTINUE
600     CONTINUE

        end



        subroutine minmax(istart,iend,points,xmin,xmax,ymin,ymax,l)

C-----------------------------------------------------------------
C       This subroutine calculates the minimum and maximum x and y value
C       of the polygon coordinates; subroutine receives info for one poly
C       at a time, and returns xm(i,min),xm(i,max),ym(i,min),ym(i,max)
C       where i is the polygon number.
C-----------------------------------------------------------------

        parameter (MAXPOLY=200,MAXPTS=210000,MIN=1,MAX=2)

        INTEGER  ISTART,IEND,POINTS(2,MAXPTS),l
        INTEGER  XMAX,XMIN,YMAX,YMIN

        XMAX =  -10000000
        XMIN =   10000000
        YMAX =  -10000000
        YMIN =   10000000

        DO 10 J = ISTART,IEND

               IF (POINTS(1,J).GE.XMAX) XMAX = POINTS(1,J)
               IF (POINTS(1,J).LT.XMIN) XMIN = POINTS(1,J)
               IF (POINTS(2,J).GE.YMAX) YMAX = POINTS(2,J)
               IF (POINTS(2,J).LT.YMIN) YMIN = POINTS(2,J)

10      CONTINUE

        RETURN
        END



        integer function ccw(p0,p1,p2)
C-------------------------------------------------------------------------
C     This function checks to see if the three points p0,p1 and p2
C     are arranged clockwise or counterclockwise, starting from p0.
C-------------------------------------------------------------------------

        integer p0(2), p1(2),p2(2)
        integer dx1, dx2, dy1, dy2

        CCW = 0

        dx1 = p1(1) - p0(1)
        dy1 = p1(2) - p0(2)

        dx2 = p2(1) - p0(1)
        dy2 = p2(2) - p0(2)

        RX1=FLOAT(DX1)
        RX2=FLOAT(DX2)
        RY1=FLOAT(DY1)
```

```
      RY2=FLOAT(DY2)

      if( RX1*RY2 .gt.RY1*RX2) then
         ccw = 1
         RETURN
      endif

      if(RX1*RY2 .lt. RY1*RX2) then
         ccw = -1
         RETURN
      endif

      if( (RX1*RX2 .lt. 0) .or. (RY1*RY2 .lt. 0))then
         ccw = -1
         RETURN
      endif
      if( (RX1*RX1 + RY1*RY1) .lt. (RX2*RX2 + RY2*RY2)) then
         ccw = 1
         RETURN
      endif

      RETURN
      end


      INTEGER FUNCTION INTERSECT(L1P1,L1P2,L2P1,L2P2)
C-----------------------------------------------------------------------
C     This function checks to see if the line segment defined by points
C     L1P1 and L1P2 intersects the line segment defined by points L2P1
C     and L2P2.
C-----------------------------------------------------------------------

      integer l1P1(2), L1P2(2),L2P1(2),l2P2(2)
      INTEGER C1,C2,C3,C4,CCW

      C1 = CCW( L1P1(1), L1P2(1), L2P1(1))
      C2 = CCW( L1P1(1), L1P2(1), L2P2(1))
      C3 = CCW( L2P1(1), L2P2(1), L1P1(1))
      C4 = CCW( L2P1(1), L2P2(1), L1P2(1))


      IF((C1*C2 .LE.0) .AND. ( C3*C4 .LT.0)) THEN
         INTERSECT = 1
      ELSE
         INTERSECT = 0
      ENDIF
      RETURN
      END


      integer function inside(ia,ib,istart,iend,points,U,B)
C-----------------------------------------------------------------------
C     This function decides if test point (ia,ib) is inside the polygon
C     being called for.
C-----------------------------------------------------------------------

      parameter (MAXPTS=210000)
      integer   count,INTERSECT,INT_MAX,npoly,points(2,maxpts)
      integer   lt(2,2), lp(2,2),ia,ib,crspt,istart,iend,seg,U
      INTEGER   nptspp(4000),B,check1,check2,lstpt
      common    int_max,NPTS,NPOLY,NPTSPP

C     LT=TEST LINE POINTS
C     LP=POLY LINE POINTS
C     CRSPT is the number of cross points between the horizontal
C     test line and the polygon segments

      crspt=0

      LT(1,1) = ia
      LT(2,1) = ib

      LT(1,2) = INT_MAX
      LT(2,2) = ib

      seg=0
```

```
        COUNT=istart

C     Step through the polygon line segments one at a time.  First
C     check to see if the test line intersects one of the polygon
C     line segment endpoints; if it does, either count it as an
C     intersection and increment the counter CRSPT or don't and
C     then move onto next segment (see explanation of this decision
C     point below).  If the test line doesn't pass through one of
C     the segment end points, then call the intersect function
C     to see if the test line and the polygon segment intersect.
C     If they do, increment the counter CRSPT.

        do 100 k=istart,iend

           if (points(2,count).ne.lt(2,1)) lstpt=k

           LP(1,1) = POINTS(1,count)
           LP(2,1) = POINTS(2,count)

           COUNT=COUNT+1

           IF(COUNT.GE.NPTSPP(U)+ISTART)THEN
              GOTO 200
           ENDIF

           LP(1,2) = POINTS(1,count)
           LP(2,2) = POINTS(2,count)


c     if first poly point intersects test line, see if second poly point
C     is above (check1=1) or below (check1=-1) test line; if the second
c     poly point is also on the test line, poly seg directly overlies test
c     so just go to next test point and start this whole process over

           if (points(2,count).eq.lt(2,1)) goto 100

           if (points(2,count-1).eq.lt(2,1)) then

              if ((points(2,count)-lt(2,1)).eq.0) goto 100

              if ((points(2,count)-lt(2,1)).gt.0) check1 = 1
              if ((points(2,count)-lt(2,1)).lt.0) check1 = -1

              if ((points(2,lstpt)-lt(2,1)).gt.0) check2 = 1
              if ((points(2,lstpt)-lt(2,1)).lt.0) check2 = -1

              if (check2.ne.check1) crspt=crspt+1
              go to 100
           endif

C     Call intersect to see if the test line intersects the
C     polygon line segment
           CHECK=INTERSECT(LP(1,1),LP(1,2),LT(1,1),LT(1,2))

             IF (CHECK .EQ.1) CRSPT = CRSPT + 1


100     CONTINUE
200     CONTINUE

        A=MOD(CRSPT,2)

C     If a = 0, that means that the total number of intersections
C     was even, and therefore the test point is NOT inside the
C     the polygon.  If a=1, that means the total number of
C     intersections was odd and the test point IS inside the polygon.

        INSIDE = A

        RETURN
        END
C*********************************************************************
```

```
      program fitplane

C*****************************************************************
C     This program finds the z value associated with each (x,y)
C     pair from the ptpoly program.  It does this by fitting a
C     plane to the nearest three digitized contour points.  Once
C     the z value is calculated, it is compared to the z values of
C     the nearest three contour points.  If this value is extrapolated
C     then the program seeks out contour points higher or lower as
C     necessary, and finds an interpolated z value.
C*****************************************************************

C     maxtst = the maximum number of test points
C     maxpts = the maximum number of contour points
C     R = the radius around each test point in which to search for
C         contour points
C     count = the number of contour points within r of the test pt.
C     xt(maxtst) = the array of test point x values
C     yt(maxtst) = the array of test point y values
C     code(maxtst) = the array of test point element code values
C     xp(maxpts) = the array of countour point x values
C     yp(maxpts) = the array of countour point y values
C     zp(maxpts) = the array of countour point z values
C     x(count),y(count),z(count) = the arrays of countour pts within
C         radius r of the given test point
C     xf(3),yf(3),zf(3) = the arrays of contour points which a plane
C        is fit to
C     zmin, zmax = the min and max  z value of the contour pts
C                  to which the plane is fit
C     newmin, newmax = the min and max z value of the contour pts
C                      which extrapolate the z value of the test pt
C     delx, dely = the difference between the x and y value of the test
C           pt and the x and y value of the contour pt
C     dx(count), dy(count) = the array of differences between the x and
C      y of the test pt and the x and y of the contour pts within r
C       of the test point
C     D = the distance between the test point and each contour point
C     Dist(count) = the array of distances between the test point
C          and the contour points within a radius r
C     lowcont = the value of the lowest contour line on the map
C     holdx,holdy, holdz, holdd = variables used for sorting the
C      contour points within r distance of the test point into
C      increasing distance
C     aa,bb,cc,dd,ee,ff = variables used to make sure that the three
C        contour points are not on a line
C     enoughlt, enougheq, enoughgt = variables used to ensure that a
C       sufficient number of countour points are found with a z value
C       less than, equal to and greater than the z values of the contour
C       point closest to the test point
C*****************************************************************************

        parameter  (maxtst=65098, maxpts=10305)

        integer  code(maxtst),count,kount,first,last,pp
        integer  enoughlt,enoughgt,total,enougheq
        real     xt(maxtst),yt(maxtst),zt(maxtst),holdd,holdx
        real     xp(maxpts),yp(maxpts),zp(maxpts),holdy,holdz
        real     delx,dely,r,x(maxpts),y(maxpts),z(maxpts)
        real     newmin,newmax,lowcont
        real     xf(3),yf(3),zf(3),dist(maxpts),dx(maxpts),dy(maxpts)
        real     aa,bb,cc,dd,ee,ff
        logical  sorted

C     Prompt user for necessary input
        write(*,*)'Enter the search radius'
        read(*,*)r

        write(*,*)'Enter the value of the lowest contour line'
        read (*,*) lowcont

C     Read test point data file and contour pt data files

        open(unit=96,file='out1.dat',status='old')
        do 21 i=1,maxtst
           read(96,*)xt(i),yt(i),code(i)
21      continue
```

```
      close(unit=96,status='old')

      open(unit=95,file='xyz.dat',status='old')
      do 22 i=1,maxpts
         read(95,*)xp(i),yp(i),zp(i)
 22   continue
      close(unit=95,status='old')

C     Begin stepping through test points (i index), looking for
C       all contour points (j index) that are within r of the test pt

      count=0
      do 40 i=1,maxtst

C     reinitialize the arrays with each new test point
      do 90 pp=1,count
            x(pp)=0
            y(pp)=0
            z(pp)=0
            dx(pp)=0
            dy(pp)=0
            dist(pp)=0
 90      continue

         count=0

         do 50 j=1,maxpts

C     check if contour point j is within a distance R of the test
C     pt i; if it is, add it to arrays x,y and z and increment count

            delx=xp(j)-xt(i)
            dely=yp(j)-yt(i)
            D=sqrt(delx**2+dely**2)
            if (D.le.R) then
                  count=count+1
                  x(count)=xp(j)
                  y(count)=yp(j)
                  z(count)=zp(j)
            endif
 50      continue

         if(count.lt.3)then
            j=0
            R=R+1
            goto 51
         endif
C     Create distance array between contour pts within r distance of
C     test point i

         do 60 k=1,count
            dx(k)=x(k)-xt(i)
            dy(k)=y(k)-yt(i)
            dist(k)=sqrt(dx(k)**2+dy(k)**2)
 60      continue

C     Sort distance array and corresponding x,y and z arrays according
C     to increasing distance from test point i

         sorted = .false.
         first=1
         last=count-1

 5       if (.not.sorted) then
            sorted=.true.
            do 70 kk=first,last
               if (dist(kk).gt.dist(kk+1)) then
                  holdd = dist(kk)
                  holdx = x(kk)
                  holdy = y(kk)
                  holdz = z(kk)

                  dist(kk) = dist(kk+1)
                  x(kk) = x(kk+1)
                  y(kk) = y(kk+1)
                  z(kk) = z(kk+1)
```

```
                        dist(kk+1) = holdd
                        x(kk+1) = holdx
                        y(kk+1) = holdy
                        z(kk+1) = holdz

                        sorted = .false.
                endif
 70             continue

                last = last-1
                go to 5

                endif

C       Initialize xf,yf and zf arrays
                do 99 pp=1,3
                   xf(pp)=0
                   yf(pp)=0
                   zf(pp)=0
 99             continue

C       Take the nearest contour point as the first point to fit a plane
C       to; now we need two more points

                xf(1)=x(1)
                yf(1)=y(1)
                zf(1)=z(1)
                kount=1
                enougheq=0
                enoughlt = 0
                enoughgt = 0

C       Step through the rest of the contour points within a distance R
C       of test pt i; we want one more contour point with a z value
C       equal to the nearest contour point, and one contour point with
C       a z value greater than the nearest contour pt.

                do 80 jj=2,count

                   if (kount.lt.3) then

                      if (zf(1).gt.lowcont) then
                         if (z(jj).eq.zf(1).and.enougheq.eq.0) then
                            enougheq=1
                            kount=kount+1
                            xf(kount)=x(jj)
                            yf(kount)=y(jj)
                            zf(kount)=z(jj)
                         elseif (z(jj).gt.zf(1).and.enoughgt.eq.0)then
                            kount=kount+1
                            enoughgt=1
                            xf(kount)=x(jj)
                            yf(kount)=y(jj)
                            zf(kount)=z(jj)
                         endif
                      elseif (zf(1).le.lowcont) then
                         if (z(jj).eq.zf(1).and.enoughlt.eq.0) then
                            enoughlt=1
                            kount=kount+1
                            xf(kount)=x(jj)
                            yf(kount)=y(jj)
                            zf(kount)=z(jj)
                         elseif (z(jj).gt.zf(1).and.enoughgt.eq.0)then
                            kount=kount+1
                            enoughgt=1
                            xf(kount)=x(jj)
                            yf(kount)=y(jj)
                            zf(kount)=z(jj)
                         endif
                      endif
                      endif
 80             continue

C       Check to make sure that the chosen three contour points are not
C       on a line; if they are go to the next test point
```

```
            aa=abs(xf(1)-xf(2))
            bb=abs(xf(1)-xf(3))
            cc=abs(xf(3)-xf(2))
            dd=abs(yf(1)-xf(2))
            ee=abs(yf(1)-xf(3))
            ff=abs(yf(3)-xf(2))

            if (aa.lt.0.05.and.bb.lt.0.05.and.cc.lt.0.05) then
               r=5
               goto 40
            elseif (dd.lt.0.05.and.ee.lt.0.05.and.ff.lt.0.05) then
               r=5
               goto 40
            endif

            if(count.gt.120) then
               r=5
               goto 40
            endif
C     if there are three points, reset the search radius; this part is
C     hardwired...
            if (kount.eq.3) r=5
C     if not enough points were found, increase r and start again with
            stepping through the contour points

            if (kount.lt.3) then
               j=0
               r=r+1
               goto 51
            endif

C     Calculate the maximum and minimum z values of the three chosen
C     contour points

      zmax=-3000
      zmin=3000

      do 66 kk=1,3
         if (zf(kk).gt.zmax) zmax=zf(kk)
         if (zf(kk).le.zmin) zmin=zf(kk)
 66   continue

C     Call subroutine plane which finds the equation of the plane which
C     passes through the three contour points

      call plane(xf,yf,zf,a,b,c)
C
      zt(i)=a*xt(i)+b*yt(i)+c

C     Now check to see if the calculated z value of the test point
C     was extrapolated (if the test pt z is greater than the max
C     z value of the 3 contours pts OR if z is less than the min
C     z value of the 3 contour pts)
C
      if (zt(i).gt.zmax) then

C     if the z value is extrapolated in the positive direction,
C     take the maximum values from the last run and find one or
C     two (as necessary)more contour points with z values greater
C     than the maximum... now the three contour points should
C     be greater than and less than the test point

        if (zmax.eq.zf(2).and.zmax.eq.zf(3)) then
            xf(1)=xf(2)
            yf(1)=yf(2)
            zf(1)=zf(2)
            xf(2)=xf(3)
            yf(2)=yf(3)
            zf(2)=zf(3)
            kount=2
         elseif (zmax.eq.zf(1).and.zmax.eq.zf(3)) then
            xf(1)=xf(1)
            yf(1)=yf(1)
            zf(1)=zf(1)
            xf(2)=xf(3)
```

```
                yf(2)=yf(3)
                zf(2)=zf(3)
                kount=2
             elseif (zmax.eq.zf(1).and.zmax.eq.zf(2)) then
                xf(1)=xf(1)
                yf(1)=yf(1)
                zf(1)=zf(1)
                xf(2)=xf(2)
                yf(2)=yf(2)
                zf(2)=zf(2)
                kount=2
             elseif (zmin.eq.zf(1).and.zmin.eq.zf(2)) then
                xf(1)=xf(3)
                yf(1)=yf(3)
                zf(1)=zf(3)
                kount=1
             elseif (zmin.eq.zf(2).and.zmin.eq.zf(3)) then
                xf(1)=xf(1)
                yf(1)=yf(1)
                zf(1)=zf(1)
                kount=1
             elseif (zmin.eq.zf(1).and.zmin.eq.zf(3)) then
                xf(1)=xf(2)
                yf(1)=yf(2)
                zf(1)=zf(2)
                kount=1
             endif

             do 49 jj=2,coun
                if (z(jj).gt.zmax.and.kount.lt.3) then
                   kount=kount + 1
                   xf(kount)=x(jj)
                   yf(kount)=y(jj)
                   zf(kount)=z(jj)
                endif
 49          continue

          elseif (zt(i).lt.zmin) then

C         if the z value is extrapolated in the negative direction,
C         take the minimum values from the last run and find one or
C         two (as necessary) more contour points with z values less
C         than the minimum... now the three contour points should
C         be greater than and less than the test point

             if (zmax.eq.zf(2).and.zmax.eq.zf(3)) then
                xf(1)=xf(1)
                yf(1)=yf(1)
                zf(1)=zf(1)
                kount=1
             elseif (zmax.eq.zf(1).and.zmax.eq.zf(3)) then
                xf(1)=xf(2)
                yf(1)=yf(2)
                zf(1)=zf(2)
                kount=1
             elseif (zmax.eq.zf(1).and.zmax.eq.zf(2)) then
                xf(1)=xf(3)
                yf(1)=yf(3)
                zf(1)=zf(3)
                kount=1
             elseif (zmin.eq.zf(1).and.zmin.eq.zf(2)) then
                xf(1)=xf(1)
                yf(1)=yf(1)
                zf(1)=zf(1)
                xf(2)=xf(2)
                yf(2)=yf(2)
                zf(2)=zf(2)
                kount=2
             elseif (zmin.eq.zf(2).and.zmin.eq.zf(3)) then
                xf(1)=xf(2)
                yf(1)=yf(2)
                zf(1)=zf(2)
                xf(2)=xf(3)
                yf(2)=yf(3)
                zf(2)=zf(3)
                kount=2
```

```
            elseif (zmin.eq.zf(1).and.zmin.eq.zf(3)) then
               xf(1)=xf(1)
               yf(1)=yf(1)
               zf(1)=zf(1)
               xf(2)=xf(3)
               yf(2)=yf(3)
               zf(2)=zf(3)
               kount=2
            endif

            do 52 jj=2,count
               if (z(jj).lt.zmin.and.kount.lt.3) then
                  kount=kount + 1
                  xf(kount)=x(jj)
                  yf(kount)=y(jj)
                  zf(kount)=z(jj)
               endif
 52         continue

         endif

C        Call subroutine plane again with new extrapolation contour
C        points

         call plane(xf,yf,zf,a,b,c)
         zt(i)=a*xt(i)+b*yt(i)+c

C        Recalculate the min and max of new extrapolation contour
C        points

            newmax=-3000
            newmin=3000

            do 600 jj=1,3
               if (zf(jj).gt.newmax) newmax=zf(jj)
               if (zf(jj).le.newmin) newmin=zf(jj)
 600        continue

           open(unit=92,file='alltst.dat',status='unknown')

C        if the program is still interpolating the z value of the
C        test point, throw out the test point; otherwise, write
C        the x,y,z and code values of the test points to a file

            if(zt(i).ge.newmin.and.zt(i).le.newmax)then
              write(92,*)xt(i),yt(i),zt(i),code(i)
            endif

40         continue

           close(unit=92,status='old')

         end
C*************************************************************************
         subroutine plane(x,y,z,a,b,c)
         dimension x(3),y(3),z(3),p1(3),p2(3)

C        This subroutine fits a plane to the three nearest contour points
C        defined by the arrays x,y and z; the subroutine returns the
C        the coefficients of the equation of the plane to the main
C        program


         p1(1)=x(2)-x(1)
         p1(2)=y(2)-y(1)
         p1(3)=z(2)-z(1)
         p2(1)=x(3)-x(1)
         p2(2)=y(3)-y(1)
         p2(3)=z(3)-z(1)

         crossa=p1(2)*p2(3)-p1(3)*p2(2)
         crossb=p1(3)*p2(1)-p1(1)*p2(3)
         crossc=p1(1)*p2(2)-p1(2)*p2(1)

         c1=crossa*x(1)
         c2=crossb*y(1)
```

```
      c3=crossc*z(1)
      csum=c1+c2+c3
      a=-crossa/crossc
      b=-crossb/crossc
      c= csum/crossc

      return
      end
```

APPENDIX B
Computer Program for Variogram Estimation

```
      program gamv3main
c-----------------------------------------------------------------
c
c         MAIN (DRIVER) PROGRAM FOR THE SUBROUTINE "GAMV3"
c         ***********************************************
c
c SUMMARY:
c  -The semi-variogram of three-dimensional irregularly spaced data
c    is computed. The program tests for missing values and any
c    number of variables can be analysed.
c
c INPUT:
c  -some dimension parameters must be checked in this main:
c       ndatmx = the maximum number of data (set at 500)
c       nlagmx = the maximum number of lags (set at 30)
c       nndmax = the maximum number of directions (set at 10)
c       nnvmax = the maximum number of variables (set at 5)
c  -a parameter file containing all the parameters for variogram
c       calculation.
c  -the data (no missing values) must be in another file.
c       stored x,y,z,vr.
c
c OUTPUT:
c  -the output is stored in two files:
c       1. documented output (file name given in parameter file).
c       2. semivariogram values written by increasing lag and then
c          by the direction and finally by the number of variables.
c
c NOTES:
c  -Detailed documentation is contained in the code for the
c    subroutine. To set the input parameters the user should refer
c    to this source of information.
c
c AUTHOR: Clayton Deutsch                          DATE: June 1987
c-----------------------------------------------------------------
        parameter(ndatmx=60000,nlagmx=500,nndmax=5,nnvmax=1)
        dimension azm(nndmax),plg(nndmax),atol(nndmax),ptol(nndmax)
        dimension test(nnvmax),x(ndatmx),y(ndatmx),z(ndatmx)
                                  d   i   m   e   n   s   i   o   n
vr(ndatmx*nnvmax),nd(nnvmax),ud(nnvmax),vd(nnvmax)
        dimension np(nlagmx*nndmax*nnvmax),dg(nlagmx*nndmax*nnvmax)
                                  d   i   m   e   n   s   i   o   n
gam(nlagmx*nndmax*nnvmax),ug(nlagmx*nndmax*nnvmax)
        character*30 file0,file1,file2,file3,ans
        common inp,iout,iout2,dummy,nv,nam,ans

c
c read in the parameters from the parameter file:
c
     write(*,*)'input the name of the parameter file'
     read(*,'(a)')file0

        open(1,file=file0,status='old')
        rewind(1)
```

```
          read(1,*) file1
          read(1,*) file2
          read(1,*) file3
          iout2=77
      iout=7
          open(iout,file=file2,status='unknown')
          read(1,*)nt
          read(1,*)lmax
          read(1,*)xlag
          read(1,*)dtol
          read(1,*)ndi
          read(1,*)(azm(i),i=1,ndi)
          read(1,*)(plg(i),i=1,ndi)
          read(1,*)(atol(i),i=1,ndi)
          read(1,*)(ptol(i),i=1,ndi)
          read(1,*)nv
          read(1,*)(test(i),i=1,nv)
          read(1,*)is
          close(1)
c
          write(*,*)'Enter the maximum dz value'
          read(*,*) zmax
c read in the data:
c
          inp=2
          open(inp,file=file1,status='unknown')
          rewind(inp)
          do 5 i=1,nt
            read(2,*)x(i),y(i),z(i),vr(i)
 5        continue

          close(inp)
c
c calculate the semi-variogram:
c
          call gamv3(lmax,xlag,dtol,ndi,azm,plg,atol,ptol,test,nt,
     +       x,y,z,vr,nd,ud,vd,np,dg,gam,ug,is,zmax)
c
c write the undocumented output:
c
          open (3,file=file3,status='unknown')
          rewind(3)
          icn=0
          do 10 k=1,nv
          do 10 j=1,ndi
          write(3,*)lmax
          do 10 i=1,lmax
          icn=icn+1
          write(3,*)dg(icn),gam(icn)
 10       continue
          write(3,*)' '
          close(3)
c
c finished:
```

```
      dg(il)=dg(il)/npp
      gam(il)=gam(il)/npp
310   ug(il)=ug(il)/npp/2.
400   continue
c
c       edition of results
      if(is.eq.0) go to 3000
c
c       print out results
c       definition of the number of pages by variable
c
      imp=(ndi-1)/4+1
      idm=float(ndi)/float(imp)+0.9999
c
c       edition of results per variable
c
      do 600 iv=1,nv
      do 500 im=1,imp
      write(iout,2001) nam(iv),im
      write(iout,2002) test(iv),ud(iv),vd(iv),nd(iv),nt,xlag,dtol
      id1=1+idm*(im-1)
      id2=min0(ndi,idm*im)
      write(iout,2004) (ia,azm(id),id=id1,id2)
      write(iout,2009) ( ia,plg(id),id=id1,id2)
      write(iout,2005) (ia,atol(id),id=id1,id2)
      write(iout,2008) (ia,ptol(id),id=id1,id2)
      write(iout,2006) (ia,id=id1,id2)
      il0=ndi*lmax*(iv-1)+lmax*(id1-1)
      ilm=il0+lmax*(id2-id1)
c
c       printing of results per lag/direction for
c       the current variable
c
      do 410 l=1,lmax
      il1=l+il0
      il2=l+ilm

        write(iout2,3001)dg(l),gam(l)
        write(iout2,*)0.075
        write(iout2,3002)np(l)

      write(iout,2007)l,(np(il),dg(il),gam(il),ug(il),
     *il=il1,il2,lmax)
410   continue
500   continue
600   continue
      write(iout,2011)
c
c       formats for edition of results
c
3001  format(2x,f13.6,3x,f13.6)
3002  format(4x,i4,'$')
2001  format(5x,' semi - variogram          ',a8,10x,'***page:',
     *i2,3x,'*** gam-v3 ***'/
```

```
      if(abs(cd).lt.ct(id)) go to 120
  122 if (cd .lt. 0.) xy = -xy
      ce=(xy*sz(id)+dz*cz(id))/h
      if(abs(ce).lt.cs(id)) go to 120
c
c       case when the current direction fits the current pair
c
      il0=l+lmax*(id-1)
c
c       the calculation of semi-variogram's parameters
c      will be made for this pair of data points for all variables
c
      do 110 iv=1,nv
      ip=i+nt*(iv-1)
      ip1=j+nt*(iv-1)
c
c      the parameter of the lag (il) is set for the current
c      variable
c
      il=il0+ndi*lmax*(iv-1)
      if(vr(ip).le.test(iv).or.vr(ip1).le.test(iv)) go to 110
      np(il)=np(il)+1
      dg(il)=dg(il)+h
      vrr=(vr(ip1)-vr(ip))
      gam(il)=gam(il)+0.5*vrr*vrr
      ug(il)=ug(il)+(vr(ip)+vr(ip1))
110   continue
120   continue
      go to 200
c
c       duplicated data message
c
199   write(iout,2010)i,x(i),y(i),j,x(j),y(j)
c
200   continue
300   continue
c
c      results are computed
c
      do 400 iv=1,nv
      if (nd(iv).eq.0) go to 400
c
c       overall statistics' parameters  per variable are derived
c
      vd(iv)=(vd(iv)-ud(iv)*ud(iv)/nd(iv))/nd(iv)
      ud(iv)=ud(iv)/nd(iv)
c
c       variogram's parameters per lag/direction/variable
c       are computed
c
      il0=ndi*lmax*(iv-1)+1
      il1=il0+lmax*ndi-1
      do 310 il=il0,il1
      npp=max0(1,np(il))
```

```
      nd(iv)=1
      ud(iv)=vrit
50    vd(iv)=vrit*vrit
c
c      computation of overall statistics' parameters  per variable
c       and of variogram's parameters per/lag/direction/variable
c
      nt1=nt-1
      do 300 i=1,nt1
c
c       a new seed point is considered
c
c       computation of statistics' parameters  for each variable
c
      ind=0
      do 210 iv=1,nv
      ip=i+nt*(iv-1)
      vrip=vr(ip)
      if(vrip.le.test(iv)) go to 210
      nd(iv)=nd(iv)+1
      ud(iv)=ud(iv)+vrip
      vd(iv)=vd(iv)+vrip*vrip
      ind=ind+1
210   continue
c
c       the end point of the current pair is selected
c       if at least for one variable, the first data of
c       the current pair is good (ind=1)
c
      if(ind.eq.0) go to 300
      i1=i+1
      do 200 j=i1,nt
c
c       definition of the lag corresponding to the current pair
c
      dx=x(j)-x(i)
      dy=y(j)-y(i)
      xy=sqrt(dx*dx+dy*dy)
      dz= z(j)-z(i)
      h=sqrt(dx*dx+dy*dy+dz*dz)
      adz=abs(dz)
      if(h.lt.0.001*dtol)go to 199
      if (adz.gt.zmax) go to 200
      l=int(h/xlag+0.5)+1
      if(l.gt.lmax.or.abs(h-(l-1)*xlag).gt.dtol) go to 200
c
c       definition of the direction corresponding to the
c       current pair. all directions are considered
c       (overlapping of direction tolerance cones is allowed)
c
      do 120 id=1,ndi
      xy=sqrt(dx*dx+dy*dy)
      if(xy.eq.0) go to 122
      cd=(dx*cx(id)+dy*cy(id))/xy
```

```
c
      double precision nam(8)
c
      common inp,iout,iout2,dummy,nv,nam,ans
c
      data ia/' '/
c
c       distance of tolerance is defined
c
      if(dtol.le.0.0) dtol=xlag/2.

c       for each direction, angle and its tolerance are defined

      pi=3.14159265
      do 1 kd=1,ndi
      if(atol(kd).le.0.or.atol(kd).gt.90) atol(kd)=45.
      if(ptol(kd).le.0.or.ptol(kd).gt.90) ptol(kd)=45.
      a=pi*azm(kd)/180.
      b=pi*plg(kd)/180.
      t=pi*atol(kd)/180.
      s=pi*ptol(kd)/180.
      cx(kd)=cos(a)
      cy(kd)=sin(a)
      cz(kd)=cos(b)
      ct(kd)=cos(t)
      sz(kd)=sin(b)
      cs(kd)=cos(s)
      if(ct(kd).le..001) ct(kd)=0.
      if(cs(kd).le..001) cs(kd)=0.
 1    continue
c
c        dimension of vario-related arrays
c
      lmm=nv*lmax*ndi
c
c       initialization of variogram's parameters
c       per lag/direction/variable
c
      do 40 il=1,lmm
      np(il)=0
      dg(il)=0.0
      gam(il)=0.0
40    ug(il)=0.0
c
c       initialization of statistics' parameters per variable
c       (using the last data value for each variable)
c
      do 50 iv=1,nv
      ud(iv)=0.
      vd(iv)=0.
      nd(iv)=0.
      it=nt*iv
      vrit=vr(it)
      if(vrit.le.test(iv)) go to 50
```

```
c               ud(nv)           -average of data /variable
c               vd(nv)           -variance of data  /variable
c               np(lmax*ndi*nv)  -number of pairs used
c                                 per lag/direction/variable
c               dg(lmax*ndi*nv)  -mean distance array
c                                 per lag/direction/variable
c               gam(lmax*ndi*nv)-semi-variogram array
c                                 per lag/direction/variable
c               ug(lmax*ndi*nv)  -weighted average of data
c                                 (mv.gt.0) used to calculate
c                                 semi-variogram per lag/direction
c                                 /variable
c                                  for ug data are weighted
c                                  by number of times they enter
c                                  the particular lag calculation
c                                  of the variogram. ug indicates
c                                  proportional effect but not an
c                                  unbiased estimate of local mean.
c
c      working arrays:
c
c       cx,cy,cz,sz,ct,cs       - sine and cosine of direction and
c                                  tolerance angles
c
c  options
c  *******
c               is.eq.1          -edit results (1 page/variable)
c                                maximum: 4 directions/page/variable
c
c  common
c  ******
c               inp               -input unit number
c               iout              -printer unit number
c               dummy             -not used
c               nv               -number of variables being analyzed
c                                   maximum = 6
c               nam(nv)           -array of variables'names (a8)
c
c REVISIONS:
c  Author                 Revision                              Date
c  -----                  --------                              ----
c  R. Mohan Srivastava    problem with direction cosines    August
1987
c                         with dipping search direction
c                         corrected:  if cd<0, then the
c                         horizontal component of the
c                         unit vector from i to j must be
c                         negative.
c
                             d   i   m   e   n   s   i   o   n
azm(3),plg(3),atol(3),ptol(3),test(1),x(1),y(1),z(1)
     1,vr(1)
      dimension nd(1),ud(1),vd(1),np(1),dg(1),gam(1),ug(1)
      dimension cx(6),cy(6),cz(6),sz(6),ct(6),cs(6)
```

```
c
        stop
        end
                  s u b r o u t i n e      g a m v 3
(lmax,xlag,dtol,ndi,azm,plg,atol,ptol,test,nt,
     *x,y,z,vr,nd,ud,vd,np,dg,gam,ug,is,zmax)
c
c
c     three dimensional semi-variogram for several variables .
c       maximum of variables allowed=6 .
c       irregularly spaced data .
c      grouping of data into classes of directions and distances.
c       computation of main statistics per variable.
c       computation of average per lag/direction/variable .
c
c
c  parameters
c  **********
c       input:
c
c               lmax            -maximum number of lags
c               xlag            -length of the unit lag
c               dtol            -distance tolerance
c                                 if dtol.le.0.,then dtol=xlag/2.
c                   ndi                 -number of directions to be
considered
c                  azm(ndi)          -angle defining the horizontal
direction
c                                   o degree denotes west-east
c                   plg(ndi)           -plunge angle (angle with the
vertical)
c                                    0=vertical, 90=horizontal
c               2*atol(ndi)     -tolerance angle for the azimuth
c                                  if atol(ndi).le.0.0,then
c                                  atol(ndi)=45.0 degrees
c               2*ptol(ndi)     -tolerance angle for the plunge
c                                  if ptol(id).le.0 then ptol(id)=45.
degrees
c               test(nv)        -indicator value of missing data
c                                 values per variable
c                                  if vr(nt*nv).le.test(nv),then
c                                  this data value is considered as
c                                  missing and is ignored
c               nt              -number of data points per variable
c                                  including missing data values
c               x(nt)           -coordinates of data points
c               y(nt)              (center point of the data)
c               z(nt)
c              vr(nt*nv)       -data values array,stored columnwise
c                                  variable per variable
c
c      output:
c
c               nd(nv)             -number of data/variable
```

```
     *7x,'**************** ',5x,'(irregular 2 dimensional grid
)'//)
                  2                   0                   0                   2
format(2x,'test=',e12.5,2x,'mean=',e12.5,2x,'variance=',e12.5,
     5x,'# of data=',i4,'/',i4,4x,'lag=',f7.2,4x,'lag tolerance=',
     2f7.2,//)
2004  format(1h ,4x,'!',4(a1,5x,'azimuth   =',f6.1,7x,'!'))
2009  format(1h ,4x,'!',4(a1,5x,' plunge   =',f6.1,7x,'!'))
2005  format(1h ,4x,'!',4(a1,5x,'azim. tol.=',f6.1,7x,'!'))
 2008 format(1h ,4x,'!',4(a1,5x,'plun. tol.=',f6.1,7x,'!'))
2006  format(1h ,'lag !',
     *4(a1,' np  dist  1/2 vario   av/lag!'))
2007  format(1h ,i5,1x,'!',4(i5,f7.2,2x,e11.5,f7.3,'!'))
2010  format(1h1,'duplicated data***gam-v3***  data',i5,
     *' x= ',f9.4,' y= ',f9.4
     *,'  data  ',i5,' x= ',f9.4,' y= ',f9.4)
2011  format('1')
3000  return
      end
```

APPENDIX C
Sensitivity Analysis for Variograms esitmated in N60E direction

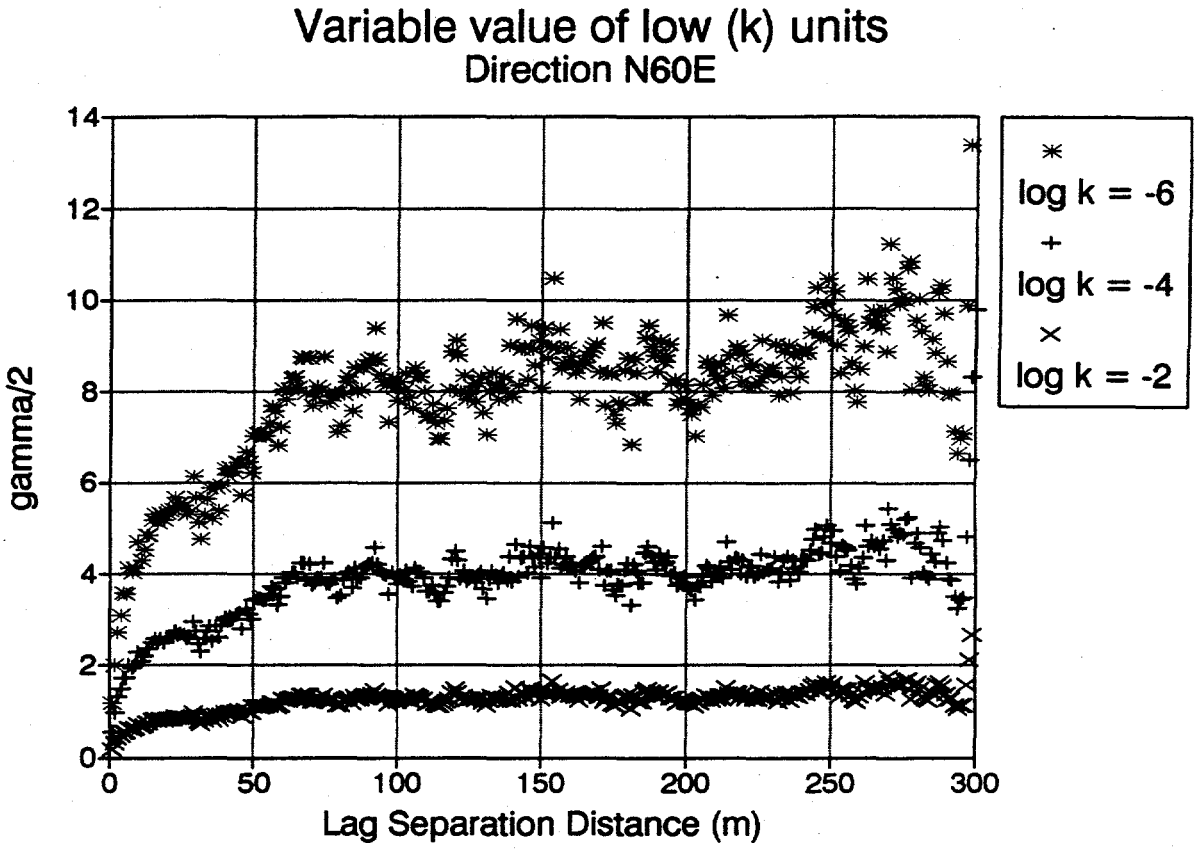
Variable value of low (k) units
Direction N60E
gamma/2
Lag Separation Distance (m)
log k = -6
log k = -4
log k = -2
0
2
4
6
8
10
12
14
0
50
100
150
200
250
300

Direction N45E

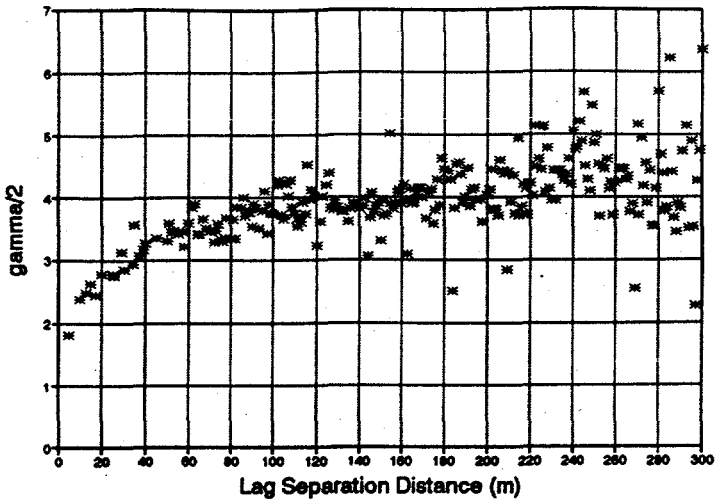

Direction N60E

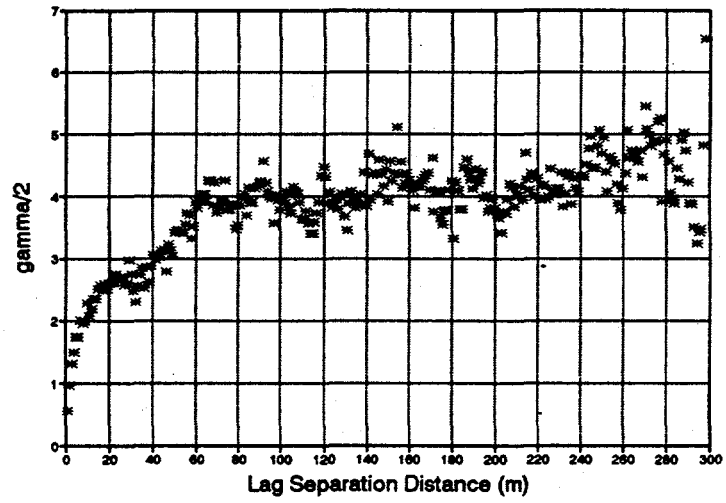

Direction N90E

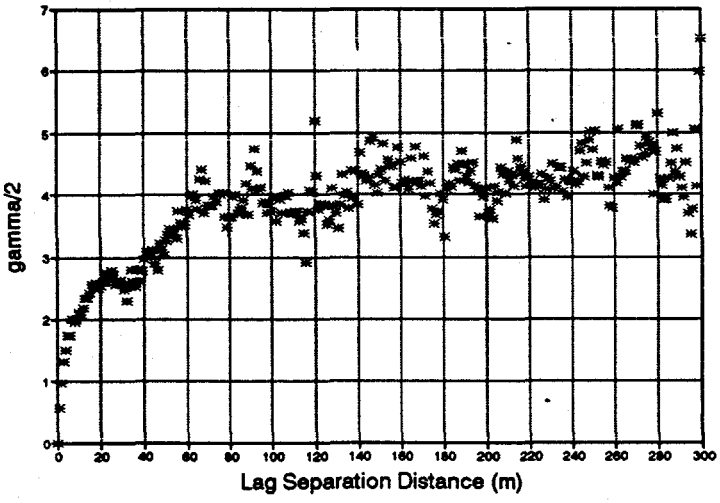

Angle Tol. = 10 degrees (anisotropic)
N60E

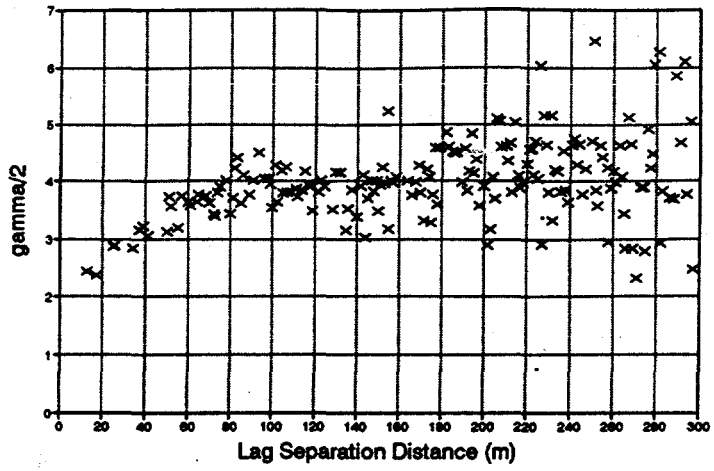

Angle Tol. = 30 degrees (anisotropic)
N60E

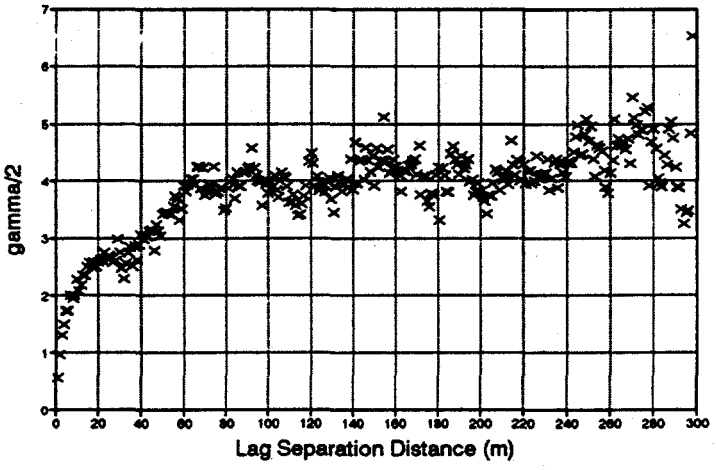

Angle Tol. = 50 degrees (isotropic)
N60E

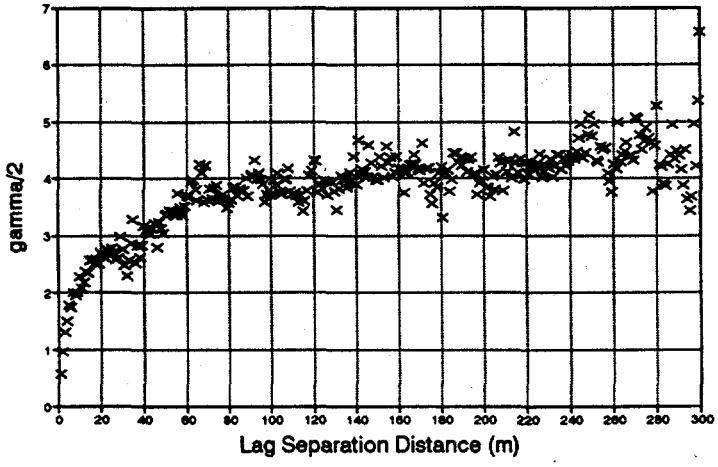

Vert. Distance Tol. = 0.10 m
N60E

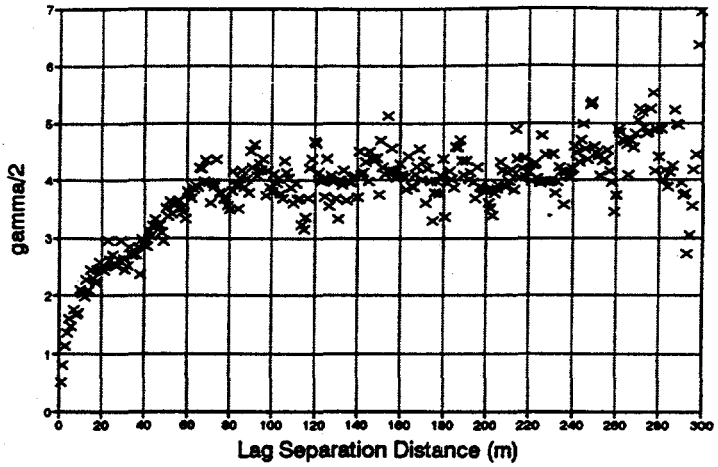

Vert. Distance Tol. = 0.25 m
N60E

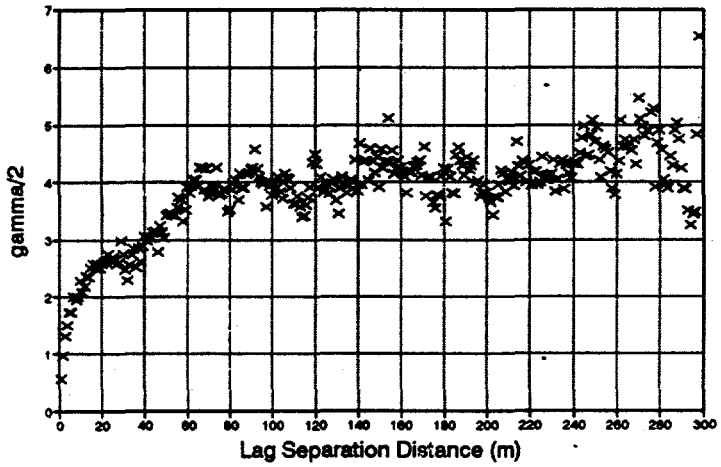

Vert. Distance Tol. = 1.0 m
N60E